EGFR phosphorylation regulates endosomal binding kinetics of Rab5 and Rab7a

Maria Winther

Thesis for the Master's degree in Molecular Biosciences

60 credits

Department of Biosciences

Faculty of Mathematics and Natural Sciences

UNIVERSITY OF OSLO

2021

Table of contents

Acknowledgements

The work presented in this study was carried out in the laboratory of Professor Oddmund Bakke at the Department of Biosciences, Faculty of Mathematics and Natural Sciences, University of Oslo.

First, I would like to thank Professor Oddmund Bakke for including me as a Master student in his lab. Thank you for the discussions, your ideas and feedback, I have really enjoyed my time as a master student in the Bakke-Progida lab.

A humongous thanks to my superb supervisors Frode Skjeldal and Linda Haugen. I will always be grateful your help, support, patience and encouraging words during my time in the Bakke lab, always welcomely sharing your time.

Lastly, I want to thank my fellow master students who I shared office with, Anna, Felicia and Marie. It has been a pleasure to fail, and every now and then master, experiments with you and hanging out with you through the struggles of the pandemic. You have been the fluorescence to my days.

Oslo, October 2021
Maria Winther

Abbreviations

DMEM	Dulbecco's Modified Eagle Medium
DTT	Dithiothreitol
EE	Early endosome
EEA1	Early Endosome Antigen 1
EGF	Epidermal growth factor
EGFP	Enhanced green fluorescent protein
EGFR	Epidermal growth factor receptor
Eps15	Epidermal growth factor receptor pathway substrate 15
ESCRT	Endosomal sorting complexes required for transport
FBS	Fetal bovine serum
FRAP	Fluorescence recovery after photobleaching
GAP	GTPase-activating protein
GDI	GDP dissociation factor
GDP	Guanine diphosphate
GEF	Guanine nucleotide exchange factor
GTPase	Guanosine triphosphate
Hrs	Hepatocyte growth factor-regulated tyrosine kinase substrate
IF	Immobile fraction
ILVs	Intralumenal vesicles
kDa	Kilo Dalton
LE	Late endosome
MF	Mobile fraction
MVB	Multivesicular bodies
PBS	Phosphate-Buffered Saline
PM	Plasma membrane
PTEN	Phosphatase and tensin homologue deleted on chromosome 10
PVDF	Polyvinylidene fluoride
Rab	Ras-related in brain
RE	Recycling endosome
REP	Rab escort protein

RNAi	RNA interference
RTK	Receptor tyrosine kinase
SDS-PAGE	Sodium dodecyl sulphate polyacrylamide gel electrophoresis
siRNA	Small interfering RNA
SNAREs	Soluble NSF attachment protein receptor
Srb	Scrambled
$T_{1/2}$	Recovery halftime
TIRF	Total internal reflection fluorescence
wt	wild type

Abstract

Upon ligand binding the EGFR is activated, autophosphorylated, internalized and trafficked through the endosomal pathway where the correct sorting and trafficking is critical for appropriate signal attenuation. Here we show by FRAP experiments that the EGFR regulates the endosomal binding kinetics of Rab5 and Rab7a in a phosphorylation-dependent manner. By introducing three mutated EGFRs with the deleted phosphorylation sites, Y1045, Y1068 and Y1086 we could show a complete rearrangement of the Rab5 and Rab7a binding dynamics. Furthermore, by TIRF microscopy we could show a delayed internalization of the mutants and specifically of the triple mutated receptor (Y1045, Y1068 and Y1086) that might also be recycled back to the plasma membrane. Moreover, we could show that a knockdown of Rab22a would impair the trafficking of the wt-receptor through Rab5 positive endosomes by inhibiting the detachment of Rab5, and the transport of the triple mutant would be discontinued. These findings suggest impaired recruitment of Rabex-5 to the triple mutated receptor upon Rab22a knockdown. Collectively, we have found that the EGFR regulates its own progression through the endosomal pathway by controlling the Rab5 and Rab7a binding dynamics. This indicates that the EGFR can regulate the pivotal Rab5 to Rab7a conversion and regulate its own progression through the endocytic pathway.

1. Introduction

1.1 Intracellular trafficking

Eukaryotic cells are structured into subcellular compartments termed organelles in which specific functions occur. These structures form a complex trafficking network throughout the cell in which the compartments can transport different molecules. There are two main trafficking pathways in the cell; the endocytic pathway, which involves the uptake of extracellular material which is transported inward through the cell, and the exocytic pathway which rids the cell of molecules by transporting it out of the cell (Figure 1.1)(Satori, Henderson et al. 2013). These two pathways are connected by a bidirectional transport between the trans-Golgi network and endosomes which allows for a direct route of newly synthesized molecules required in endosomes (Progida, Cogli et al. 2010).

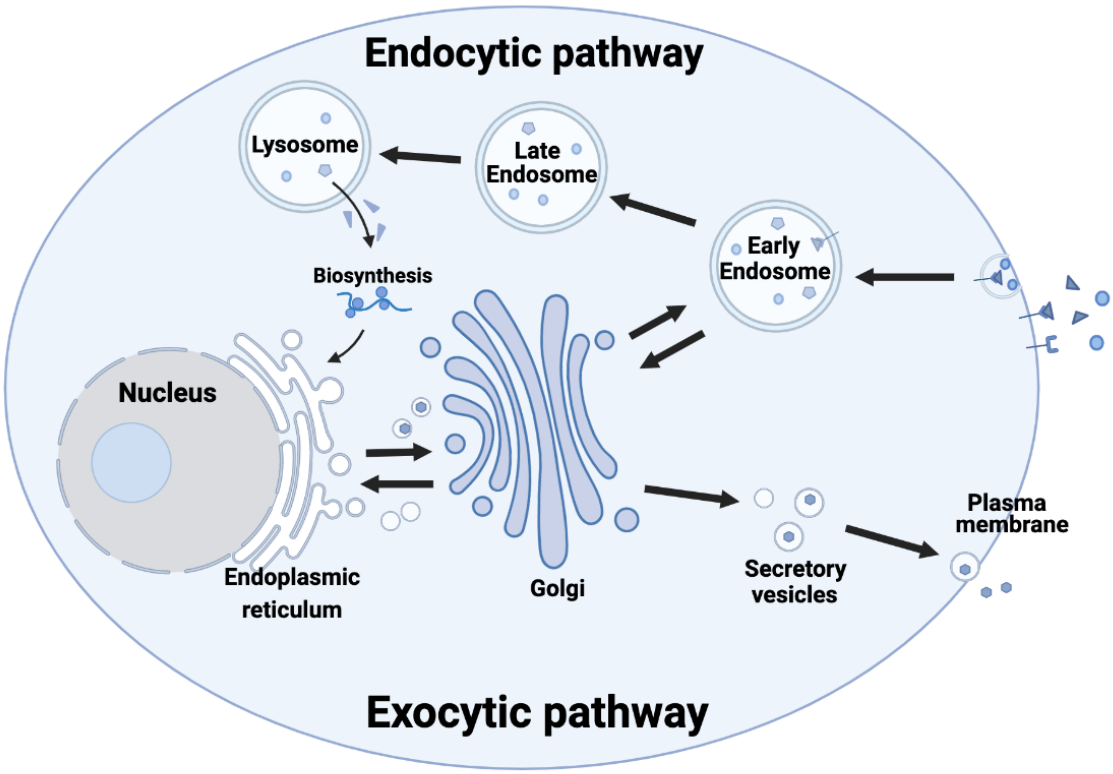

Figure 1.1: Schematic figure of the endocytic and exocytic pathway. The endocytic pathway describes the transport of cargo from the extracellular environment into the cell. This pathway includes early endosomes, late endosomes and lysosomes. The exocytic pathway describes the transport of newly synthesized molecules inside the cell to the extracellular environment. This pathway includes transport from the ER through Golgi and further delivery of molecules to the plasma membrane and extracellular environment by secretory vesicles. Figure inspired by (Tokarev, Alfonso et al.).

Activation and internalization of receptors on the plasma membrane stimulates different signaling pathways in the cell, where functional trafficking is critical for appropriate signaling and eventually signal attenuation by degradation. This complex network of intracellular trafficking is strongly regulated which is important for correct sorting of molecules, signal transduction and cell membrane homeostasis (Palade 1975, Bonifacino and Glick 2004).

1.2 Endocytosis

Endocytosis is a basic cellular process in which substances are brought into the cell. The term endocytosis is derived from the three Greek words; *endo* meaning "inside", *kytos* meaning "cell", and *osis* meaning "process" (Khan and Steeg 2021). Substances that are to be taken up by the cell become enclosed by the cell membrane and the newly formed vesicle is pinched off and further trafficked within the cell. Molecules from the cell surface can be acquired through various endocytic mechanisms including phagocytosis (cell eating), pinocytosis (cell drinking) and receptor-mediated endocytosis (Figure 1.2) (Cooper 2000). The internalized cargo-containing vesicle is dependent on further mechanisms in order to fuse with its target membrane (Mayor and Pagano 2007).

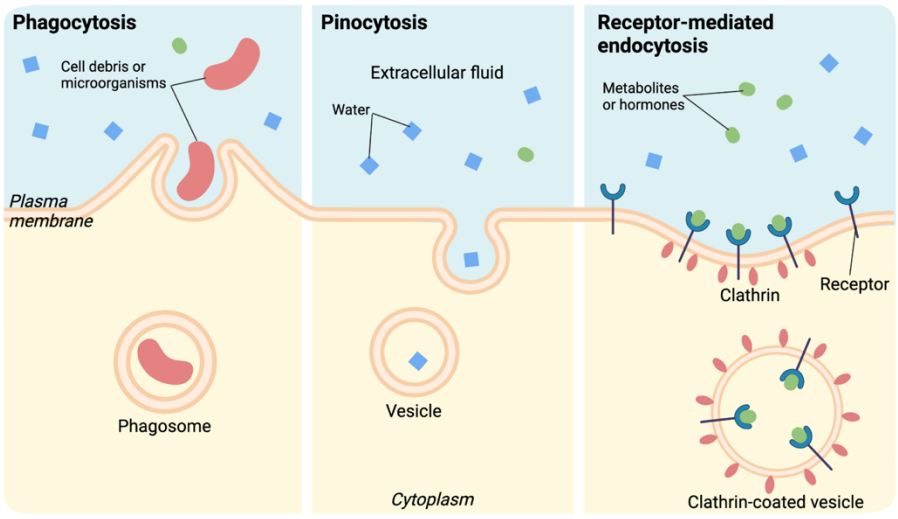

Figure 1.2: Schematic figure of endocytosis. Phagocytosis (cell eating) enables the cell to engulf large surface-bound particles, e.g. a pathogen, and internalize it into phagosomes. Pinocytosis (cell drinking) is the engulfment of extracellular medium which is internalized into vesicles. Receptor-mediated endocytosis is the internalization of receptors through clathrin-coated pits into a clathrin-coated vesicle. Figure: modification of work by Mariana Ruiz Villarreal.

Endocytosis of signaling receptors is an important mechanism for attenuating the strength and duration of signaling. Signaling from internalized receptor/ligand complexes may be terminated by endosomal trafficking destined for degradation in lysosomes. Aberrant endocytosis is shown to be implicated in several cancer types, including ovarian, breast, bladder and prostate cancer (Mills, Mosesson et al. 2008).

1.2.1 Clathrin-Mediated Endocytosis (CME)

Clathrin-mediated endocytosis (CME) is the main internalization route for surface-bound receptors and cargo in mammalian cells (Bitsikas, Corrêa et al. 2014). Iron-bound transferrin receptors (TFRs), low-density lipoprotein receptor (LDLRs) and the epidermal growth factor receptor (EGFR) are classic examples of cargo internalized by CME. CME is initiated as endocytic coat proteins in cytosol cluster to the plasma membrane (Figure 1.3). The coat assembly further recruits additional coat proteins from the cytosol. Some of these coat proteins important for CME are the clathrin triskelia and the adaptor protein-2 (AP2). Cargo recruitment assembles cargo on the plasma membrane to the coated regions and membrane bending is further induced by the assembling coat which leads to the formation of a 'clathrin-coated pit'. The vesicle formation and scission process is achieved by BAR domain proteins in cooperation with dynamin, constricting the neck of the forming vesicle and leading to separation of the vesicle from the plasma membrane. Coat and scission proteins collaborate with actin to induce shaping of the membrane. Lastly, the clathrin-coat is disassembled from the newly formed vesicle which enables fusion with endosomes and further trafficking within the cell (Taylor, Perrais et al. 2011) (Massol, Boll et al. 2006, Kaksonen and Roux 2018).

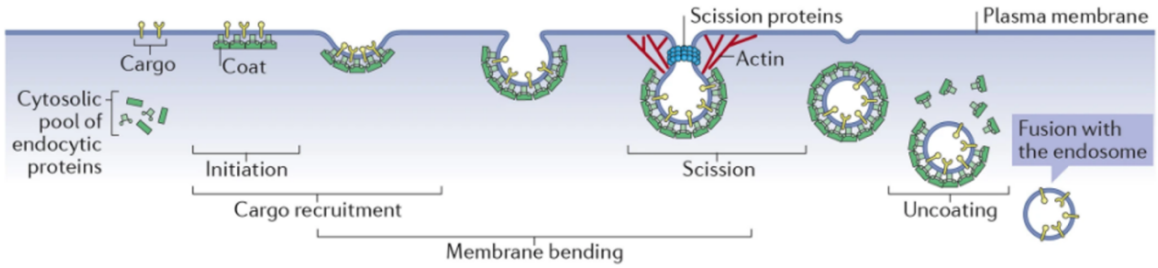

Figure 1.3: Clathrin-mediated endocytosis. Cargo is recruited to coated region of the plasma membrane and the region is bent into a clathrin-coated pit. Coat and scission proteins collaborate with actin to induce shaping of the membrane. The scission process tightens the neck of the forming vesicle and separates it from the plasma membrane. Following is the uncoating of the vesicle which enables fusion with endosomes and further trafficking within the cell. Figure from (Kaksonen and Roux 2018).

1.2.2 Clathrin-Independent Endocytosis (CIE)

Another mechanism of endocytosis of cargo is clathrin-independent endocytosis (CIE). Examples of CIE are pinocytosis, phagocytosis and caveolae-mediated endocytosis. In contrast to CME, this mechanism of cargo internalization does not involve the clathrin protein. Pinocytosis allows the cell to engulf extracellular medium and internalize it into vesicles. These vesicles are finally fused to lysosomes where the extracellular compounds are degraded and nutrients can be extracted (Lewis 1937, King and Kay 2019).

Phagocytosis enables the cell to engulf surface-bound particles such as a pathogen into a forming organelle called a phagosome. After the particle is bound to a surface receptor there is a rearrangement of the actin cytoskeleton leading to a remodeling of the plasma membrane. The subsequent budding off from the plasma membrane forms a phagosome that is increasingly acidified through the endocytic pathway. Finally, the acidic phagosome fuses with the lysosome into a phagolysosome, where the cargo is degraded (Desjardins, Huber et al. 1994, Swanson 2008).

Caveolae-mediated endocytosis (CavMe) is a CIE pathway which involves invagination of the plasma membrane forming a vesicular structure called caveolae (meaning little caves). Caveolae are membrane domains enriched in cholesterol and sphingolipids (Kiss and Botos 2009). The process of caveolae formation is driven by caveolin and cavin proteins, where caveolin-1 and cavein1 have been shown to sort specific lipids from the plasma membrane (Zhou, Ariotti et al. 2021). CavMe is induced upon ligand binding of receptors located in caveolae. Kinases and phosphatases regulate the budding of the caveolae, and the pinching off from the plasma membrane requires Dynamin (Khan and Steeg 2021).

1.3 The family of Rab-GTPases

Rab GTPases with nearly 70 family members is the largest family of small GTPases (Figure 1.4). The distinctive Rab GTPases locate to their specific membrane compartments and act as key regulators of intracellular membrane trafficking. Due to the specific properties and location of the Rab GTPases they contribute to maintain membrane identity and control the specificity and directionality of vesicular transport (Stenmark 2009, Pfeffer 2013, Wandinger-Ness and Zerial 2014).

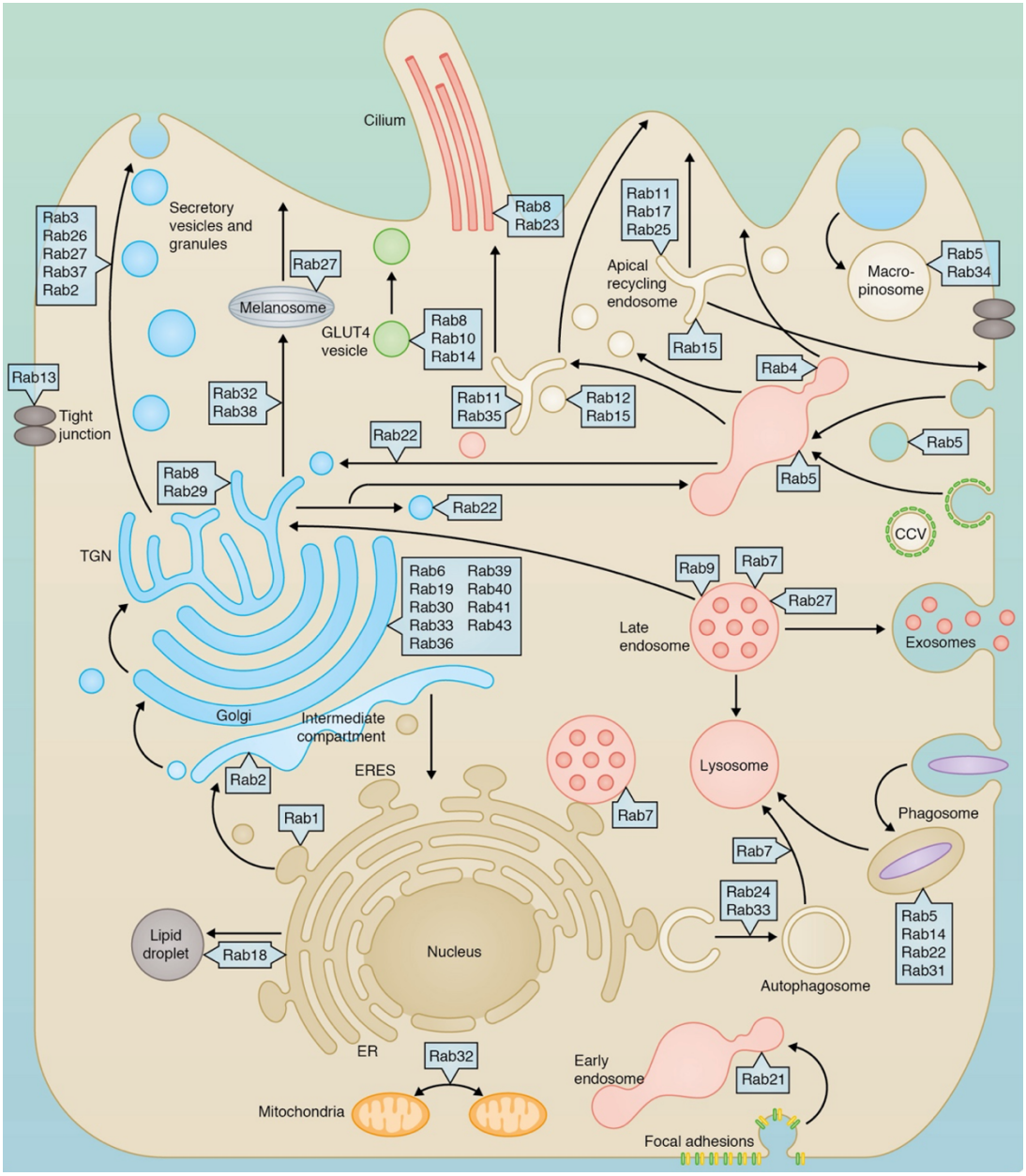

Figure 1.4: Rab GTPases and their intracellular location. The Rab proteins are located at their specific membrane structures throughout the cell, important for correct sorting and trafficking of cargo. Figure from (Zhen and Stenmark 2015).

A specific Rab GTPase can be located to more than one intracellular compartment. One example is Rab7b which is located both on late endosomes (LE) and the trans-Golgi network (TGN), regulating vesicular transport from LE to the TGN (Progida, Cogli et al. 2010, Progida, Nielsen et al. 2012).

Particular Rab proteins give specificity to organelles such as Rab5 and Rab7a on the early and late endosome, respectively, where Rab5 has been shown to regulate the maturation and

fusion of early endosomes (Gorvel, Chavrier et al. 1991, Skjeldal, Haugen et al. 2021). However, an organelle may have several different membrane-bound Rab proteins. For example, Rab5, Rab4, Rab21 and Rab22a all locate to the early endosome, carrying out specific functions (Wandinger-Ness and Zerial 2014).

Several diseases have been linked to mutations of Rab proteins. An example of this is the hereditary motor and sensory neuropathy called Charcot-Marie Tooth Type 2B (CMT2B) which has been linked to mutations of the Rab7a gene. Further, mutations in the Rab27a gene has been linked to the autosomal recessive disease Griscelli Syndrome (GS), which is characterized by a pigment deficiency in addition to immunodeficiency (Griscelli and Prunieras 1978, Van Gele, Dynoodt et al. 2009). Moreover, upregulated expression of Rab5 is an early known neuronal response in the progressive neurogenerative disorder Alzheimer's disease (Kim, Sato et al. 2016).

In addition to their roles in intracellular trafficking, Rab proteins are involved in a variety of other cellular processes. Rab20 has been shown to have an antibacterial function, which was shown by a knockdown experiment of Rab20 in *M. tuberculosis* infected macrophages. Knockdown of Rab20 inhibited the normal phagolysosomal function to become acidic and proteolytic, leading to bacterial replication (Schnettger, Rodgers et al. 2017).

Rab proteins have also been shown to be involved in cellular migration. Studies of Rab13 knock out mice showed smaller spleen and lymph nodes due to the impaired migration of lymphocytes (Nishikimi, Ishihara et al. 2014). Moreover, Rab GTPases are involved in cell division. Studies have shown that Rab35 is required for cytokinesis (Klinkert, Rocancourt et al. 2016), and that Rab11 is required for correct organization of microtubules and the mitotic spindle (Hehnly and Doxsey 2014).

1.3.1 Rab GTPases as molecular switches

Small Rab GTPases act as molecular switches, being active in its GTP-bound state and inactive in its GDP-bound state. The nucleotide cycle of small Rab GTPases is regulated by guanine-nucleotide exchange factors (GEFs) and GTPase-activating proteins (GAPs). Some GEFs and GAPs are specific for single Rab GTPases, while others are specific for a Rab GTPase subfamily (Zhen and Stenmark 2015).

The active (GTP-bound) state of the Rab allows for effector protein interaction. The Rab-GTP is converted back to its inactive state by a GTPase-activating protein (GAP) and an inorganic phosphate is released (Figure 1.5). The Rab escort protein (REP) recognizes the newly synthesized Rab-GDP and presents it to a geranylgeranyl transferase (GGT). The GGT prenylates the C-terminal of the Rab-GDP, which is essential for membrane anchoring. The Rab GDP dissociation inhibitor (GDI) recognizes the prenylated Rab-GDP, making the Rab-GDP soluble in cytosol. The GDI-displacement factor (GDF) targets Rab-GDP to a specific membrane by promoting GDI release of the Rab-GDI complex (Pfeffer, Aivazian et al. 2003, Stenmark 2009).

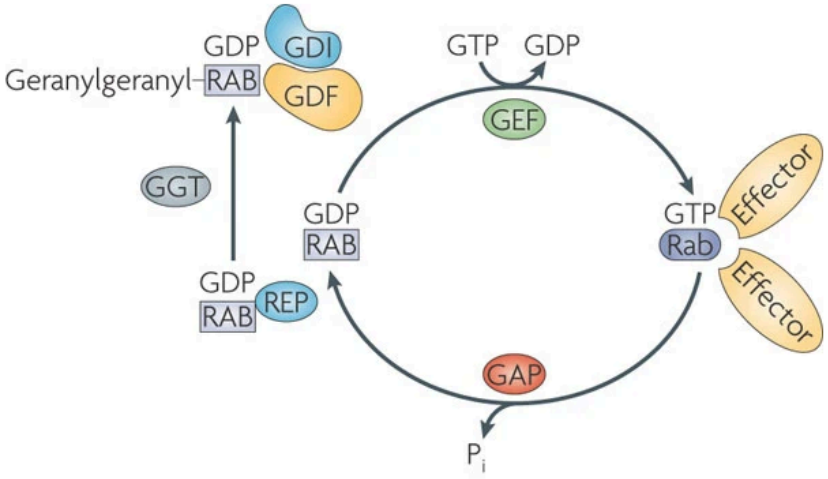

Figure 1.5: The GDP-GTP cycle of Rab GTPases. Guanine-nucleotide exchange factor (GEF) catalyzes the conversion from Rab-GDP to Rab-GTP, which allows for effector binding. Rab-GTP to Rab-GDP conversion requires a GTPase-activating protein (GAP). Rab escort protein (REP) presents Rab-GDP to a geranylgeranyl transferase (GGT) which prenylates the C-terminal of Rab-GDP. Rab GDP dissociation inhibitor (GDI) recognizes Rab-GDP forming a complex. GDI displacement factor (GDF) promotes GDI release from the GDI-Rab complex and targets Rab-GDP to a specific membrane. Figure from (Stenmark 2009).

Following Rab activation there are conformational differences between the two states in mainly two regions; switch I and switch II. When GTP is bound, these two regions are able to interact with effector proteins (Eathiraj, Pan et al. 2005), while in the GDP-bound state the switch region seems to be unfolded not allowing effector proteins to bind (Gabe Lee, Mishra et al. 2009). Thus, Rab GTPases are able to interact with their effectors when in a GTP-bound state (Pylypenko, Hammich et al. 2018). Rab effectors include fusion regulators, molecular tethers, kinases and phosphatases (Gillingham, Sinka et al. 2014). Some Rab effectors have

GAP or GEF activity. One example of this is the Rabaptin-5/Rabex-5 complex. The Rabaptin functions as an effector for Rab5, while Rabex-5 harbor GEF activity towards Rab5. This results in a positive feedback loop of Rab5 accumulation on the EE (Zhu, Liang et al. 2009).

1.4 The endosomal network

The endosomal network is comprised of several membrane-enclosed compartments crucial for appropriate sorting of endocytosed molecules. All endocytosed molecules are transported to early endosomes and either recycled back to the plasma membrane or to lysosomes for degradation. The endosomal compartments include early endosomes, recycling endosomes, multivesicular bodies, late endosomes, and lysosomes. The intralumenal pH decreases through the endosomal pathway with early endosomes maintain a pH of 6.5, late endosomes a pH of 5.5 and lysosomes a pH of 4.5 (Hu, Dammer et al. 2015). Trafficking through the endosomal compartments is a highly regulated process with distinct associated proteins maintaining the identity and progression of the various compartments.

1.4.1 The early endosome (EE)

The early endosome (EE) is defined as the first endosomal compartment that receives cargo from the plasma membrane (Helenius, Mellman et al. 1983). Cargo can be internalized via CME or CIE which forms a vesicle that is delivered to the EE (Mayor and Pagano 2007). Cargo delivered to EEs can either be directly recycled back to the plasma membrane from EE through the fast recycling route regulated by Rab4 (van der Sluijs, Hull et al. 1992) or through the slower recycling route through recycling endosomes regulated by Rab11 (Takahashi, Kubo et al. 2012). The cargo can also be sorted from the EE to the TGN. Furthermore, cargo destined for degradation is transported to the late endosome and further to lysosomes (Hu, Dammer et al. 2015).

After the formation of an endocytic vesicle Rab5 will be recruited and the newly formed early endosome will immediately start to interact and fuse with other Rab5 positive early endosomes. Rab5 is the main determinant of the early endosome and is one of the main regulators of endosomal maturation and progression (Rink, Ghigo et al. 2005, Skjeldal, Haugen et al. 2021). In addition, Rab5 regulates mechanisms such as the motility of EEs on the microtubular network (Zerial, Severin et al. 1999) and the activation of signaling pathways from EEs (Miaczynska, Christoforidis et al. 2004).

An important effector of Rab5 is the phosphatidylinositol-3-OH kinase (PI(3)K) which generates phosphatidylinositol 3-phosphate (PI3P) on the EE membrane. The PI3P act as a binding site for tethering proteins such as the early endosomal antigen 1 (EEA1) essential for membrane docking, which in combination with soluble *N*-ethylmaleimide-sensitive factor attachment receptor (SNARE) proteins will lead to membrane fusion (Zerial, McBride et al. 1999). The EE may fuse with other EEs (homotypic fusion) as well as with incoming endocytosed vesicles (heterotypic fusion) (McBride and Zerial 2001). The fusion of EE is dependent on the presence of Rab5 on both the donor and acceptor membrane (Barbieri, Hoffenberg et al. 1998, Rubino, Miaczynska et al. 2000). The EE decides the fate of the internalized cargo, targeting it for recycling or degradation.

1.4.2 The recycling endosome (RE)

Despite most ligand/receptor complexes being transported to the late endosomes and subsequent to lysosomes for degradation, recycling of receptors to the plasma membrane often occurs (Hopkins 1983, Dunn, McGraw et al. 1989). The recycling endosome (RE) has a higher intralumenal pH compared to early endosomes and is defined as a distinct organelle that receives cargo that will be recycled back to the plasma membrane (Yamashiro, Tycko et al. 1984, Sipe and Murphy 1987). Consistent with the findings that the identity of the endosomes are maintained by occupation of distinct Rab GTPases on the endosomal membrane, the Rab GTPase composition on REs differ from that of EEs with Rab11 being a key RE marker (Lock and Stow 2005). The biogenesis of REs is not well-understood. Studies support the notion that they arise from EEs as a set of extended tubular structures (Maxfield and McGraw 2004, Klumperman and Raposo 2014).

Several proteins have been shown to play important roles in the transport of cargo from the EE to the RE, one of them being the Eps homology domain 4 (EHD4) protein (Sharma, Naslavsky et al. 2008). A second protein EHD3 is suggested to be a linker between EE and RE. EHD3 binds to both Rabenosyn-5 and Rab11 family-interacting protein 2 (RAB11FIP2) which are effectors of Rab5 and Rab11, respectively (Naslavsky, Rahajeng et al. 2006). Studies have shown a second Rab11 effector RAB11FIP5 to be important for trafficking of cargo from EE to RE. Upon loss of RAB11FIP5 transport of cargo from EE to RE was inhibited and enhanced recycling of the cargo was measured. This enhanced recycling was

assumed to be due to the cargo being trafficked through the faster recycling route from EE directly to the plasma membrane (Schonteich, Wilson et al. 2008).

Before cargo recycling to the plasma membrane the tubular structure of RE appears to break up into vesicles that further fuse with the cell surface. This process requires involvement of several proteins, including Arf6 and Rab11 (Grant and Donaldson 2009). A protein that has been shown to be important for the biogenesis of RE is the GTPase Rab22a. Previous studies show that in absence of Rab22a these tubular REs do not form and vesicles at the cell periphery are less abundant (Weigert, Yeung et al. 2004).

1.4.3 The late endosome (LE)

Maturation from EE to late endosome (LE) is characterized by the switch of the endosomal marker Rab5 to Rab7a, respectively (Poteryaev, Datta et al. 2010). There are two Rab7 proteins in mammals, Rab7a and Rab7b. Rab7a is primarily located on late endosomes and plays a key role in transport from EE to LE and further from LE to lysosomes (Bucci, Thomsen et al. 2000). In contrast, Rab7b regulates transport from LE to the TGN and is located to both compartments (Progida, Cogli et al. 2010, Progida, Nielsen et al. 2012).

LEs are enriched in phosphatidylinositol (3,5) biphosphate (PI(3,5)P2), and have a lower intralumenal pH compared to EEs (Griffiths 1989). The morphological characteristics of LEs is that they contain intraluminal vesicles (ILVs), a change that takes place upon maturation from early to late endosomes. When LEs acquire ILVs they are referred to as multivesicular bodies (MVBs). The formation of MVBs requires a set of protein complexes known as the Endosomal Sorting Complex Required for Transport (ESCRT) machinery. ESCRT-0 initiates the MVB pathway by binding PI3P and clustering ubiquitinated membrane proteins. ESCRT-0 then recruits ESCRT-I which too binds ubiquitinated cargo. Further, ESCRT-II interacts with ESCRT-I, PI3P and the ubiquitinated cargo, and ESCRT-III is assembled in a stepwise manner inducing the recruitment of cargo and inward budding of the vesicle (Schmidt and Teis 2012). Previous studies have shown that depletion of the ESCRT-II subunit vps22 significantly reduced degradation of EGFR and its ligand EGF (Malerød, Stuffers et al. 2007).

The subsequent fusion of late endosomes or MVBs with lysosomes is mediated by SNARE proteins (Antonin, Holroyd et al. 2000). The intralumenal pH of lysosomes is lower than that of LEs and MVBs and contain more than 60 acid hydrolases that degrade various substrates.

The lysosomal compartment is responsible for degradation of various molecules received via several routes including the endocytic pathway (De Duve and Wattiaux 1966, Ballabio and Bonifacino 2020).

1.4.4 Endosomal maturation

The endosomal maturation refers to the transition from EE to LE and is characterized by the exchange of Rab5 to Rab7a on the endosomal membrane. The detachment of Rab5 is initially dependent on Rab7a before it locates to domains on the endosomal membrane and detaches forming a new Rab5 endosome (Skjeldal, Haugen et al. 2021). This maturation is crucial for the correct sorting of endocytosed cargo such as signaling receptors.

The conversion from Rab5-GDP to Rab5-GTP requires guanine nucleotide exchange factors (GEFs). One known Rab5 GEF is Rabex5 which is recruited to the EE by the Rab5 effector Rabaptin-5. Rabaptin-5 binds Rab5-GTP on the EE membrane leading to Rabex-5 recruitment. This leads to additional activation of Rab5 by Rabex-5, which in turn leads to further recruitment of Rabaptin-5 in a positive feedback loop (Horiuchi, Lippé et al. 1997, Lippé, Miaczynska et al. 2001). A major player in the activation of Rab5 is Rab22a. The small GTPase Rab22a is found on several endosomal compartments but are particularly abundant on the EE and the RE. Rab22a recruits the Rab5 GEF Rabex-5 to the EE and upon knockdown of Rab22a in HeLa cells Rabex-5 was not targeted to the EE (Zhu, Liang et al. 2009). In addition, previous studies have shown a decrease in endocytosis of a fluid marker upon transfection with a negative mutant of Rab22a (Mesa, Salomón et al. 2001). As Rab22a is essential for the activation and subsequent maturation of the EE, it plays a cruical role in the endocytic pathway.

As the Rab5-positive EE matures it becomes increasingly acidic, initializes ILV formation and internalize cargo destined for degradation into the newly formed ILVs (Scott, Vacca et al. 2014). The exchange of Rab5 with Rab7a on the endosomal membrane is a carefully regulated process (Rink, Ghigo et al. 2005). This exchange is dependent on the two cytosolic factors Mon1/SAND-1 and Ccz1 (Figure 1.6). Mon1/SAND-1 and Ccz1 bind to Rab5-GTP and PI3P on the EE and promotes the dissociation of Rabex-5, thus interrupting the positive feedback loop of Rab5 activation. The Mon/SAND-1 and Ccz1 thereafter recruits Rab7a to the maturing membrane and activates it through its GEF activity towards Rab7a-GDP (Nordmann, Cabrera et al. 2010, Poteryaev, Datta et al. 2010)(Langemeyer, Borchers et al.

2020). Following this step, the Rab7a-positive LE will mature and induce lysosomal degradation (Vanlandingham and Ceresa 2009).

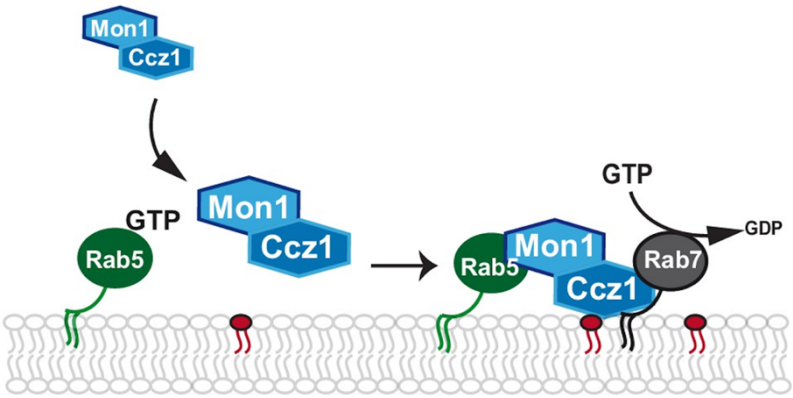

Figure 1.6: Exchange of Rab5 to Rab7a upon endosomal maturation. Mon1/SAND-1 and Ccz1 bind Rab5-GTP and PI3P (in red) and promote Rab7a recruitment. The mon1/SAND-1/Ccz1 complex act as a GEF for Rab7a, activating and stabilizing it on the endosomal membrane. Figure from (Langemeyer, Borchers et al. 2020)

1.5 Epidermal growth factor receptor (EGFR)

The epidermal growth factor receptor (EGFR; also known as ErbB1/Her1) was the first receptor tyrosine kinase (RTK) to be identified (Carpenter, King et al. 1978) and has been the pre-dominant experimental model when studying RTKs for the last four decades (Pinilla-Macua, Grassart et al. 2017). EGFR is a 170 kDa glycoprotein important for regulation of several cellular processes such as proliferation, migration and tissue maintenance (Grandal and Madshus 2008). Mutations and overexpression of EGFR has been identified in several cancers, such as cancer in breast, lung, and brain. Extracellular ligands bind to the receptor which transduce the signal by activating intracellular signaling pathways (Wieduwilt and Moasser 2008). Ligand binding induces dimerization and activation of the receptor following internalization. The internalized EGFR is either recycled back to the plasma membrane or progresses through the endosomal pathway for degradation in lysosomes (Tomas, Futter et al. 2013).

1.5.1 EGFR ligands

Currently, seven ligands are known to bind and activate EGFR; epidermal growth factor (EGF), transforming growth factor-alpha (TGF-α), heparin-binding EGF-like growth factor

(HBEGF), betacellulin, amphiregulin, epiregulin and epigen (Singh, Carpenter et al. 2016). All seven ligands are synthesized as transmembrane proteins containing an N-terminal extension called the EGF-module, which is the structure that binds to the EGFR. The protein may be biologically active while anchored, however the EGF-module is most often cleaved by a metalloprotease and the soluble growth factor is released (Schneider and Wolf 2009).

Studies have shown a difference in EGFR trafficking when activated by different ligands. One example of this is the change in EGFR trafficking when activated by TGF-α compared to EGF. EGFR activation by TGF-α show a higher receptor recycling rate and less receptor degradation due to the ligand more readily dissociating from the receptor in the acidic interior of the early endosomes. EGF inhabits a different pH-sensitivity and remains bound to the EGFR and is trafficked through maturing endosomes destined for degradation (Decker 1990, Ebner and Derynck 1991).

1.5.2 The ErbB family

After the identification of EGFR, three additional family members were discovered: ErbB2/Her2, ErbB3/Her3 and ErbB4/Her4. The ErbB family share a common structure composed of a ligand-binding extracellular domain, a single transmembrane domain, and a cytoplasmic domain with a conserved tyrosine kinase (TK) domain flanked by a regulatory region, the C-terminal tail (Figure 1.7)(Ferguson 2008).

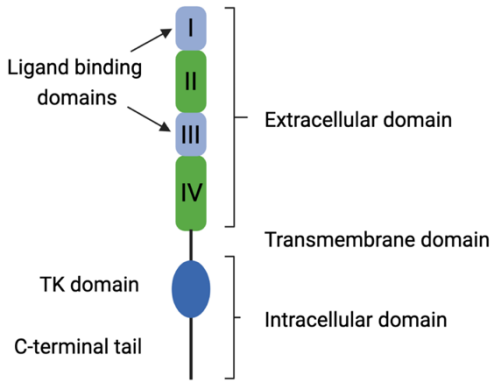

Figure 1.7: Schematic figure of the EGFR structure. The extracellular domain of EGFR is comprised of four domains where domains I and III are the ligand binding domains. Between the extracellular and intracellular domain is the transmembrane domain. The intracellular domain comprises a juxtamembrane region, the tyrosine kinase (TK) domain and the regulatory C-terminal tail.

Though the overall structures of the ErbBs are similar, the ligand binding domain of ErbB2 and the kinase domain of ErbB3 differ from the rest. Upon ligand binding, the ligand binding domain of EGFR, ErbB3 and ErbB4 undergoes a conformational change which exposes their dimerization arm enabling them to form homo- and heterodimers (Ferguson, Berger et al. 2003). In contrast, the dimerization arm of ErbB2 is always exposed and there is no known ligand for this ErbB family member. However, due to its conformation ErbB2 is the preferred dimerization partner of other ErbBs (Tzahar, Waterman et al. 1996). EGFR, ErbB2 and ErbB4 all contain a kinase domain on their cytoplasmic tail which can be activated. In contrast, ErbB3 has been shown to have an inactive kinase domain (Guy, Platko et al. 1994).

1.5.3 EGFR activation

Before ligand activation, the EGFR monomer adopts a tethered conformation on the plasma membrane due to interaction between domains II and IV of the EGFR (Figure 1.8). The dimerization arm is extended upon ligand binding which promotes dimerization. The EGFR can form homodimers or heterodimers with its ErbB family members (Garrett, McKern et al. 2002, Ogiso, Ishitani et al. 2002).

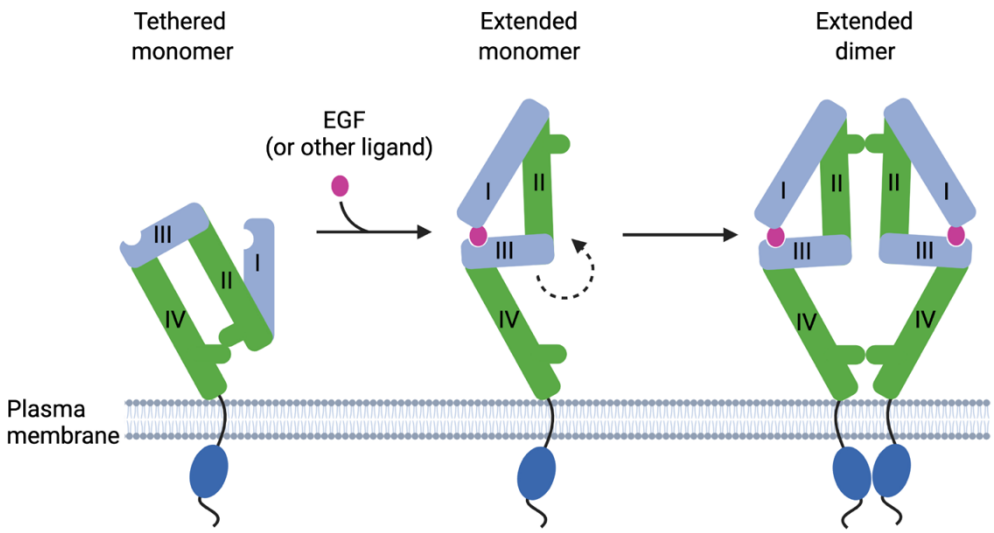

Figure 1.8: Schematic figure of conformational change and dimerization of EGFR upon ligand binding. Before binding of ligand, the EGFR monomer is present in a tethered state. Upon ligand binding to domains I and III, the dimerization arm (domain II) is extended which promotes dimerization of the EGFR. Figure inspired by (Nevo 2021).

Following dimerization, the TK domain is activated. Subsequent phosphorylation of C-terminal tyrosine residues act as docking sites for recruited adaptor proteins (Pawson and Schlessingert 1993) such as the E3 ubiquitin ligase Casitas B-lineage Lymphoma (Cbl). Upon

recruitment, Cbl is phosphorylated by the receptor leading to activation of the ubiquitin ligase. This in turn leads to ubiquitination of the EGFR which mediates receptor internalization and lysosomal sorting (Conte and Sigismund 2016). Cbl can bind directly to the EGFR at phosphorylated Y1045 (pY1045) or indirectly through recruitment by growth factor receptor binding protein 2 (Grb2) (Figure 1.9). In addition to Cbl, Grb2 is recruited to the receptor following receptor autophosphorylation. Grb2 is a small adaptor protein containing an SH2 domain flanked by two SH3 domains (Lowenstein, Daly et al. 1992, Rozakis-Adcock, Batzer et al. 1992) and couples EGFR to intracellular signaling (Jiang, Huang et al. 2003). Grb2 may directly bind to the EGFR at pY1068 and pY1086 or indirectly through the Src homology and collagen (Shc) adaptor protein. Shc binds directly to the receptor at pY1148 and pY1173 (Okutani, Okabayashi et al. 1994) (Batzer, Rotin et al. 1994).

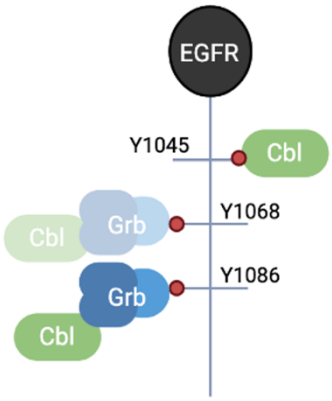

Figure 1.9: Schematic figure of Cbl and Grb2 binding sites on the EGFR. Cbl can bind directly at Y1045 or indirectly through Grb2 at Y1068/Y1086.

The receptor is rapidly internalized, mainly through clathrin-mediated endocytosis. The receptor/ligand complex may be recycled back to the plasma membrane from EEs, or transported through late endosomes to lysosomes for degradation (Sorkin and Goh 2009).

1.5.4 EGFR mutants

Previous studies in the lab have shown that EGFR trafficking is altered when three different mutants carrying mutations in the Cbl and/or Grb2 binding sites were introduced (Merete Storflor, Master thesis 2015)(Figure 1.10). The different EGFR mutants decelerated the progression of the receptor by constraining the detachment of Rab5 on EGFR positive endosomes. Moreover, the studies also showed a major reduction in degradation of the triple mutant EGFR (3Y-EGFR) compared to wild-type (wt) after EGF-Alexa 647 stimulation in PAE cells (data not shown). Altered speed of progression might be an indication of a change in Rab5 to Rab7a conversion, which initiated the investigation of Rab5/Rab7a binding dynamics on endosomes positive for the different receptors (Table 3.1).

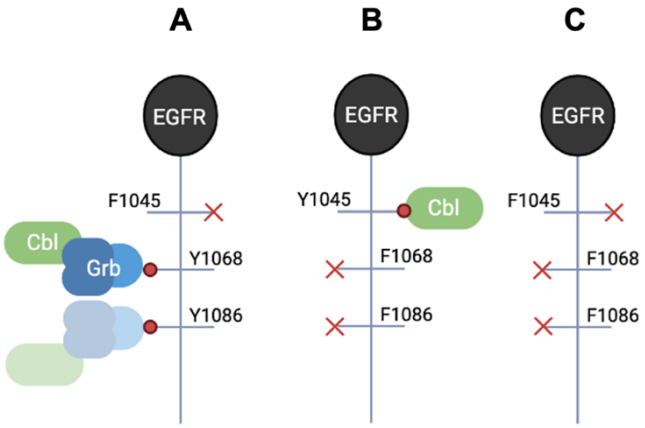

Figure 1.10: Three EGFRs with mutations in Cbl and/or Grb2 binding sites. A) EGFR with single mutation Y1045F on direct binding site for Cbl (1Y-EGFR). **B)** EGFR with mutations Y1068F and Y1086F in direct binding sites for Grb2 (2Y-EGFR). **C)** EGFR with three mutations Y1045F, Y1068F and Y1086F on direct binding sites for Cbl and Grb2 (3Y-EGFR).

2. Aim of study

Ligand activated EGFRs are autophosphorylated, ubiquitinated, internalized and sent to the endocytic pathway for recycling or degradation (Sorkin and Goh 2009). Mutations on the main binding sites for Cbl and Grb2 have been shown to alter the internalization, trafficking and degradation (Grøvdal, Stang et al. 2004, Fortian, Dionne et al. 2015).

Previous studies in the lab of Professor Oddmund Bakke have shown that the well-known Rab GTPases, Rab5 and Rab7a, change their maturation characteristics by altered detachment pattern in cells expressing these specific receptor mutants (Merete Storflor, Master thesis 2015).

The scientific aim of this study is to understand:

- The internalization trafficking and recycling of wt-EGFR and receptor mutants:
    - 1Y-EGFR/1Y-EGFR-GFP with mutated Y1045F phosphorylation site
    - 2Y-EGFR/2Y-EGFR-GFP with mutated Y1068F/Y1086F phosphorylation sites
    - 3Y-EGFR/3Y-EGFR-GFP with mutated Y1045F/Y1068F/Y1086F phosphorylation sites
- If the EGFR regulate its own fate according to its phosphorylation state.
- To understand if EGFR can regulate its progression through the pathway by controlling the endosomal maturation.
- To understand how the degree of phosphorylation might change the endosomal binding dynamics of Rab5 and Rab7a.
- To understand the role of Rab22a in the trafficking of EGFR and regulating the binding characteristic of Rab5
- To understand the temporal interplay between an activated EGFR receptor and the Rab GTPases, Rab5 and Rab7a.

3. Materials and methods

3.1 Cell lines

Cell lines used in these experiments were Porcine Aortic Endothelial (PAE) cells stably transfected with either wt-EGFR, 1Y-EGFR, 2Y-EGFR or 3Y-EGFR kept in Ham's F-12 medium, and HeLa Kyoto cells from a human cervical cancer cell line kept in Dulbecco's Modified Eagle Medium (DMEM). Both medium types were supplemented with 25 U/ml penicillin/streptomycin and 10% calf serum. The cells were incubated at 37°C with 5% CO_2 and with a humidity of 95%.

3.2 Cell treatment

3.2.1 Constructs

Table 3.1: DNA constructs.

Construct name	Referred to as	Producer/Reference
pEGFP-EGFR	wt-EGFR-GFP	Sorkin, A.
pEGFP-EGFR Y1045F	1Y-EGFR-GFP	Mutagenex Inc.
pEGFP-EGFR Y1068/1086F	2Y-EGFR-GFP	Mutagenex Inc.
pEGFP-EGFR 3YF	3Y-EGFR-GFP	Mutagenex Inc.
mCherry-Rab5	mCh-Rab5	(Haugen, Skjeldal et al. 2017)
mApple-Rab5a	mAp-Rab5	Addgene
EGFP-Rab7a	EGFP-Rab7a	Progida, C
mApple-Rab7a	mAp-Rab7a	Addgene

3.2.2 Transfection

Cells were plated on 35 mm glass-bottom Petri dishes (MatTek) over night and transfected when the cells were 70-90% confluent. The cells were transiently transfected with Lipofectamine 2000 (Invitrogen by Thermo Fisher Scientific) and 0.5 µg DNA per construct (Table 3.1). DNA and Lipofectamine 2000 were diluted in separate Eppendorf tubes with 100

µl Opti-MEM (Gibco Reduced Serum medium), incubated for 5 minutes at room temperature (RT) and mixed. The solution was incubated for 20 minutes at RT and added to the plated cells. Transfected cells were ready for imaging the following day.

3.2.3 Transformation

Competent Top10F cells were thawed on ice and plasmid was added (1 µg plasmid/200 µl cells). This was incubated on ice for 30 minutes, heat-shocked at 42°C for 2 minutes to induce plasmid uptake and incubated on ice for 2 minutes. Further, 1 ml 1xLB (Supplementary Table S1) was added to 200 µl cells and incubated at 37°C for 30 minutes. Cells were centrifuged at 4000 rpm for 4 minutes at RT and the majority of the supernatant was removed, leaving ~100 µl to resuspend the pellet. The cells were then plated on agar plates containing antibiotics, either ampicillin (100 µg/ml) or kanamycin (50 µg/ml) and incubated overnight at 37 °C. A colony was carefully picked and added to 100 ml LB medium containing antibiotics and incubated at 37°C with shaking overnight. The following day DNA was isolated using the Wizard Plus Midiprep kit protocol (Supplementary Table S2). DNA concentration was measured using the NanoDrop ND-1000 spectrometer (Saveen & Werner).

3.2.4 RNA interference

HeLa cells for knockdown experiments were seeded out in 35 mm glass-bottom petri dishes for imaging and a 6-well plate for Western Blot. Cells were washed 3x with 1xPBS and incubated in 1.5 ml DMEM supplemented with 10% FCS. Two transfection solutions were made: 1; 250 µl DMEM and 2.5 µl siRNA/Scrambled and 2; 250 µl DMEM and 6µl Lipofectamine RNAi MAX (Invitrogen by Thermo Fisher Scientific). The two solutions were mixed and incubated for 20 minutes at RT and added to the plated cells. Medium was changed the following day and two days after knockdown the cells were transfected with mCh-Rab5 and wt-EGFR-GFP/3Y-EGFR-GFP (3.2.2 Transfection). The following day, cells in the glass-bottom petri dishes were imaged and the cells in 6-well plates were lysed for Western Blot.

siRNA sequences used to knockdown Rab22a, purchased from Dharmacon™:

#1: GUAGGUAAAUCGAGUAUUG
#2: GGACUACGCCGACUCUAUU
#3: CCUUAGCACCAAUGUACUA
#4: CGCGAUAAACAUAAAUGAA

Dharmacom 5x siRNA buffer (GE Healthcare, Dharmacom) was used to dilute the siRNA-sequences. All siRNAs showed a knockdown of Rab22a (Results, Figure 4.19). Cells transfected with siRNA#2 was used for imaging due to the state of the cells after knockdown. Knockdown of Rab22a with siRNA#1, siRNA#3 and siRNA#4 led to morphological changes of the cells.

3.3 Protein Techniques

3.3.1 Cell Lysis

Lysis buffer (Supplementary Table S3) was prepared on ice in a prechilled Eppendorf tube. Cells were washed twice with cold 1xPBS on ice, before 50 µl lysis buffer was added to each 6 well-dish and placed on a tilting shaker for 15 minutes. The cells were scraped off, transferred to pre-chilled Eppendorf tubes and centrifuged at 13000 rpm at 4°C for 10 minutes. The supernatant was transferred to new Eppendorf tubes before the protein concentration was measured using Bradford assay. To measure protein concentration, 1µl lysate was mixed with 200 µl Bradford reagent (Bio-Rad Laboratories, Inc.) diluted in 800µl dH_2O and incubated at RT for 5 minutes. Protein concentration was measured by absorbance and lysate was stored at -80°C.

3.3.2 SDS-PAGE

Lysate was thawed on ice and Laemmli (Supplementary Table S4) was added to 50 µg protein sample before incubating for 5 minutes at 95°C to denature the proteins. For separation of proteins, sodium dodecyl-polyacrylamide gel electrophorese (SDS-PAGE) was performed. Samples were loaded to a 10 well 4-20% Gel (Bio-Rad Laboratories, Inc.) and Precision Plus Protein™ Keleidoscope™ (Bio-Rad Laboratories, Inc.) was used as a pre-stain standard. The gel was run at 10 minutes at 80V and ~1 hour at 100V in 1x Running Buffer (Supplementary Table S5).

3.3.3 Western Blotting

The proteins were transferred from the SDS-PAGE gel to an Immobile Polyvinylidene fluoride (PVDF) membrane (Bio-Rad Laboratories, Inc.). The membrane was activated in methanol for 30 seconds, washed with dH_2O for 2 minutes and then kept in Transfer buffer

for at least 5 minutes (Supplementary table S6). The transfer was run for 3 hours at 150mA at 4°C with stirring.

After the transfer the membrane was blocked for 1 hour in Milk/PBST (5% Bio-Rad nonfat dry milk in 1xPBS with 0.05% Tween) at RT to decrease non-specific binding. Primary antibody (pAb) (Supplementary Table S7) was mixed with Milk/PBST, added to the membrane and incubated overnight at 4°C. The following day the membrane was washed 3 x 5-10 minutes with PBST (1xPBS with 0.05% Tween) before incubating the membrane for 1 hour at RT with the secondary antibody(sAb) (Supplementary Table S7). The Amersham™ ECL™ Prime Western Blotting Detection Reagent (GE Healthcare) was used for the detection of proteins. Solution A and B was mixed 1:1, added to the membrane and incubated for 5 minutes in absence of light. Protein bands were detected with Amersham Hyperfilm™ ECL high performance chemiluminescence film (GE Healthcare) using the OPTIMAX X-Ray Film Processor (PROTEC GmbH & Co. KG). Quantification of protein bonds were performed with ImageJ Gel analyzer.

3.3.4 Membrane stripping

Membrane stripping was performed by incubating the membrane in Restore™ Western Blot Stripping Buffer (Thermo Scientific) for 3 minutes. After stripping the membrane was washed 3x10 minutes with PBST and re-immunoblotted as described in section 3.3.3.

3.4 Imaging and analysis

Live fluorescent imaging is a valuable tool to study temporal protein dynamics in cells. By transfecting fluorescently tagged proteins to the cell one can perform measurements such as localization, dynamic interactions and colocalization over time. This can provide us with further knowledge of the kinetics and mobility of intracellular organelles and their associated proteins.

3.4.1 Confocal microscopy

Live cell imaging can be performed by various techniques such as widefield microscopy and confocal microscopy. The technique used in this study is confocal microscopy. Confocal microscopy has improved the quality of fluorescence imaging from widefield fluorescence imaging by blocking out-of-focus light emitted from the illuminated sample. This is due to the

pinhole that allows fluorescence only from a specific focal point to pass through and reach the detector, which excludes emitted light from the outside the focal point. The result is higher resolution imaging with a better signal to noise ratio in a single focal plane (Minsky 1961).

3.4.2 Microscopes

Imaging was done on four different inverted microscopes; 1) Olympus SpinSR10 spinning disk confocal super resolution microscope, 2) Olympus iX81 FluoView 1000 inverted confocal microscope 3) Zeiss LSM880 Fast AiryScan microscope, and 4) Leica DMI6000B TIRF microscope (Table 3.2).

1) The Olympus SpinSR10 spinning disk confocal super resolution microscope is equipped with a Yokogawa CSU-W1 confocal spinning disk containing multiple pinholes allowing simultaneous point scans throughout the sample. The microscope is equipped with a sDMOS Hamamatsu Orca Fusion camera with a 2048x2048 chip. Imaging was carried out with a PlanApo 60x/1.42 immersion oil objective.

2) Imaging with Olympus iX81 FluoView 1000 confocal microscope was done by single point scanning across the sample. The PlanApo 60x/1.3 oil immersion objective was used for image acquisition.

3) The Zeiss LSM880 microscope is equipped with an AiryScan detector for super-resolution imaging, which leads to a 1.8x increase in resolution compared to diffraction limited microscopy. The LD LCI 63x/1.4 immersion oil objective was used for image acquisition.

4) Imaging with inverted Leica TIRF DMI6000B was carried out using HCX PlanApo 100x/1.47 immersion oil objective. The microscope is equipped with a cooled Andor iXon3 EMCCD camera with a 1024x1024 chip.

Table 3.2: Microscopes and objectives used for imaging.

Microscope	Magnification	Numerical Aperture	Immersion
Olympus SpinSR10 spinning disk confocal super resolution	60x	1.42	Oil
Olympus iX81 FluoView 1000 confocal microscope	60x	1.3	Oil
Zeiss LSM880 Fast AiryScan	63x	1.4	Oil
Leica TIRF DMI6000B	100x	1.47	Oil

Before imaging, the cells were washed twice with 1xPBS and imaged in Dulbecco's Modified Eagle Medium containing HEPES. All microscope incubation chambers are set to a stable temperature of 37°C.

3.4.3 Fluorescence Recovery After Photobleaching (FRAP)

Fluorescent recovery after photobleaching (FRAP) is a microscopy-based method used to study the mobility of fluorescently tagged molecules (Pincet, Adrien et al. 2016). A region of interest (ROI) containing fluorescent marked proteins is exposed to high laser intensity which causes the fluorophores emission to fade immediately. The bleached proteins detach and are exchanged by the diffusion and binding of nearby proteins with intact fluorophores which gives a fluorescent intensity recovery over time (Sprague and McNally 2005). From this data one can gain knowledge about the kinetics of a protein of interest, such as the proteins mobile fraction (MF), immobile fraction (IF) and halftime recovery ($T_{1/2}$). The MF represents the fraction of proteins that are exchanged in the ROI within our chosen time frame, whereas the IF represents the remaining protein fraction which is not exchanged. $T_{1/2}$ is the time at which the fluorescence recovery intensity reaches 50% of the recovered fluorescence (Figure 3.1).

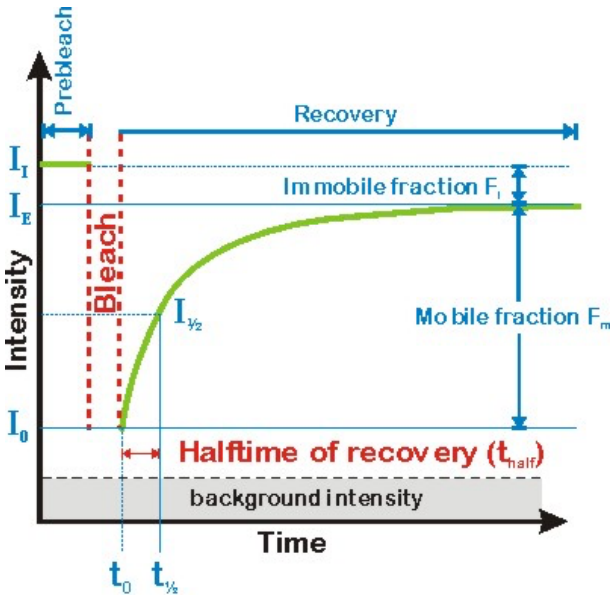

Figure 3.1: FRAP figure depicting mobile fraction (F_m), immobile fraction (F_I) and halftime recovery ($I_{1/2}$) (EMBL 2004).

The FRAP experiments were performed at the Olympus SpinSR10 spinning disk confocal super resolution microscope which is equipped with a cellFRAP module. This unique setup has two stand-alone lasers, with the wavelengths of 405nm and 561nm, specific for bleaching that allows us to acquire images and bleach simultaneously. Hence, the lag period between image acquisition and bleaching is minimized and the immediate recovery after bleaching can be measured. Bleaching is performed by using the click-and-bleach on the center of endosomes.

In this project endosomes positive for mCh-/mAp-Rab5 or mAp-/EGFP-Rab7a were bleached to an intensity of ~30%. Rab7a-EGFP and mCh-/mAp-Rab5/mAp-Rab7a were bleached with 405 and 561 nm lasers, respectively. The bleaching time was set to 50 milliseconds and the laser power to 100%. In FRAP experiments involving EGF, EGF-Alexa Fluor 647 (EGF-Alexa 647) (50 ng/ml) was added to the imaging dish ~10 minutes before imaging.

HeLa cells were transfected with mCh-Rab5/mAp-Rab7a and the various EGFP-tagged receptors, and PAE cells were transfected with mAp-Rab7a/EGFP-Rab7a. HeLa cells were imaged every 257 milliseconds for 500 frames and PAE cells were imaged every 786 milliseconds for 500 frames. When performing FRAP experiments to investigate the effect of EGF-positive EGFRs on mCh-Rab5/mAp-Rab5/mAp-Rab7a/EGFP-Rab7a recovery, a dual channel image of the specific Rab and EGF-Alexa 647 was acquired before bleaching. This was done to make sure the vesicles were EGF-positive when bleached.

FRAP analysis: The FRAP experiments were analyzed in ImageJ using a tracking algorithm developed by Felix Margadant, Xu Xiaochun and Hu Xian (Unpublished) which allows tracking of an endosome with drift correction (Figure 3.2). In cases where the tracker did not manage to follow the endosome, manually tracking was performed marking the center of the endosome for each frame of the movie. The tracker measures the intensity of the endosomal coat and results in an intensity profile of the endosome from frame 1-500.

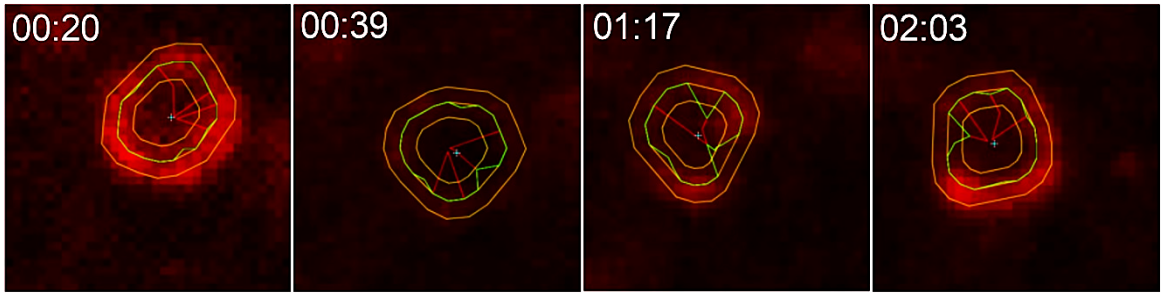

Figure 3.2: Endosome tracker developed by Felix Margadant, Xu Xiaochun and Hu Xian (Unpublished).

In addition, an intensity of the background was made to correct for sample bleaching by measuring the intensity of an area in cytosol. The fluorescence intensity of the background and the endosomes were plotted into Microsoft Excel and the data was normalized using the following function:

$$F(t) = \frac{I_{total(0)}}{I_{bleached(0)}} \; x \; \frac{I_{bleached(t)}}{I_{total(t)}}$$

Where $I_{total(0)}$ is the intensity of the cell before bleaching, $I_{bleach(0)}$ is the intensity of the bleached area before bleaching, $I_{total(t)}$ is the intensity of the cell over time and $I_{bleach(0)}$ is the intensity of the bleached area over time (Helenius, Kartenbeck et al. 2001).

GraphPad Prism 8 was used to calculate I_0, I_{max} and $T_{1/2}$ using a non-linear regression fit with the following function:

$$Y = \frac{I_0 + (I_{max} \cdot T_{half})}{1 + (\frac{X}{T_{half}})}$$

IF and MF were calculated as follows (Lippincott-Schwartz, Snapp et al. 2001):

$$IF = \frac{1 - I_{max}}{1 - I_0}$$

$$MF = 1 - IF$$

3.4.5 Total Internal Reflection Fluorescence (TIRF) microscopy

Total internal reflection microscopy (TIRFM) is a microscopy method that enables us to perform imaging of a very thin section of the cells. This is due to the critical angle of the laser and the difference in refractive index between the glass cover slip and the cell medium. As stated in Snell's Law, when light passes through a medium with a higher refractive index to a medium with a lower refractive index the velocity of the light changes and causes the light to bend. Total internal reflection fluorescent microscopy (TIRFM) exploits this by positioning the laser at a critical angle causing the light in the glass cover slip to be totally internally reflected. At this critical angle an electromagnetic wave called the evanescent wave is created which exponentially decays inward in the cell medium. Due to this exponential decay of the light only fluorophores closest to the glass cover slip are excited and we are able to perform imaging of a very thin section of cells, such as the plasma membrane (Fish 2009). In these experiments we performed imaging with a penetration depth of 110nm.

TIRF analysis: HeLa cells transiently transfected with wt-, 1Y-, 2Y- or 3Y-EGFR-GFP were imaged every 10 seconds for 200 frames. EGF-Alexa 647 (50ng/ml) was added after frame 2 (~ 20 seconds).

TIRF movies were analyzed using Imaris 9.5.1 (Bitplane, Oxford Instruments) to measure the recruitment of EGFRs to the plasma membrane as EGF-Alexa 647 was added during imaging. The Spots creation wizard was then used to detect the receptor clusters present on the plasma membrane, giving a spot count for each selected frame of the movie. The spots were then masked in a different color for better visualization.

4. Results

4.1 FRAP analysis: Effects of EGFR on Rab5/Rab7a endosomal binding kinetics

Previous studies in our lab have shown that receptor phosphorylation is essential for trafficking and degradation (Merete Storflor, Master thesis 2015). This particular study could show that mutations in specific tyrosine phosphorylation sites changed the ubiquitination and the trafficking of the EGFR. More specific, mutated phosphorylation sites changed the colocalization characteristics between EGF-Alexa647 with Rab5 and Rab7a, indicative of altered trafficking.

A pivotal point in endosomal trafficking is early endosomal maturation, which is characterized by the Rab5 to Rab7a conversion (Rink, Ghigo et al. 2005, Skjeldal, Haugen et al. 2021). This specific switch is regulating the transport of EGFR through the endocytic pathway by exchanging Rab5 and Rab7a on the endosomal membranes. The binding kinetics of Rab5 and Rab7a may be altered during endosomal maturation and our goal in this study is to identify any EGFR induced changes in the binding kinetics of the respective Rabs.
To study the Rab5 and Rab7a binding kinetics on endosomes, in the presence of EGF stimulated or unstimulated EGFR, we utilized two cellular systems:

1. HeLa cells transiently transfected with EGFP-wtEGFR, EGFP-1Y-EGFR, EGFP-2YEGFR or EGFP-3YEGFR (wt-EGFR-GFP, 1Y-EGFR-GFP, 2Y-EGFR-GFP, or 3Y-EGFR-GFP) co-transfected with fluorescently labeled Rab5 or Rab7a.
2. PAE cells, without endogenous EGFR, stably transfected with wt-EGFR, 1Y-EGFR, 2Y-EGFR or 3Y-EGFR and co-transfected with fluorescently labeled Rab5 or Rab7a.

4.1.1 Endosomal binding kinetics of Rab5 in presence of EGF-activated EGFRs in HeLa cells

HeLa cells were transiently transfected with mCh-Rab5 in four consecutive experiments with either; wt-,1Y-, 2Y- or 3Y-EGFR-GFP and stimulated with EGF-Alexa 647 before bleaching. EGF-Alexa 647 localized to the plasma membrane and was internalized into mCh-Rab5 positive vesicles. EGF-Alexa 647 was internalized for ~10 minutes until we could observe colocalization of mCh-Rab5, EGF-Alexa 647 and the different types of receptors, as depicted in the representative Figure 4.1. On these triple-positive vesicles we bleached mCh-Rab5 to analyze the binding dynamics in the presence of the wt-EGFR versus the different mutants.

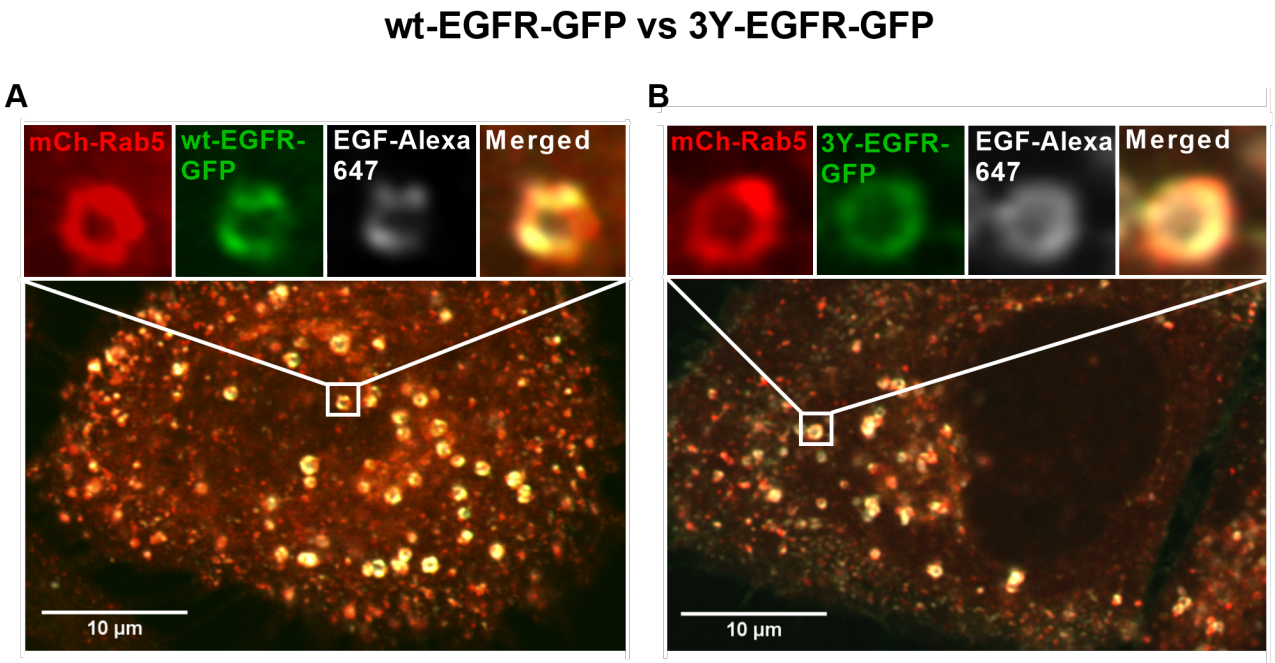

Figure 4.1: EGF-Alexa 647 uptake in HeLa cells. A) HeLa cells transfected with mCh-Rab5 and wt-EGFR-GFP, 10 min after stimulation with EGF-Alexa 647 (50ng/ml). **B)** HeLa cells transfected with mCh-Rab5 and 3Y-EGFR-GFP, 10 min after stimulation with EGF-Alexa 647 (50ng/ml).

Single endosomes positive for mCh-Rab5 were bleached and cells were imaged with a 257 milliseconds interval (Figure 4.2). An image of mCh-Rab5 and EGF-Alexa 647 was captured ~1 second before the experiment to confirm their colocalization before the FRAP experiment.

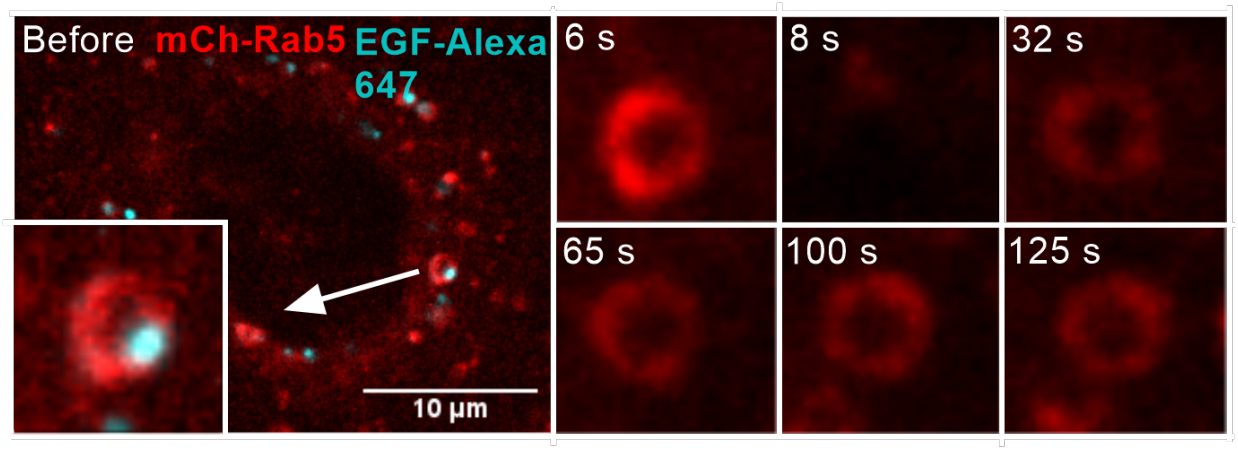

Figure 4.2: Bleaching on mCh-Rab5 positive endosomes in HeLa cells co-transfected with wt-EGFR-GFP and mCh-Rab5, ~10 min after stimulation with EGF-Alexa 647 (50ng/ml). Cells were imaged every 257ms for ~2min. Dual-channel imaging of mCherry-Rab5 and EGF-Alexa 647 was performed ~1 sec before bleaching.

The temporal fluorescence intensity recovery of mCh-Rab5 was measured using the endosome tracker plugin in ImageJ developed by Felix Margadant, Xu Xiaochun and Hu Xian (Materials and methods, FRAP analysis). This enabled us to follow the same endosome and measure the average intensity on the bleached mCh-Rab5 positive endosome over time. Bleaching experiments were complicated as the mCh-Rab5 positive endosomes are promiscuous, have many interaction partners, they move fast and change size over time.

Following bleached mCh-Rab5 positive endosomes we measured a $T_{1/2} = 27 \pm 1.4$ seconds when colocalized with EGF-Alexa 647 activated wt-EGFR-GFP as a control experiment, similar to previously published results (Anna Vik Rødseth, Master thesis 2021)(Skjeldal, Haugen et al. 2021). However, introducing the three different mutants, 1Y-, 2Y-, 3Y-EGFR-GFP, we could measure a significant increase in the mCh-Rab5 $T_{1/2}$ for all three mutants. We could show that mCh-Rab5 when colocalizing with different mutants were; 1Y-EGFR-GFP $T_{1/2} = 30 \pm 1.5$ seconds, 2Y-EGFR-GFP $T_{1/2} = 35 \pm 1.9$ seconds and 3Y-EGFR-GFP $T_{1/2} = 39 \pm 1.8$ seconds (Figure 4.3 B, Table 4.1). We could furthermore measure a major change in the IF and MF of mCh-Rab5 as the IF decreases and the MF increases. Calculating the endosomal fractions of mCh-Rab5 when colocalizing with; wt-EGFR-GFP to be IF = 16% and MF = 84%, with 1Y-EGFR-GFP to be IF = 7% and MF = 93%, with 2Y-EGFR-GFP similar to 3Y-EGFR-GFP, IF = 1% and MF = 99% (Figure 4.3 C, Table 4.1).

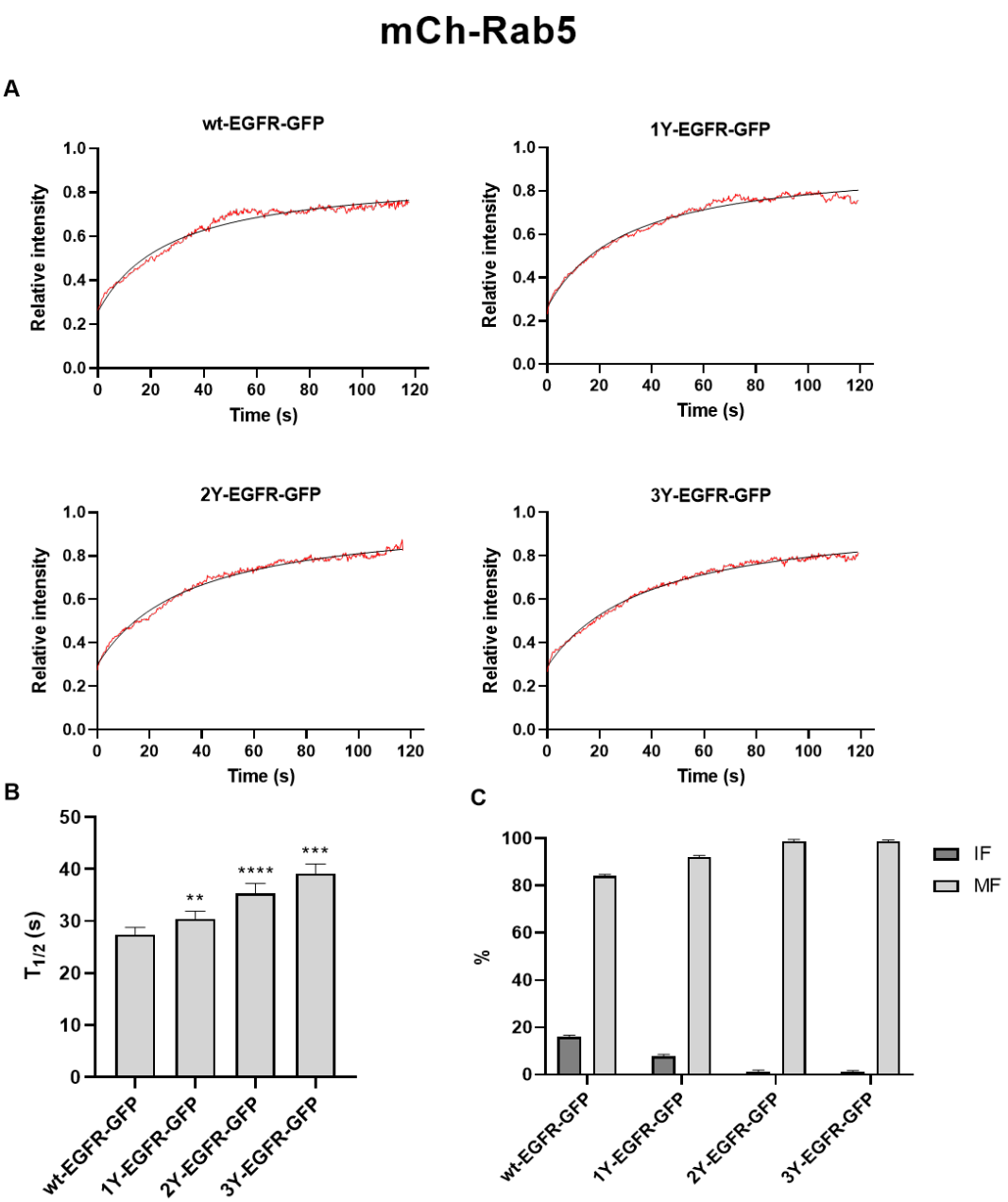

Figure 4.3: mCh-Rab5 fluorescence recovery, $T_{1/2}$, IF and MF when colocalized with the various EGFRs positive for EGF-Alexa 647 (50ng/ml). Cells were imaged every 257ms for ~2min.

A) mCh-Rab5 fluorescence recovery when co-transfected with: wt-EGFR-GFP n=11, 1Y-EGFR-GFP n=12, 2Y-EGFR-GFP n=10, 3Y-EGFR-GFP n=10. **B)** mCh-Rab5 $T_{1/2}$ when co-transfected with: wt-EGFR-GFP = 27.43 ± 1.4 s (SEM), 1Y-EGFR-GFP = 30.50 ± 1.5 s (SEM), 2Y-EGFR-GFP = 35.37 ± 1.9 s (SEM), 3Y-EGFR-GFP = 39.20 ± 1.8 s (SEM). Students t-test was performed testing mutant EGFRs against the wt-EGFR-GFP, all showing statistical significance. P-values: 1Y-EGFR-GFP p = 0.0024, 2Y-EGFR-GFP p < 0.0001, 3Y-EGFR-GFP p = 0.0004. **C)** IF and MF of mCh-Rab5 when co-transfected with: wt-EGFR-GFP IF/MF= 16%/ 84% ± 0.7% (SEM), 1Y-EGFR-GFP IF/MF = 7%/ 93% ± 0.7% (SEM), 2Y-EGFR-GFP IF/MF= 1%/ 99% ± 0.7% (SEM), 3Y-EGFR-GFP IF/MF=1%/ 99% ± 0.6% (SEM).

We could measure a ~12 second increase in mCh-Rab5 $T_{1/2}$ and a decrease in IF from 16 to 1% from wt- to 3Y-EGFR-GFP (Figure 4.3 C, Table 4.1). These results indicate an overall change in the endosomal binding kinetics of mCh-Rab5 introduced by the different mutated EGFR's. This may indicate that the EGFR can regulate the binding dynamics of Rab5 on early endosomes.

4.1.2 Endosomal binding kinetics of Rab7a in presence of EGF-activated EGFRs in HeLa cells

We have shown that the endosomal mCh-Rab5 binding kinetics when colocalized with the various EGF-activated mutant EGFRs was altered. We could measure an increased $T_{1/2}$ and MF, and a decrease in IF throughout the mutants (Figure 4.3, Table 4.1). As the transition from early to late endosome is regulated by the exchange of Rab5 to Rab7a (Skjeldal, Haugen et al. 2021), we further wanted to investigate the effect of the various EGF-positive mutant EGFRs on Rab7a binding kinetics. To measure this, HeLa cells were transiently transfected with mAp-Rab7a and the various EGFRs and stimulated with EGF-Alexa 647 for ~15 minutes prior to bleaching. The EGF-incubation time was prolonged to make sure that the EGF would reach the Rab7a-positive late endosomes, which is one step after the Rab5 to Rab7a transition.

In the control situation in HeLa cells, we bleached on endosomes positive for mAp-Rab7a, wt-EGFR-GFP and EGF-Alexa 647 and we measured a mAp-Rab7a $T_{1/2} = 22.6 \pm 2.5$ seconds, which is similar to previously published data (Merete Storflor, Master thesis 2015). When we compare the FRAP fingerprint ($T_{1/2}$, IF and MF) in the control situation of mCh-Rab5 and mAp-Rab7a, we could detect a different distribution of the fractions and the $T_{1/2}$ (Figure 4.3 C, Figure 4.4 C, Table 4.1). The mutated EGFRs altered the binding dynamics of mCh-Rab5 and we wanted to investigate if the same could occur with the late endocytic marker mAp-Rab7a.

After tracking of the bleached mAp-Rab7a positive endosome colocalized with EGF-activated wt-EGFR-GFP we measured a mAp-Rab7a $T_{1/2}$ of 22.6 ± 2.5 seconds, similar to previous published data (Distefano, Haugen et al. 2018). This experiment was performed as a control to measure if the various mutant EGFRs altered the mAp-Rab7a binding kinetics.

When mAp-Rab7a colocalized with the various EGF-activated mutants we could measure a major increase in $T_{1/2}$ for 1Y-EGFR-GFP and a significant increase in $T_{1/2}$ for 2Y- and 3Y-EGFR-GFP. When stimulated with EGF we measured mAp-Rab7a $T_{1/2}$ with 1Y-EGFR-GFP to be 30 ± 2.2 seconds, with 2Y-EGFR-GFP to be 43.5 ± 4.9 seconds and with 3Y-EGFR-GFP to be 50.1 ± 2.8 seconds (Figure 4.4 C, Table 4.1).

Further, we could calculate a different distribution of mAp-Rab7a IF and MF compared to mCh-Rab5, showing a higher IF for and lower MF of mAp-Rab7a compared to mCh-Rab5. The endosomal fractions of mAp-Rab7a when colocalizing with: wt-EGFR-GFP to be IF = 59% and MF = 41%, 1Y-EGFR-GFP to be IF = 54% and MF = 46%, 2Y-EGFR-GFP to be IF = 34% and MF = 66% and 3Y-EGFR-GFP to be IF =23% and MF = 77% (Figure 4.4 C, Table 4.1). mAp-Rab7a IF decreased and MF increased with all three EGF-activated mutants.

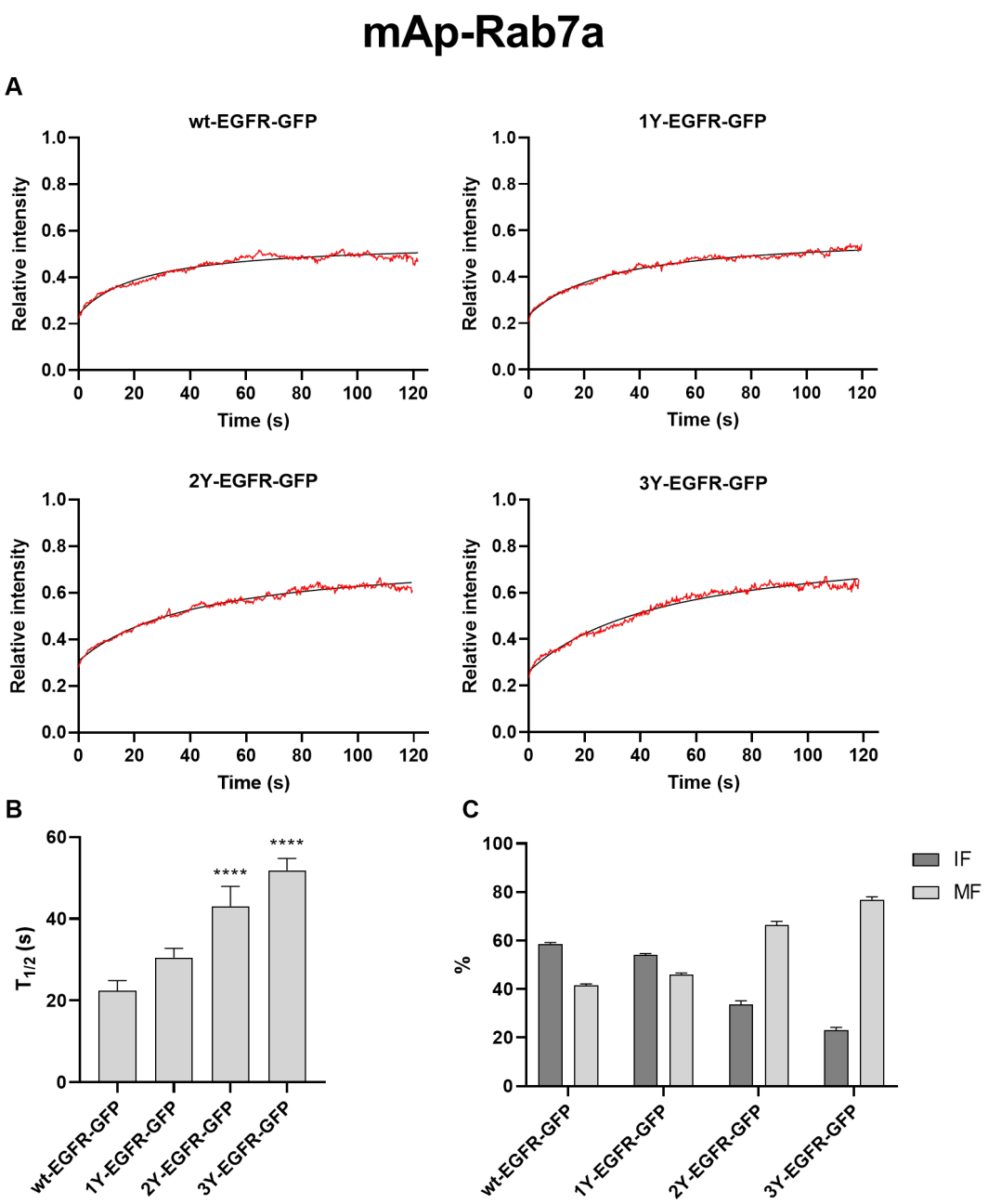

Figure 4.4: mAp-Rab7a fluorescence recovery, $T_{1/2}$, IF and MF when colocalized with the various EGFRs positive for EGF-Alexa 647 (50ng/ml). Cells were imaged every 257ms for ~2min.

A) mAp-Rab7a fluorescence recovery when HeLa cells were co-transfected with: wt-EGFR-GFP n= 10, 1Y-EGFR-GFP n= 10, 2Y-EGFR-GFP n= 10, 3Y-EGFR-GFP n= 11. **B)** mAp-Rab7a $T_{1/2}$ when co-transfected with: wt-EGFR-GFP= 22.6 ± 2.5 s (SEM), 1Y-EGFR-GFP= 30.0 ± 2.2 s (SEM), 2Y-EGFR-GFP= 43.5 ± 4.9 s (SEM), and 3Y-EGFR-GFP= 50.1 ± 2.8s (SEM). Students t-test was performed testing mutant EGFRs against the wt-EGFR-GFP, giving statistical significance for 2Y-, and 3Y-EGFR-GFP. P-values: 1Y-EGFR-GFP p= ns, 2Y-EGFR-GFP p= <0.0001, 3Y-EGFR-GFP p= <0.0001. **C)** IF and MF of mAp-Rab7a when co-transfected with: wt-EGFR-GFP IF/MF= 59%/41% ± 0.7% (SEM), 1Y-EGFR-GFP IF/MF= 54%/ 46% ± 0.6% (SEM), 2Y-EGFR-GFP IF/MF=34%/ 66% ± 1.6% (SEM), 3Y-EGFR-GFP IF/MF= 23%/ 77% ± 1.2% (SEM).

Our data show a ~27 seconds increase in mAp-Rab7a $T_{1/2}$ and a decrease in IF from 59% to 23% and MF from 41% to 77 % from wt- to 3Y-EGFR-GFP (Figure 4.4 B, Figure 4.4 C, Table 4.1). This specific reorganization of the IF and MF of mAp-Rab7a, specifically induced by the degree of phosphorylation, may change the endosomal maturation characteristics as previously observed with Rab5 (Skjeldal, Haugen et al. 2021). We could also measure a similar pattern of increasing $T_{1/2}$ and MF, and a decrease in IF for mCh-Rab5 (Figure 4.3, Figure 4.4, Table 4.1).

Combined, these results show that the EGFR regulates the binding kinetics of mCh-Rab5 and mAp-Rab7a in HeLa cells leading to a slower exchange of mCh-Rab5 and mAp-Rab7a on the early and late endosome, respectively, when EGFR phosphorylation is lacking.

4.1.3 Endosomal binding kinetics of Rab5 in PAE cells

Our analysis of bleached mCh-Rab5 and mAp-Rab7a positive endosomes in HeLa cells showed altered endosomal binding kinetics in presence of the EGF-activated EGFR mutants compared to wt-EGFR-GFP. We could measure an increase in the Rab5 and Rab7a $T_{1/2}$ when co-transfected with the various mutant EGFRs (Figure 4.3 B, Figure 4.4 B, Table 4.1), in addition major changes in IF and MF were calculated (Figure 4.3 C, Figure 4.4 C, Table 4.1).

In the previous experiments we studied the binding kinetics of Rab5 and Rab7a when co-transfected with the various EGFRs activated by EGF in HeLa cells. HeLa cells express endogenous EGFR, and we further wanted to investigate the binding kinetics of Rab5 in PAE cells without endogenous EGFR. PAE cells stably transfected with wt-, 1Y-, 2Y-, or 3Y-EGFR were then co-transfected with mAp-Rab5 and mAp-Rab5 positive endosomes were bleached in the absence of EGF (unstimulated).

When performing FRAP experiments in PAE cells we found the intensity recovery not to reach a proper plateau within 2 minutes for some of the Rab/EGFR combinations. For this reason, we expanded the timeframe of the experiment from 2 to 5 minutes with an increased time interval of 786 milliseconds between each image.

The stably transfected PAE cells had a different morphology compared to HeLa cells, being more elongated and narrower in appearance. Several mAp-Rab5 positive endosomes were present in cytosol though fewer than what was observed in HeLa cells (data not shown).

In unstimulated PAE cells expressing mAp-Rab5 positive endosomes we could measure a mAp-Rab5 $T_{1/2}$ of 19.4 ± 1.8 seconds with wt-EGFR. The FRAP fingerprint of mAp-Rab5 colocalized with wt-EGFR was set as a control experiment before analyzing mAp-Rab5 kinetics with the different EGFR mutants. When introducing the mutant receptors we could show an increase in mAp-Rab5 $T_{1/2}$ with 1Y-EGFR and a significant increase with 2Y- and 3Y-EGFR. In unstimulated PAE cells we measured a mAp-Rab5 $T_{1/2}$ to be 23.7 ± 1.9 seconds with 1Y-EGFR, 27.3 ± 1.0 seconds with 2Y-EGFR, and 33.2 ± 1.6 seconds with 3Y-EGFR (Figure 4.5 B, Table 4.1). Further, we measured a change in IF and MF for the various EGFRs. We could show the endosomal fractions of mAp-Rab5 when colocalizing with; wt-EGFR to be IF = 22% and MF = 78%, 1Y-EGFR to be IF =16% and MF = 84%, with 2Y-EGFR to be IF =18% and MF = 81% and with 3Y-EGFR to be IF = 18% and MF = 82% (Figure 4.5 C, Table 4.1).

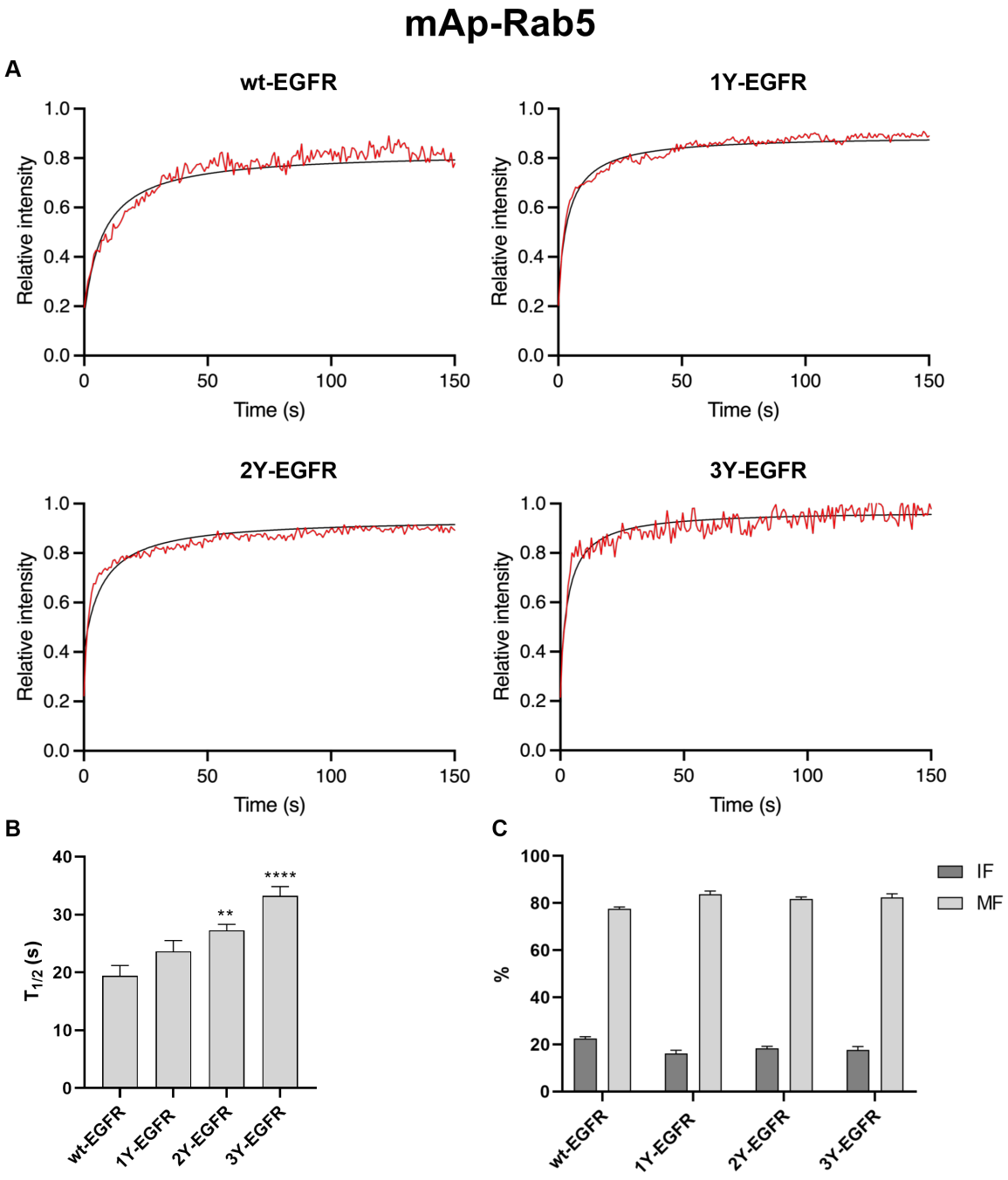

Figure 4.5: mAp-Rab5 fluorescence recovery, $T_{1/2}$, IF and MF in PAE cells stably transfected with wt-, 1Y-, 2Y- and 3Y-EGFR in absence of EGF. Cells were imaged every 786ms for 5min.

A) mAp-Rab5 fluorescence recovery in PAE cells stably transfected with: wt-EGFR n= 16, 1Y-EGFR n= 20, 2Y-EGFR n= 16, 3Y-EGFR n= 16. **B)** mAp-Rab5 $T_{1/2}$ in PAE cells stably transfected with: wt-EGFR= 19.4 ± 1.8 s (SEM), 1Y-EGFR= 23.7 ± 1.9 s (SEM), 2Y-EGFR= 27.3 ± 1.0 s (SEM), 3Y-EGFR = 33.2 ± 1.6 s (SEM). Students t-test was performed testing mutant EGFRs against the wt-EGFR, giving statistical significance 2Y- and 3Y-EGFR. P-values: 2Y-EGFR p= 0.0032, 3Y-EGFR p= <0.0001. **C)** IF and MF of mAp-Rab5 in PAE cells stably transfected with: wt-EGFR IF/MF= 22%/ 78% ± 0.8% (SEM), 1Y-EGFR IF/MF= 16%/ 84% ± 1.3% (SEM), 2Y-EGFR IF/MF=18%/ 82% ± 0.9% (SEM), 3Y-EGFR IF/MF= 18%/ 82% ±1.6% (SEM).

Our analysis showed a steady increase in mAp-Rab5 $T_{1/2}$ in unstimulated PAE cells stably transfected wt-, 1Y-, 2Y-, and 3Y-EGFR (Figure 4.5 B, Table 4.1). We measured a ~13 seconds difference of mAp-Rab5 $T_{1/2}$ in wt-EGFR compared to 3Y-EGFR PAE cells. The highest IF was measured in wt-EGFR cells with a value of 22% and the lowest IF was measured in 1Y-EGFR with a value of 16% (Figure 4.5 C, Table 4.1), however no shift in the balance of IF and MF was detected.
We found the same pattern of increasing Rab5 $T_{1/2}$ throughout the receptor mutants in both unstimulated PAE cells and EGF-stimulated HeLa cells. Interestingly, we found that Rab5 $T_{1/2}$ when in presence of the various EGF-activated receptors in HeLa cells was faster than in unstimulated PAE cells stably transfected with the various EGFRs.

4.1.4 Endosomal binding kinetics of Rab5 with EGF-activated EGFRs in PAE cells

From our measurements of mAp-Rab5 binding kinetics in PAE cells stably transfected with wt-, 1Y-, 2Y-, and 3Y-EGFR, we found that mAp-Rab5 $T_{1/2}$ differed between the mutants in absence of EGF (Figure 4.5 B, Table 4.1). Therefore, we wanted to investigate the effect of EGF-stimulated receptors on mAp-Rab5 binding kinetics in the same PAE cell system. PAE cells stably transfected with wt-, 1Y-, 2Y-, or 3Y-EGFR were co-transfected with mAp-Rab5 and stimulated with EGF-Alexa 647 ~10 minutes prior to bleaching. mAp-Rab5 positive endosomes colocalized with EGF-Alexa 647 were bleached and cells were imaged every 786 milliseconds for 5 minutes.

By tracking the bleached mAp-Rab5 positive endosomes colocalizing with EGF-Alexa 647 we could measure a mAp-Rab5 $T_{1/2}$ of 16.3 ± 2.7 seconds in wt-EGFR PAE cells, which was established as a control experiment before introducing the EGFR mutants. However, when investigating the mutant EGFRs we could measure a significant increase in mAp-Rab5 $T_{1/2}$ for all three mutants. When mAp-Rab5 colocalized with the three EGF-activated mutants we could measure a mAp-Rab5 in: 1Y-EGFR $T_{1/2}$ = 21.6 ± 0.9 seconds, 2Y-EGFR $T_{1/2}$ = 24.8 ± 2.1 seconds, 3Y-EGFR $T_{1/2}$ = 31.9 ± 2.7 (Figure 4.6 B, Table 4.1). Furthermore, when calculating the fractions, we could measure a change in IF and MF. We calculated the endosomal fractions of mAp-Rab5 when colocalizing with; wt-EGFR to be IF = 20% and MF = 80%, 1Y-EGFR to be IF = 12% and MF = 88%, 2Y-EGFR to be IF = 21% and MF = 79% and 3Y-EGFR to be IF = 23% and MF = 77% (Figure 4.6 C, Table 4.1).

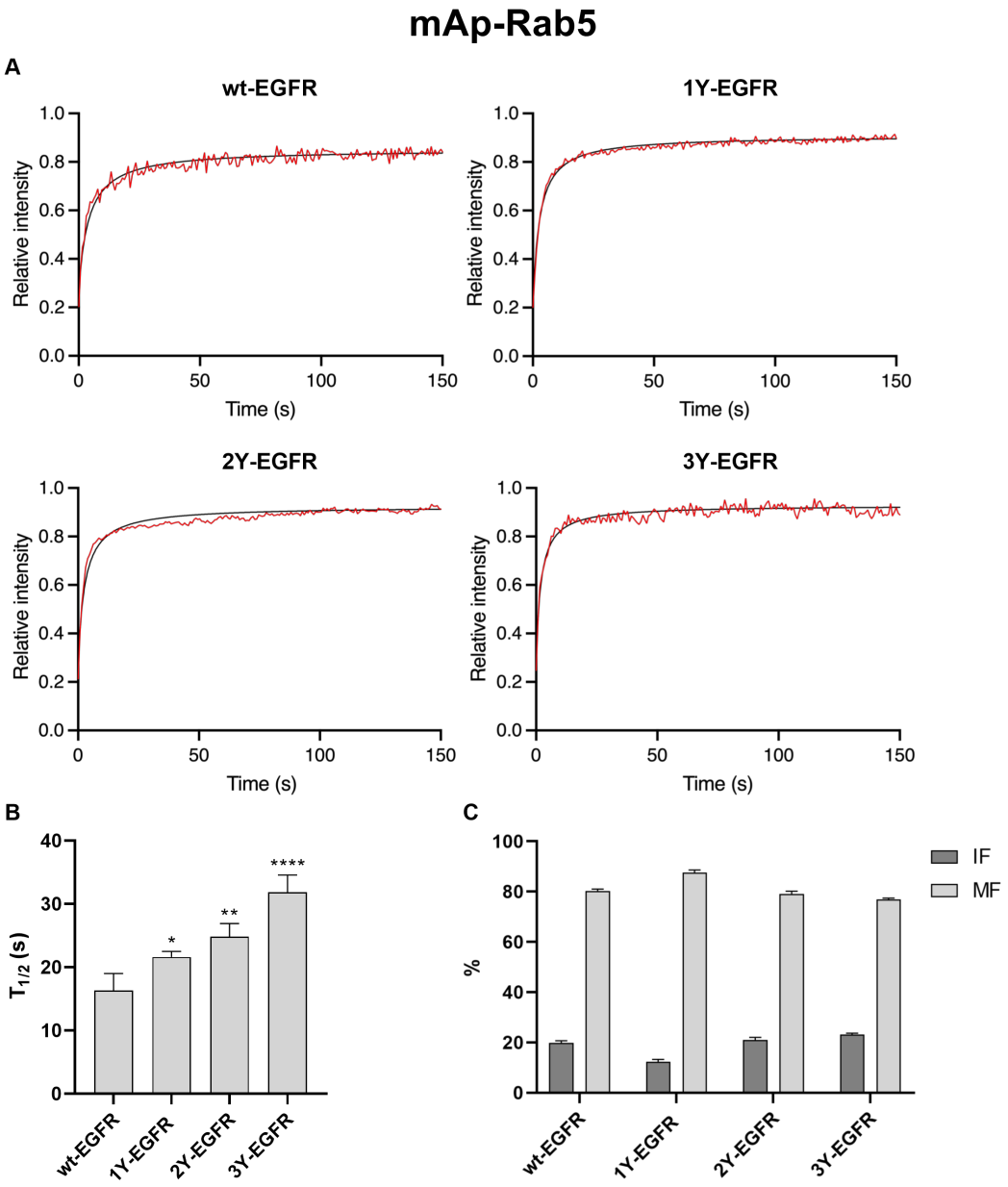

Figure 4.6: mAp-Rab5 fluorescence recovery, $T_{1/2}$, IF and MF in PAE cells stably transfected with wt-, 1Y-, 2Y- and 3Y-EGFR in presence of EGF. Cells were imaged every 786ms for 5min.

A) mAp-Rab5 fluorescence recovery in EGF-induced PAE cells stably transfected with: wt-EGFR n= 16, 1Y-EGFR n= 20, 2Y-EGFR n= 16, 3Y-EGFR n= 16. **B)** mAp-Rab5 $T_{1/2}$ when colocalized with EGF-Alexa 647 in: wt-EGFR = 16.3 ± 2.7 s (SEM), 1Y-EGFR = 21.6 ± 0.9 s (SEM), 2Y-EGFR= 24.8 ± 2.1 s (SEM), and 3Y-EGFR= 31.9 ± 2.7 s (SEM). Students t-test was performed testing mutant EGFRs against the wt-EGFR, giving statistical significance for all mutants. P-values: 1Y-EGFR p= 0.0365, 2Y-EGFR p= 0.0045, 3Y-EGFR p<0.0001. **C)** IF and MF of mAp-Rab5 when colocalized with EGF-Alexa 647 in: wt-EGFR IF/MF= 20%/ 80% ± 0.9% (SEM), 1Y-EGFR IF/MF= 12%/ 88%, 2Y-EGFR IF/MF=21%/ 79% ± 1.0% (SEM), 3Y-EGFR IF/MF= 23%/ 77% ± 0.6% (SEM).

Our results show a significant increase in mAp-Rab5 $T_{1/2}$ throughout the mutants in EGF-stimulated PAE cells (Figure 4.6 B, Table 4.1). We could show a faster mAp-Rab5 $T_{1/2}$ in EGF-stimulated PAE cells compared to unstimulated PAE cells (Figure 4.5 B, Figure 4.6 B). The highest IF of 23% was measured in 3Y-EGFR while the lowest IF of 12% was measured in 1Y-EGFR PAE cells, however we did not detect a shift in the balance of MF and IF (Figure 4.6 C, Table 4.1).

4.1.5 Endosomal binding kinetics of Rab7a in PAE cells

From our investigations we could show altered binding kinetics of mAp-Rab5 in PAE cells stably transfected with the various EGFRs, both with and without stimulation with EGF-Alexa 647. In both cases, we measured a major increase in mAp-Rab5 $T_{1/2}$ (Figure 4.5 B, Figure 4.6 B, Table 4.1) as well as differences in IF and MF (Figure 4.5 C, Figure 4.6 C, Table 4.1). Another interesting observation was that the mAp-Rab5 $T_{1/2}$ in stably transfected PAE cells increased when stimulated with EGF compared to unstimulated PAE cells.
Our analysis of endosomal binding kinetics in EGF-stimulated HeLa cells showed a major increase in mAp-Rab7a $T_{1/2}$ when colocalized with the mutant EGFRs (Figure 4.4 B, Table 4.1). Further, it showed a shift in the balance of mAp-Rab7a IF and MF measuring a decrease in IF throughout the mutant EGFRs (Figure 4.4 C, Table 4.1)

Having established the effect of the various receptors on mAp-Rab7a endosomal binding kinetics in stimulated HeLa cells, we further wanted to investigate the binding kinetics of EGFP-Rab7a in unstimulated PAE cells stably transfected with the various EGFRs. To study this, PAE cells stably transfected with wt-, 1Y-, 2Y-, or 3Y-EGFR were co-transfected with EGFP-Rab7a. EGFP-Rab7a positive endosomes were bleached and cells were imaged every 786 milliseconds for ~5 minutes.

In the control situation, the $T_{1/2}$ for EGFP-Rab7a in unstimulated wt-EGFR PAE cells was measured to 24.4 ± 3.0 seconds. When measuring the endosomes with mutant EGFRs, however, we could show an increase in $T_{1/2}$ with 1Y-EGFR and a significant increase with 2Y-, and 3Y-EGFR. In unstimulated PAE cells we measured the EGFP-Rab7a $T_{1/2}$ to be 28.6 ± 2.9 seconds with 1Y-EGFR and 30.6 ± 2.7 seconds with 2Y-EGFR. Surprisingly, when EGFP-Rab7a colocalized with 3Y-EGFR we could measure the EGFP-Rab7a $T_{1/2}$ of 210,9 ± 25.9 seconds (Figure 4.7 B, Table 4.1).

In addition, we could measure a major change in IF and MF of EGFP-Rab7a. Calculating the endosomal fraction of EGFP-Rab7a with: wt-EGFR to be IF = 5% and MF = 95%, 1Y-EGFR to be IF = 14% and MF to be 86%, 2Y-EGFR to be IF = 14% and MF = 86%, 3Y-EGFR to be IF = 5% and MF = 95% (Figure 4.7 C, Table 4.1).

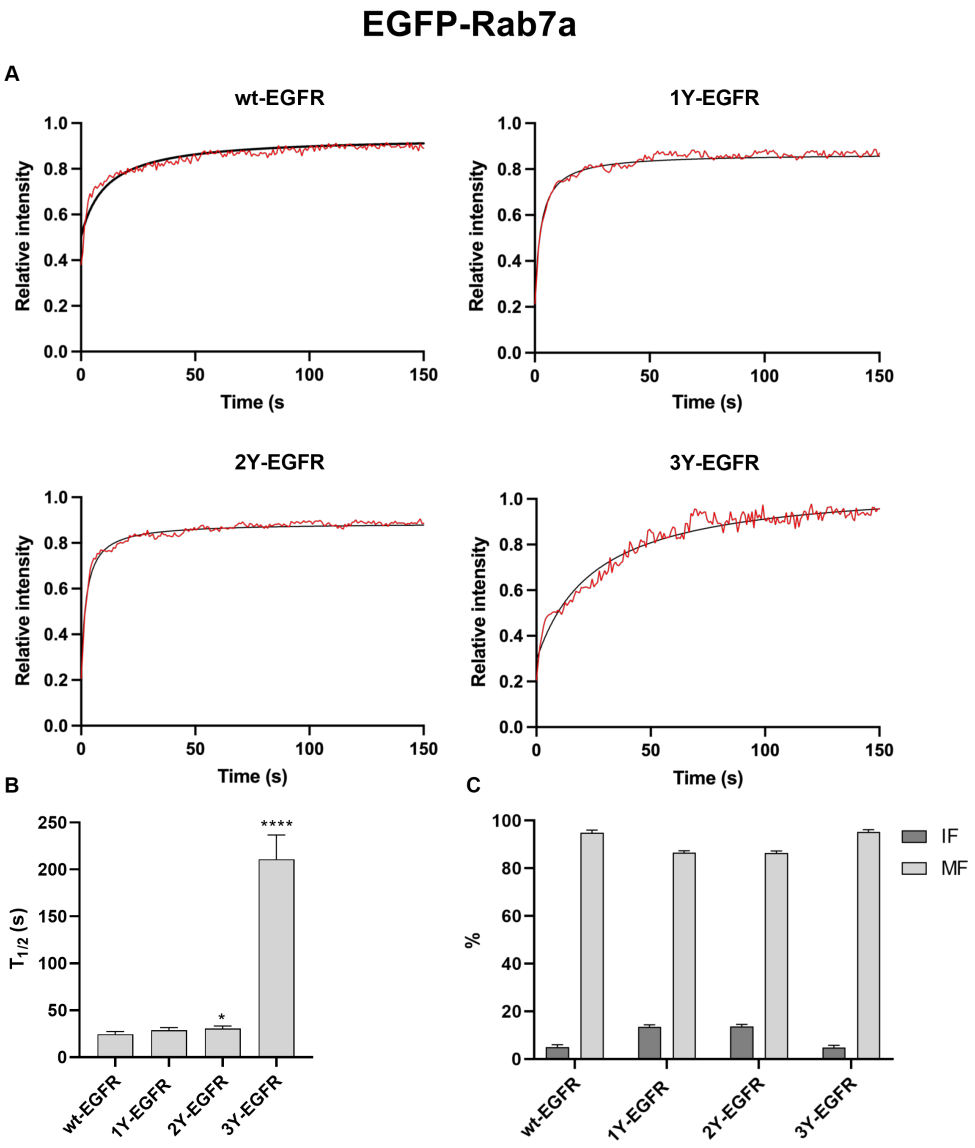

Figure 4.7: EGFP-Rab7a fluorescence recovery, $T_{1/2}$, IF and MF in PAE cells stably transfected with wt-, 1Y-, 2Y- and 3Y-EGFR in absence of EGF. Cells were imaged every 786ms for 5min.

A) EGFP-Rab7a fluorescence recovery in PAE cells stably transfected with: wt-EGFR n= 16, 1Y-EGFR n= 21, 2Y-EGFR n= 16, 3Y-EGFR n= 18. **B)** EGFP-Rab7a $T_{1/2}$ in PAE cells stably transfected with: wt-EGFR= 24.4 ± 3.0 s (SEM), 1Y-EGFR= 28.6 ± 2.9s (SEM), 2Y-EGFR= 30.6 ± 2.7s (SEM), 3Y-EGFR = 210,9 ± 25.9s (SEM). Students t-test was performed testing mutant EGFRs against the wt-EGFR, giving statistical significance for 2Y- and 3Y-EGFR. P-values: 1Y-EGFR p= ns, 2Y-EGFR p= 0.0401, 3Y-EGFR p<0.0001. **C)** IF and MF of EGFP-Rab7a in PAE cells stably transfected with: wt-EGFR IF/MF= 5%/ 95% ± 1.0% (SEM), 1Y-EGFR IF/MF= 14%/ 86% ± 0.9% (SEM), 2Y-EGFR IF/MF=14%/ 86% ± 0.9% (SEM), 3Y-EGFR IF/MF= 5%/ 95% ±1.0 % (SEM).

These results showed an increase of ~2-4 seconds in the EGFP-Rab7a $T_{1/2}$ from wt-EGFR to 2Y-EGFR in absence of EGF (Figure 4.7 B, Table 4.1). The $T_{1/2}$ of EGFP-Rab7a in 3Y-EGFR cells was calculated to ~211 seconds, which is an increase of 187 seconds compared to the wt-EGFR. In addition, major differences in IF and MF of EGFP-Rab7a were measured where both wt-EGFR and 3Y-EGFR showed an IF of 5% whereas 1Y- and 2Y-EGFR showed an IF of 14% (Figure 4.7 C, Table 4.1). This indicates that the EGFR regulate the endosomal binding kinetics of EGFP-Rab7a in unstimulated cells.

4.1.6 Endosomal binding kinetics of Rab7a in presence of EGF-activated EGFRs in PAE cells

Our analysis of EGFP-Rab7a binding kinetics in PAE cells stably transfected with wt-, 1Y-, 2Y- and 3Y-EGFR showed a large increase in $T_{1/2}$ for all mutant EGFRs (Figure 4.7 B, Table 4.1). In addition, we calculated major changes in the IF and MF of EGFP-Rab7a (Figure 4.7 C, Table 4.1). Having established this, we further wanted to investigate the effect of EGF-Alexa 647 on EGFP-Rab7a binding kinetics in the various stably transfected PAE cells. To study this, the stably transfected PAE cells were co-transfected with EGFP-Rab7a and stimulated with EGF-Alexa 647 ~15 minutes prior to bleaching. EGFP-Rab7a positive endosome colocalizing with EGF-Alexa 647 were bleached and cells were imaged every 786 milliseconds for 5 minutes.

Tracing the bleached endosomes, we could measure the EGFP-Rab7a $T_{1/2}$ of 15.6 ± 4.1 seconds when colocalized with EGF-stimulated wt-EGFR for this control experiment. However, EGFP-Rab7a with the EGF-activated mutated EGFRs showed a significant increase in $T_{1/2}$ throughout the mutants. When colocalized with the EGF-activated mutated EGFRs we could measure EGFP-Rab7a: 1Y-EGFR $T_{1/2}$ = 24.4 ± 3.2 seconds, 2Y-EGFR $T_{1/2}$ = 28.5 ± 3.2 seconds. Interestingly, we found EGFP-Rab7a $T_{1/2}$ when colocalized with EGF-activated 3Y-EGFR to 543.6 ± 186.6 seconds (Figure 4.8 B, Table 4.1). We could furthermore measure a change in the IF and MF of EGFP-Rab7a with the various EGF-activated EGFRs. Calculating the endosomal fractions of EGFP-Rab7a in EGF-stimulated PAE cells when colocalizing with: wt-EGFR to be IF = 7% and MF = 93%, with 1Y-EGFR to be IF = 13% and MF = 87%, with 2Y-EGFR to be IF = 13% and MF = 87%, with 3Y-EGFR to be IF = 12% and MF = 88% (Figure 4.8 C, Table 4.1).

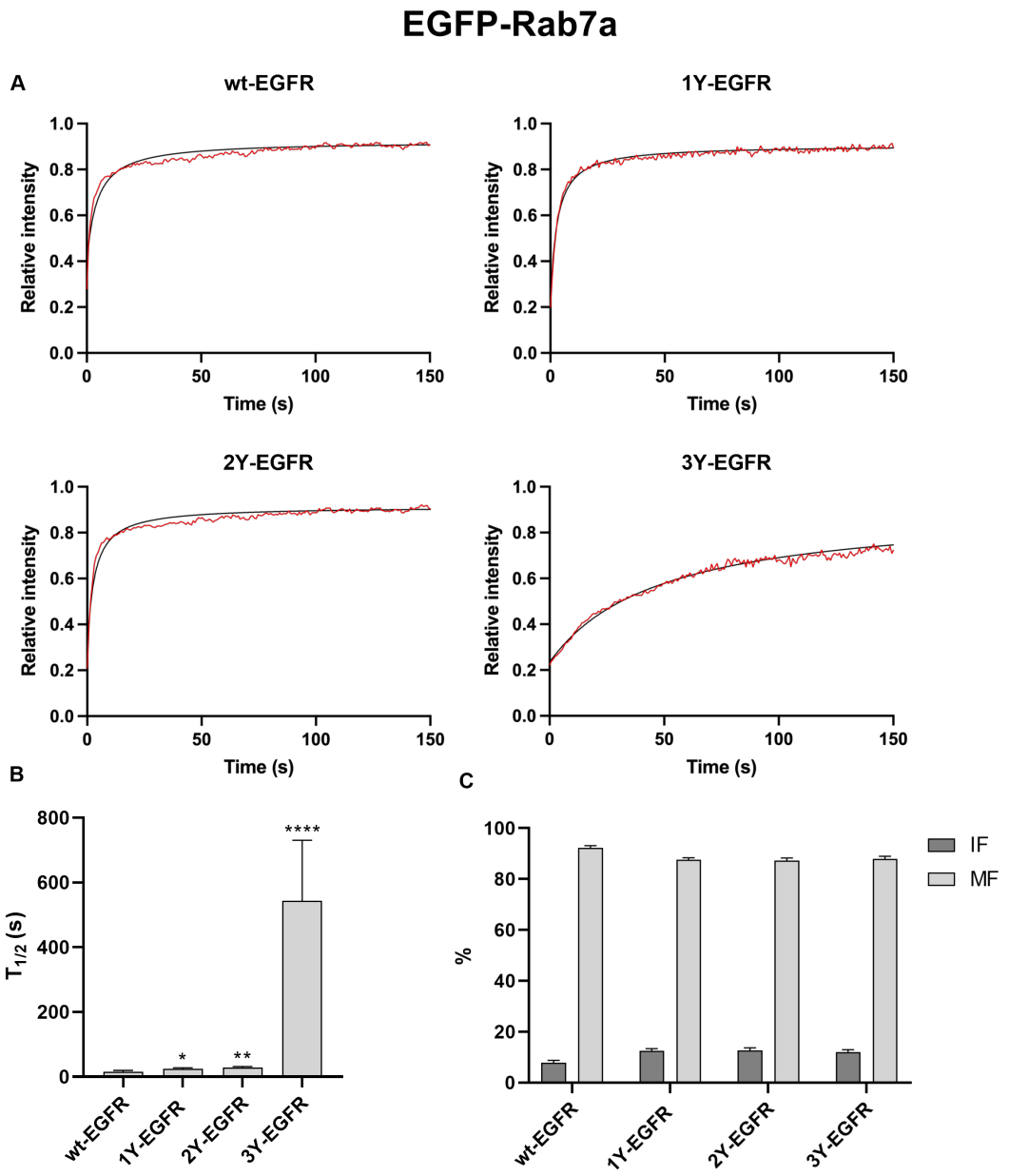

Figure 4.8: EGFP-Rab7a fluorescence recovery, $T_{1/2}$, IF and MF in PAE cells stably transfected with wt-, 1Y-, 2Y-, and 3Y-EGFR in presence of EGF. Cells were imaged every 786ms for 5min.

A) EGFP-Rab7a fluorescence recovery in EGF-induced PAE cells stably transfected with: wt-EGFR n= 17, 1Y-EGFR n= 18, 2Y-EGFR n= 17, 3Y-EGFR n= 16. **B)** EGFP-Rab7a $T_{1/2}$ when colocalized with EGF-Alexa 647 in: wt-EGFR= 15.6 ± 4.1 s (SEM), 1Y-EGFR= 24.4 ± 3.2 s (SEM), 2Y-EGFR= 28.5 ± 3.2 s (SEM), and 3Y-EGFR= 543.6 ± 186.6 s (SEM). Students t-test was performed testing mutant EGFRs against the wt-EGFR giving statistical significance for all mutants. P-values: 1Y-EGFR p= 0.0213, 2Y-EGFR p= 0.0025, 3Y-EGFR p<0.0001. **C)** IF and MF of EGFP-Rab7a when colocalized with EGF-Alexa 647 in: wt-EGFR IF/MF= 7%/ 93% ± 0.9% (SEM), 1Y-EGFR IF/MF= 13%/ 87% ± 0.9% (SEM), 2Y-EGFR IF/MF=13%/ 87% ± 1.0% (SEM), 3Y-EGFR IF/MF= 12%/ 88% ± 0.9% (SEM).

We could show similar characteristics of EGFP-Rab7a $T_{1/2}$ in EGF-stimulated PAE cells compared to unstimulated PAE cells. However, we measured a faster EGFP-Rab7a $T_{1/2}$ in stimulated PAE cells (Figure 4.7 B, Figure 4.8 B, Table 4.1). In 3Y-EGFR co-transfected with EGFP-Rab7a, $T_{1/2}$ for EGFP-Rab7a was measured to ~544 seconds when colocalized with EGF-Alexa 647, showing that the effect of the 3Y mutation on EGFP-Rab7a $T_{1/2}$ was even stronger when the cells were EGF stimulated.

Overall, our investigations of Rab5 and Rab7a in HeLa and PAE cells show altered endosomal binding kinetics when subjected to mutant versions of the EGFR (Table 4.1). In both HeLa and PAE cells we could measure a slower exchange of Rab5 and Rab7a on the early and late endosome, respectively, throughout the mutant EGFRs (Table 4.1). In addition, we found a redistribution of IF and MF for Rab5 and Rab7a in stimulated HeLa cells with a pattern of decreasing IF throughout the mutant EGFRs (Figure 4.3 C, Figure 4.4 C, Table 4.1).

Table 4.1: $T_{1/2}$, IF and MF of Rab5 and Rab7a in HeLa and PAE cells. HeLa cells co-transfected with wt-, 1Y-, 2Y-, and 3Y-EGFR-GFP stimulated with EGF-Alexa 647, and PAE cells stably transfected with wt-, 1Y-, 2Y- and 3Y-EGFR with and without stimulation with EGF-Alexa 647.

	mCh-Rab5	**$T_{1/2}$ ± SEM (s)**	**IF (%)**	**MF (%)**
HeLa cells	wt-EGFR-GFP + EGF-Alexa 647	27.43 ± 1.4	16	84
	1Y-EGFR-GFP + EGF-Alexa 647	30.50 ± 1.5	7	93
	2Y-EGFR-GFP + EGF-Alexa 647	35.37 ± 1.9	1	99
	3Y-EGFR-GFP + EGF-Alexa 647	39.20 ± 1.8	1	99
	mAp-Rab7a	**$T_{1/2}$ ± SEM (s)**	**IF (%)**	**MF (%)**
	wt-EGFR-GFP + EGF-Alexa 647	22.6 ± 2.5	59	41
	1Y-EGFR-GFP + EGF-Alexa 647	30.0 ± 2.2	54	46
	2Y-EGFR-GFP + EGF-Alexa 647	43.5 ± 4.9	34	66
	3Y-EGFR-GFP + EGF-Alexa 647	50.1 ± 2.8	23	77
PAE cells	**mAp-Rab5**	**$T_{1/2}$ ± SEM (s)**	**IF (%)**	**MF (%)**
	wt-EGFR	19.4 ± 1.8	22	78
	1Y-EGFR	23.7 ± 1.9	16	84
	2Y-EGFR	27.3 ± 1.0	18	82
	3Y-EGFR	33.2 ± 1.6	18	82
	wt-EGFR+ EGF-Alexa 647	16.3 ± 2.7	20	80
	1Y-EGFR+ EGF-Alexa 647	21.6 ± 0.9	12	88
	2Y-EGFR+ EGF-Alexa 647	24.8 ± 2.1	21	79
	3Y-EGFR+ EGF-Alexa 647	31.9 ± 2.7	23	77
	EGFP-Rab7a	**$T_{1/2}$ ± SEM (s)**	**IF (%)**	**MF (%)**
	wt-EGFR	24.4 ± 3.0	5	95
	1Y-EGFR	28.6 ± 2.9	14	86
	2Y-EGFR	30.6 ± 2.7	14	86
	3Y-EGFR	210,9 ± 25.9	5	95
	wt-EGFR+ EGF-Alexa 647	15.6 ± 4.1	7	93
	1Y-EGFR+ EGF-Alexa 647	24.4 ± 3.2	13	87
	2Y-EGFR+ EGF-Alexa 647	28.5 ± 3.2	13	87
	3Y-EGFR+ EGF-Alexa 647	543.6 ± 186.6	12	88

4.2 TIRFM analysis of EGF-induced recruitment of EGFR to the plasma membrane

We have shown that the phosphorylation of EGFR affects the binding kinetics of Rab5 and Rab7a and potentially change the trafficking and degradation of the receptor. Previous studies of the various EGFR mutants have indicated an altered endosomal maturation pattern, delaying the progression from early to late endosomes (Merete Storflor, Master thesis 2015). Activated EGFRs are ubiquitinated, which is crucial for receptor PM internalization (Goh, Huang et al. 2010, Sigismund, Algisi et al. 2013) and the trafficking through the endosomal pathway for lysosomal degradation (Grovdal, Stang et al. 2004, Huang, Kirkpatrick et al. 2006). The four types of receptors are internalized and progress through the endocytic pathway and they colocalize with Rab7a (Figure 4.1). Previous results have shown that the degradation changes upon the different mutations at the respective tyrosine residues (1045/1068/1086) (Grøvdal, Stang et al. 2004) (Unpublished data from the Bakke lab). Previous work in the lab have shown that endosomal maturation, Rab5 and Rab7a binding kinetics, ubiquitination and degradation changes when we introduce the respective mutants (Merete Storflor, Master thesis 2015). However, little is known about the recycling of these mutant receptors. Consequently, we wanted to decipher the internalization and recycling characteristics of the different receptors by TIRFM imaging.

4.2.1 wt-EGFR-GFP is recruited to the plasma membrane after EGF-Alexa 647 stimulation

To investigate EGFR internalization and recycling we transfected HeLa cells with the various EGFRs and stimulated the cells with EGF during imaging. As a control experiment, we transfected HeLa cells with wt-EGFR-GFP and stimulated the cells with EGF-Alexa 647 during imaging. The cells were imaged every 10 seconds for ~ 33 minutes.

EGF-Alexa 647 was added to the cells during image acquisition, and we could detect a signal with EPI-fluorescence, but no signal in the TIRF plane. The EGF-Alexa 647 will then stimulate the cells on the opposite side of the TIRF plane. However, after one minute, post EGF-Alexa 647 addition, we could detect wt-EGFR-GFP positive spots on the PM (Figure 4.9). The number of wt-EGFR-GFP spots increased with time and eventually decreased. We could also detect a weak signal of EGF-Alexa 647 towards the end of the movie (Figure 4.9).

Spot counts of the receptor clusters over time were performed with Imaris 9.5.1 (Bitplane, Oxford Instruments).

Having analyzed the data, we could measure wt-EGFR-GFP recruitment to the plasma membrane at 4 minutes and 50 seconds (Figure 4.9). The highest number of wt-EGFR-GFP clusters was detected at 7 minutes. From that time point until the end of the observation period the number of receptor clusters decreased, indicating internalization of activated wt-EGFR-GFP. As the receptor clusters decreased, we detected an increasing signal of EGF-Alexa 647 towards the end of the movie.

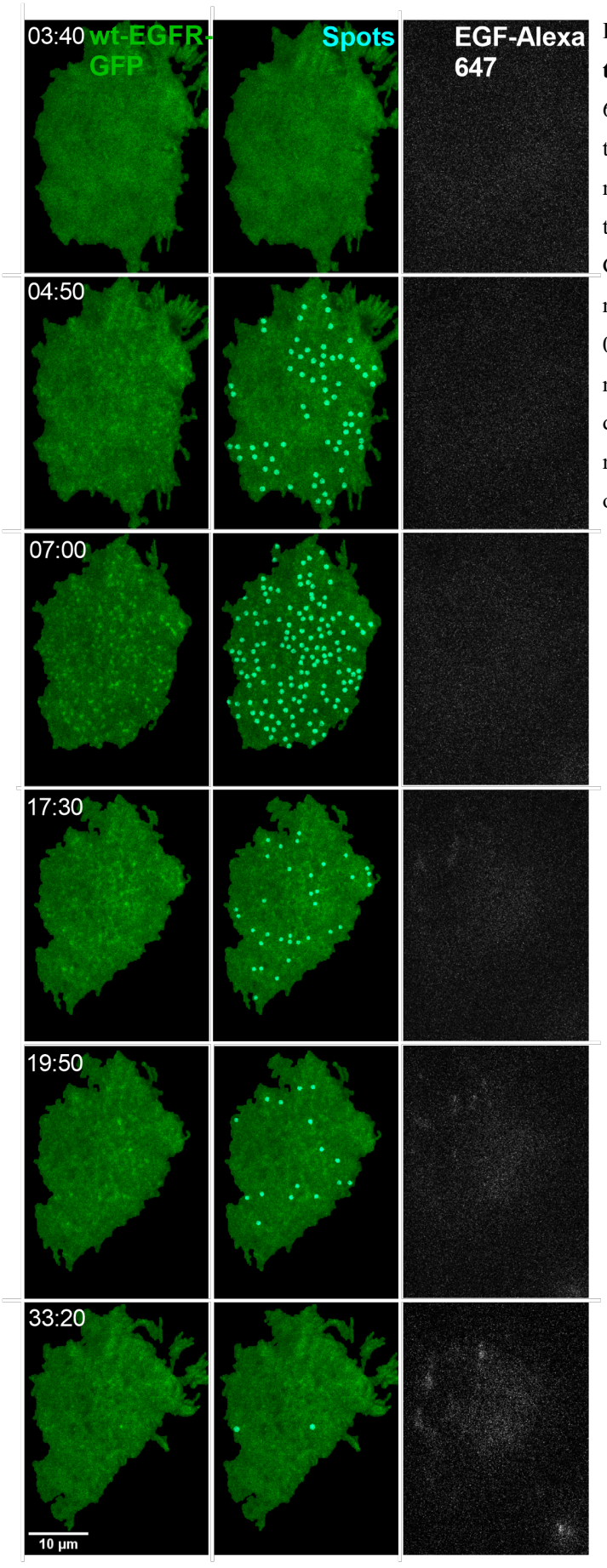

Figure 4.9: Montage of HeLa cell transiently transfected with wt-EGFR-GFP. EGF-Alexa 647 (50ng/ml) was added after ~20 seconds. First time point at 03:40 min shows the plasma membrane before recruitment of wt-EGFR-GFP to the plasma membrane. Clusters of wt-EGFR-GFP begin to appear at 04:50 min. Highest number of receptor clusters was measured at 07:00 minutes. From 17:30 min and out the number of clusters at the plasma membrane decreases. EGF-Alexa 647 was detected at 17:30 min with some increase in signal toward the end of the movie.

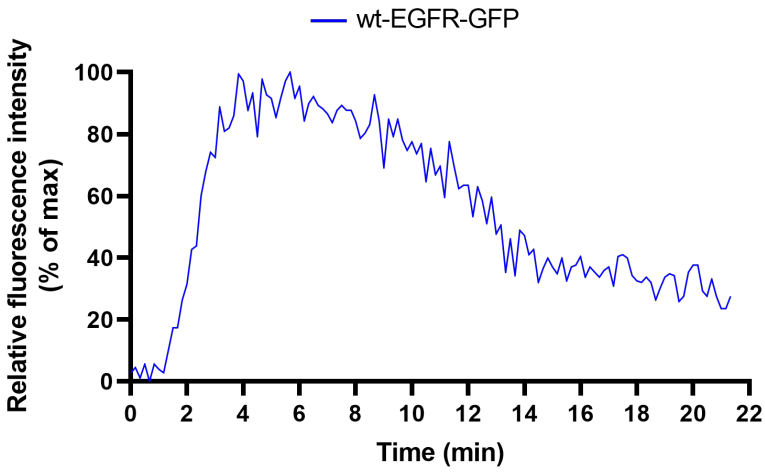

Figure 4.10: Recruitment and internalization of wt-EGFR-GFP at the plasma membrane. The graph represents an average of five experiments (n = 5).

Results of wt-EGFR-GFP showed recruitment of wt-EGFR-GFP to the plasma membrane upon EGF-Alexa 647 stimulation which increased reaching a high, before decreasing throughout the movie (Figure 4.10). We detected signal of EGF-Alexa 647 at ~ 17 minutes which may indicate some receptor recycling back to the plasma membrane.

4.2.2 1Y-EGFR-GFP shows delayed recruitment to the plasma membrane

Our data showed that the wt-EGFR-GFP was recruited to the plasma membrane at 4 minutes and 50 seconds, and we could count the highest number of receptors at 7 minutes. Having established this as a control experiment, we wanted to investigate the recruitment of the 1Y-EGFR-GFP. To study this, HeLa cells were transiently transfected with 1Y-EGFR-GFP and stimulated with EGF-Alexa 647 during imaging at ~20 seconds.

We could measure a delayed recruitment of 1Y-EGFR-GFP to the plasma membrane compared to the wt-EGFR-GFP, with receptors being recruited at 6 minutes and 20 seconds (Figure 4.11). Number of 1Y-EGFR-GFP clusters increased reaching the highest number of spots at 10 minutes and 50 seconds. We further measured a decrease in number of clusters towards the end of the movie, only detecting a few spots in the last frame. At 17 minutes and 30 seconds we detected a weak signal of EGF-Alexa 647 which slightly increased towards the last frame.

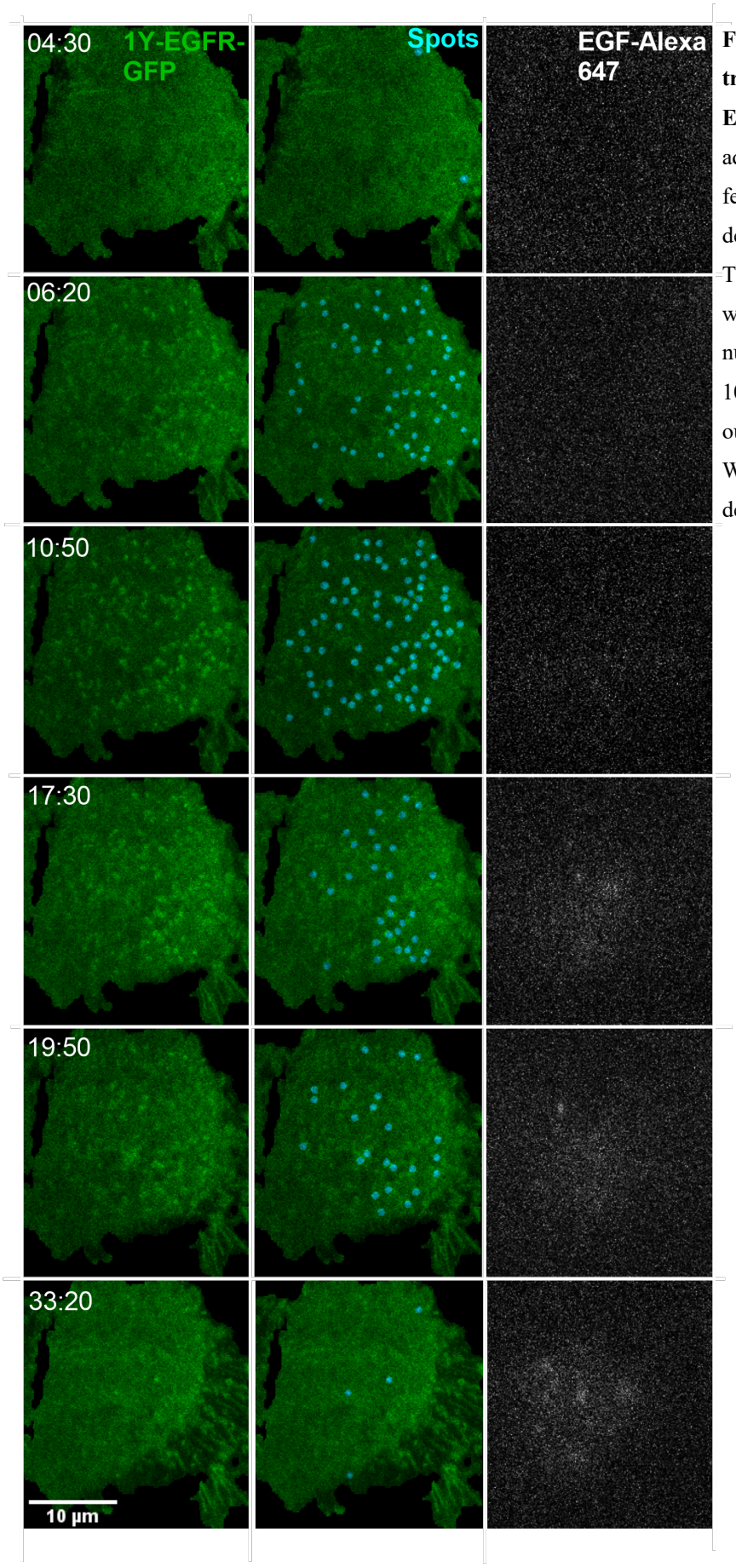

Figure 4.11: Montage of HeLa cell transiently transfected with 1Y-EGFR-GFP. EGF-Alexa 647 was added after ~20 s. At 04:30 min only a few 1Y-EGFR-GFP clusters were detected on the plasma membrane. The recruitment of 1Y-EGFR-GFP was detected at 06:20 min. Highest number of receptor clusters appear at 10:50 min. From 17:30 minutes and out the number of clusters decreases. Weak signals of EGF-Alexa 647 were detected at 17:30 min and out.

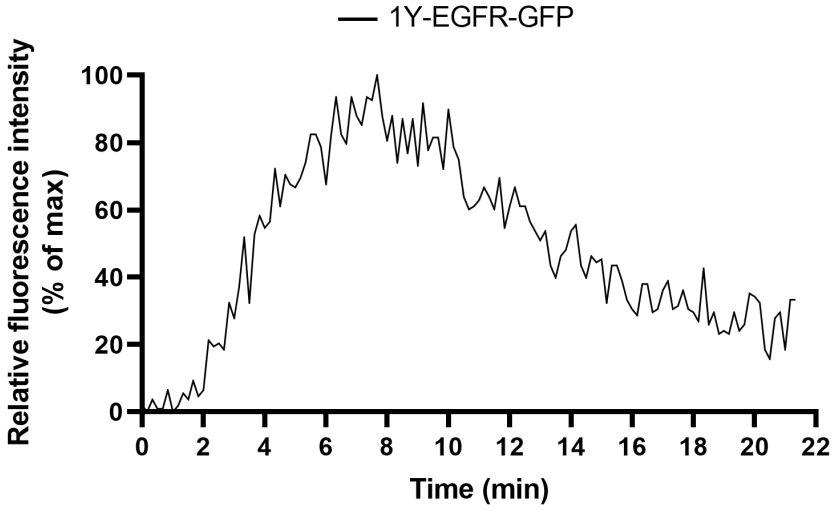

Figure 4.12: Recruitment and internalization of 1Y-EGFR-GFP at the plasma membrane. The graph represents an average of five experiments (n = 5).

Our analysis shows a delay in 1Y-EGFR-GFP recruitment to the plasma membrane compared to wt-EGFR-GFP with a difference of 1 minute and 30 seconds (Figure 4.12). The highest number of 1Y-EGFR-GFP clusters was detected at 10 minutes and 50 seconds which is 3 minutes and 50 seconds later than for the wt-EGFR-GFP. From this time point and out the number of clusters decreased, indicating internalization of 1Y-EGFR-GFP. EGF-Alexa 647 was detected at 17 minutes and 30 seconds, increasing as the receptors were internalized which indicated recycling of 1Y-EGFR-GFP to the plasma membrane.

4.2.3 2Y-EGFR-GFP shows further delay in recruitment to the plasma membrane

Analysis of 1Y-EGFR-GFP showed a delayed recruitment to the plasma membrane compared to the wt-EGFR-GFP. We further wanted to investigate the recruitment of the 2Y-EGFR-GFP. To study this, HeLa cells were transiently transfected with 2Y-EGFR-GFP. Cells were stimulated with EGF-Alexa 647 during imaging at ~20 seconds.

Measuring the 2Y-EGFR-GFP recruitment to the plasma membrane we could detected a further delay in recruitment compared to the wt- and 1Y-EGFR-GFP. Recruitment of 2Y-EGFR-GFP was detected at 8 minutes which further increased reaching the highest number of spots at 12 minutes (Figure 4.13). Further, we could measure a decrease in 2Y-EGFR-GFP receptor clusters towards the end of the movie. Spots of EGF-Alexa 647 were detected at the

three first timepoints, however this signal lay outside the cell of interest. As the number of clustered receptors decreased at 17 minutes and 30 seconds, we could detect strong EGF-Alexa 647 signals which slowly increased towards the last time point.

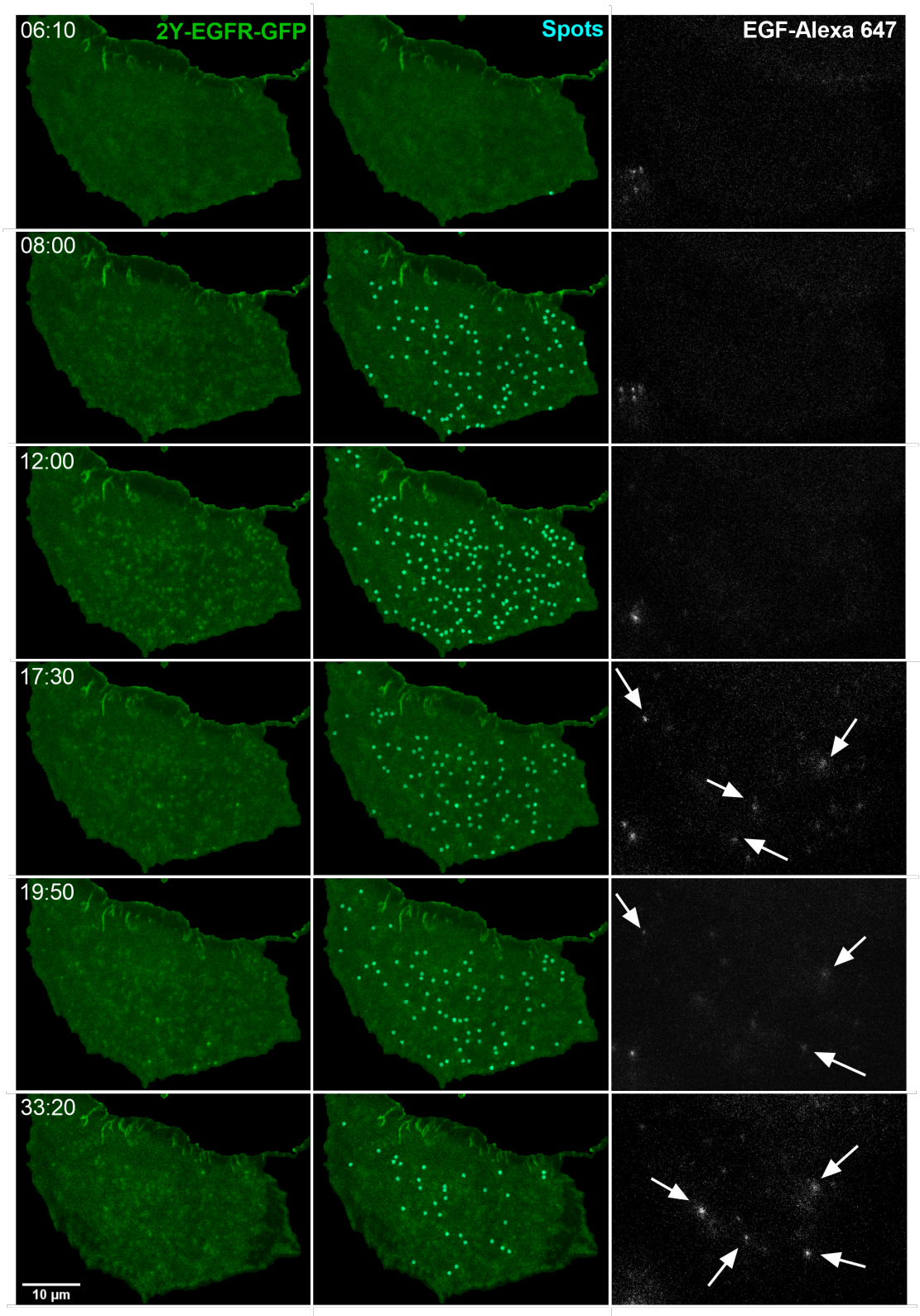

Figure 4.13: Montage of HeLa cell transiently transfected with 2Y-EGFR-GFP. EGF-Alexa 647 was added after approximately ~20 seconds. At 06:10 min only one 2Y-EGFR-GFP cluster was detected at the plasma membrane. The recruitment of receptors was detected at 08:00 min. Highest number of receptor clusters was detected at 12:00 min. From 17:30 min and out the number of clustered receptors decreased. Clear spots of EGF-Alexa 647 were detected on the plasma membrane at 17:30 min and out (white arrows).

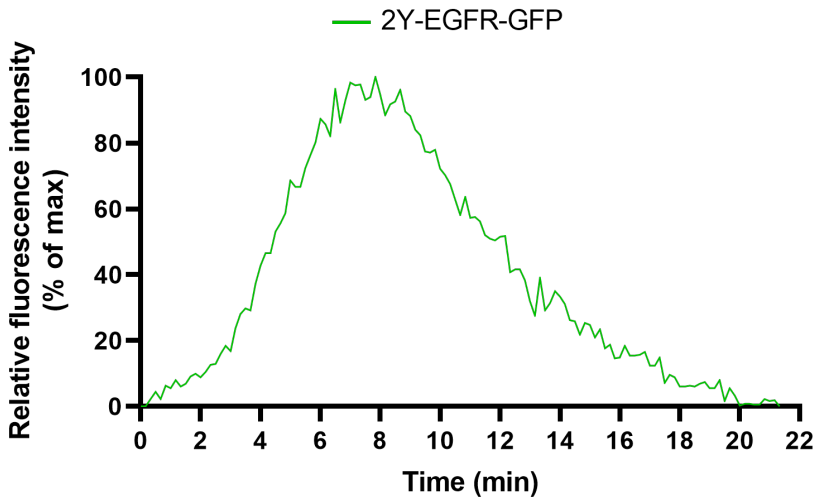

Figure 4.14: Recruitment and internalization of 2Y-EGFR-GFP at the plasma membrane. The graph represents an average of five experiments (n=5).

2Y-EGFR-GFP was recruited to the plasma membrane at 8 minutes (Figure 4.13, Figure 4.14). This is a delay of 3 minutes and 10 seconds compared to wt-EGFR-GFP. The highest number of receptor clusters was detected at 12 minutes which is a delay of 1 minute and 10 seconds compared to the wt-EGFR-GFP.

EGF-Alexa 647 was detected at 17 minutes and 30 seconds in addition to the two last time points. The EGF-Alexa 647 signal was stronger compared to wt- and 1Y-EGFR-GFP indicating a higher rate of recycling of 2Y-EGFR-GFP back to the plasma membrane.

4.2.4 3Y-EGFR-GFP shows delayed recruitment to the plasma membrane

Analysis of 2Y-EGFR-GFP showed a delay of 3 minutes and 10 seconds in recruitment to the plasma membrane compared to the wt-EGFR-GFP and the highest number of receptor clusters was measured at 12 minutes which was 1 minute and 10 seconds later than for the wt-EGFR-GFP. We further wanted to measure the recruitment of 3Y-EGFR-GFP to the plasma membrane and to investigate this, HeLa cells were transiently transfected with 3Y-EGFR-GFP. Cells were stimulated with EGF-Alexa 647 during imaging at ~20 seconds.

Our analysis shows major 3Y-EGFR-GFP recruitment to the plasma membrane at 6 minutes and 30 seconds (Figure 4.15). Interestingly, at 10 minutes and 30 seconds we could measure a

slight decrease in number of spots following a further increase at 17 minutes and 30 seconds. Number of 3Y-EGFR-GFP clusters increased towards the end of the movie with the highest number of spots counted in the last frame of the movie. In contrast to the experiments with wt-, 1Y- and 2Y-EGFR-GFP, strong signals of EGF-Alexa 647 were visible at all chosen time points.

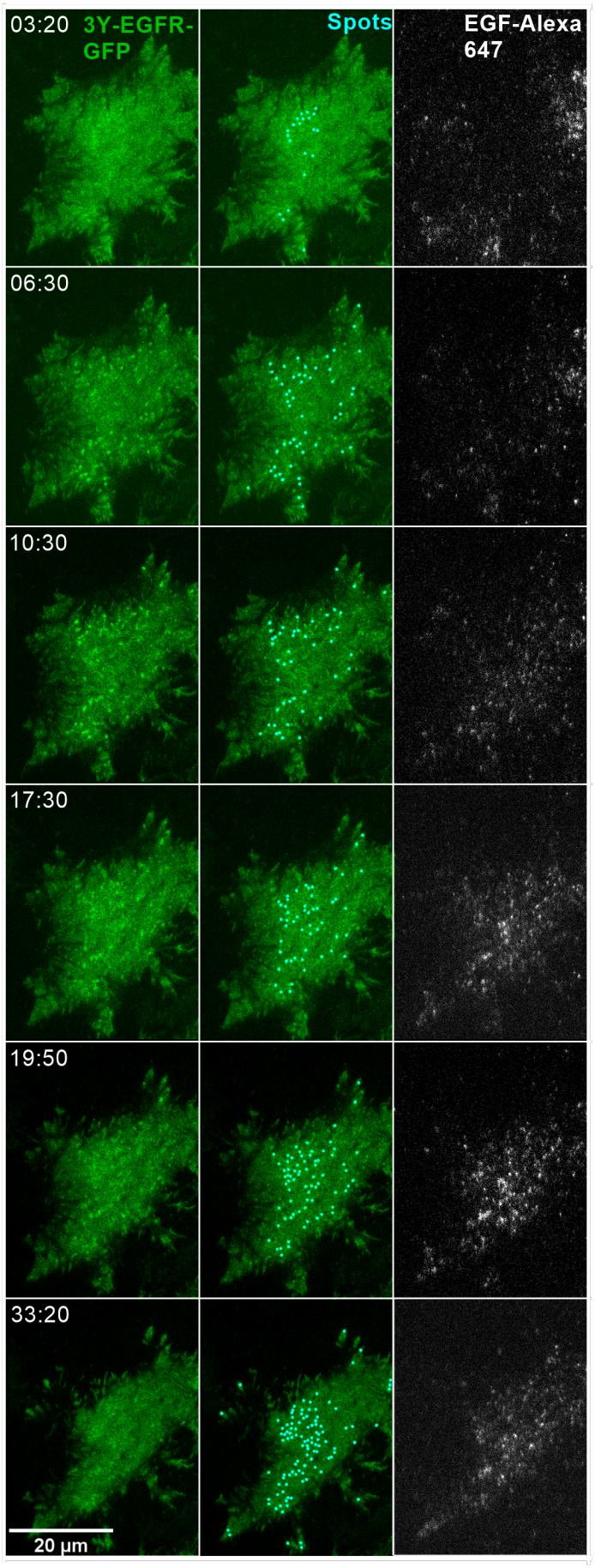

Figure 4.15: Montage of HeLa cell transiently transfected with 3Y-EGFR-GFP. EGF-Alexa 647 was added after approximately ~20s. A few 3Y-EGFR-GFP clusters were detected on the plasma membrane at 03:20min. The recruitment of receptors was detected at 06:30min. A slight decrease in 3Y-EGFR-GFP clusters was measured at 10:30 min. At 17:30min the number of clusters had increased. Further increase in receptor clusters was measured at 19:50min. At 33:20min the highest number of 3Y-EGFR-GFP receptor clusters was detected. Strong signals of EGF-Alexa 647 were detected throughout the movie.

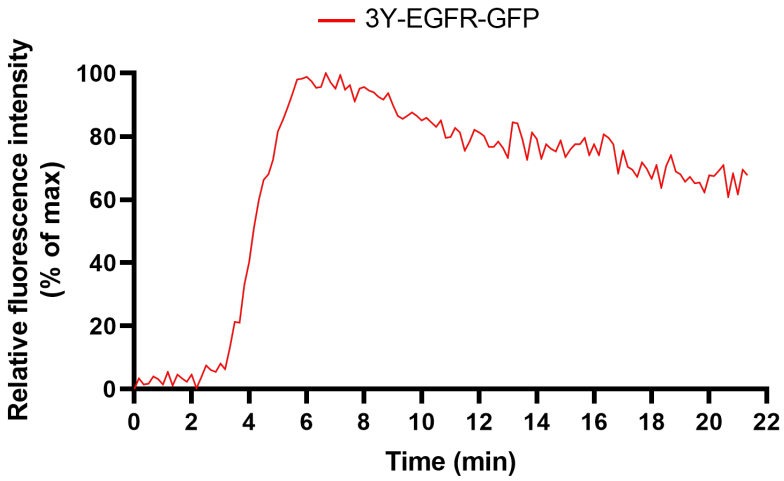

Figure 4.16: Recruitment and internalization of 3Y-EGFR-GFP at the plasma membrane. The graph represents an average of five experiments (n=5).

3Y-EGFR-GFP was recruited to the plasma membrane at 6 minutes and 30 seconds (Figure 4.15, Figure 4.16). This was 1 minute and 40 seconds slower compared to wt-EGFR-GFP. We detected a high amount of 3Y-EGFR-GFP receptor still present on the plasma membrane at the end of the movie (Figure 4.16). We detected EGF-Alexa 647 signal at all chosen time points. The strongest EGF-Alexa 647 signal was detected at 19 minutes and 50 seconds.

TIRF experiments were performed to investigate the recruitment of wt-, 1Y-, 2Y- and 3Y-EGFR-GFP to the plasma membrane after stimulation with EGF. Data from our spot count of the various receptors was plotted and normalized using GraphPad Prism 8 to examine if there was a difference in recruitment, internalization and receptor recycling between the EGFRs. The wt-EGFR-GFP showed the fastest recruitment to the plasma membrane among the various EGFRs after EGF-stimulation (Figure 4.17). We could measure a slower recruitment initiation of 1Y-EGFR-GFP compared to the wt-EGFR-GFP, though they showed a similar amount of receptorclusters left on the plasma membrane during internalization. In both wt- and 1Y-EGFR-GFP ~30% of clustered receptors were still present on the plasma membrane. Our analysis showed a further delay in 2Y-EGFR-GFP recruitment initiation on the plasma membrane, reaching a peak approximately at the same time as 1Y-EGFR-GFP. We measured no clusters of 2Y-EGFR-GFP on the plasma membrane at the end of the experiment. Interestingly, when measuring recruitment of 3Y-EGFR-GFP to the plasma membrane upon EGF stimulation we could detect major differences compared to the wt-, 1Y- and 2Y-EGFR-

GFP. The initiation of 3Y-EGFR-GFP recruitment was the slowest of all the various receptors. However, the highest number of 3Y-EGFR-GFP was detected approximately at the same time as for 1Y- and 2Y-EGFR-GFP. We measured the internalization of 3Y-EGFR-GFP to highly differ from wt-, 1Y- and 2Y-EGFR-GFP. At the end of the experiment ~70% of the clustered 3Y-EGFR-GFP were still present on the plasma membrane.

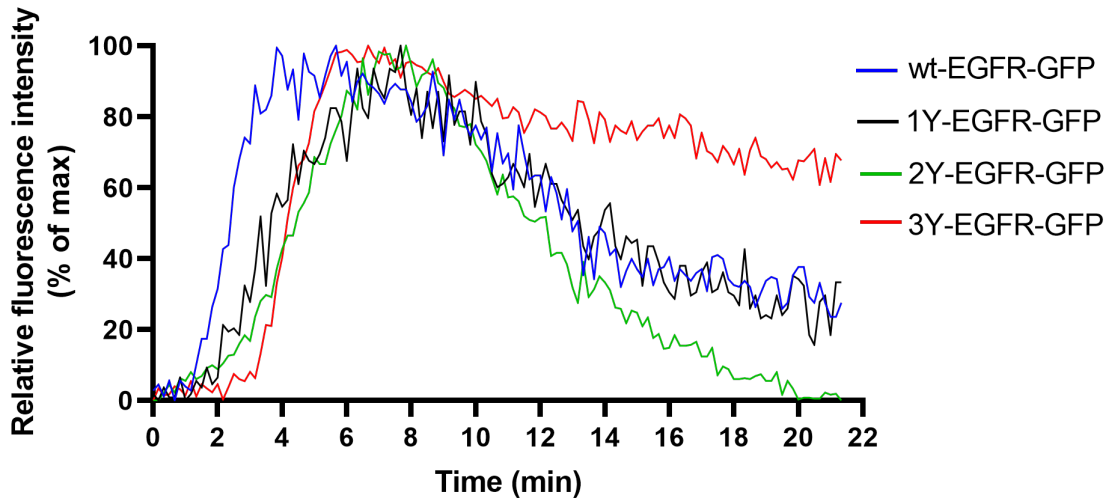

Figure 4.17: Relative receptor recruitment to the plasma membrane of wt-, 1Y-, 2Y- and 3Y-EGFR-GFP when stimulated with EGF-Alexa 647 in HeLa cells. HeLa cells were transiently transfected with wt-, 1Y-, 2Y- or 3Y-EGFR-GFP and imaged for ~33 min. Stimulation with EGF-Alexa 647 was performed at ~20 sec after start of imaging. Each graph represents an average of five experiments (n = 5).

The analysis of our TIRF experiments show differences in recruitment of wt-, 1Y-, 2Y- and 3Y-EGFR-GFP to the plasma membrane when stimulated with EGF-Alexa 647. We could measure a delay in receptor recruitment of 1Y-, 2Y- and 3Y-EGFR-GFP to the plasma membrane compared to the wt-EGFR-GFP (Figure 4.17). In addition, we measured a major difference in receptor internalization of 3Y-EGFR-GFP compared to wt-, 1Y- and 2Y-EGFR-GFP, where a high amount of receptor clusters still was present at the plasma membrane for 3Y-EGFR-GFP at the end of the movie.

4.2.5 Internalized EGF-Alexa 647 with the various EGFRs

Our TIRF experiments showed a delay in receptor recruitment to the plasma membrane between wt-EGFR-GFP and the mutant EGFRs (Figure 4.17). We could also detect a stronger EGF-Alexa 647 signal for 2Y- and 3Y-EGFR-GFP after receptor internalization (Figure 4.13, Figure 4.15) indicating a higher rate of receptor recycling compared to wt- and 1Y-EGFR-

GFP. In addition, we measured a slow internalization rate of the 3Y-EGFR-GFP compared to wt-, 1Y- and 2Y-EGFR-GFP, and a major amount of 3Y-EGFR-GFP present at the membrane at the end of the experiment (Figure 4.17). Therefore, we further wanted to investigate the amount of internalized EGF-Alexa 647 with the various EGFRs. HeLa cells were transiently transfected with wt-, 1Y-, 2Y- or 3Y-EGFR-GFP and stimulated with EGF-Alexa 647 (50ng/ml). A z-stack of 5 images was acquired 35 minutes post stimulation with EGF-Alexa 647.

Internalized EGF-Alexa 647 was present in all EGFR variants. Interestingly, we observed a difference in the amount of internalized EGF-Alexa 647 between the various receptors (Figure 4.18). Cells transfected with wt- and 1Y-EGFR-GFP showed the highest and similar amount of internalized EGF-Alexa 647. Less signal was detected for 2Y-EGFR-GFP. The 3Y-EGFR-GFP clearly differed from the other receptor variants with the lowest amount of internalized EGF-Alexa 647 which could indicate a high receptor recycling rate.

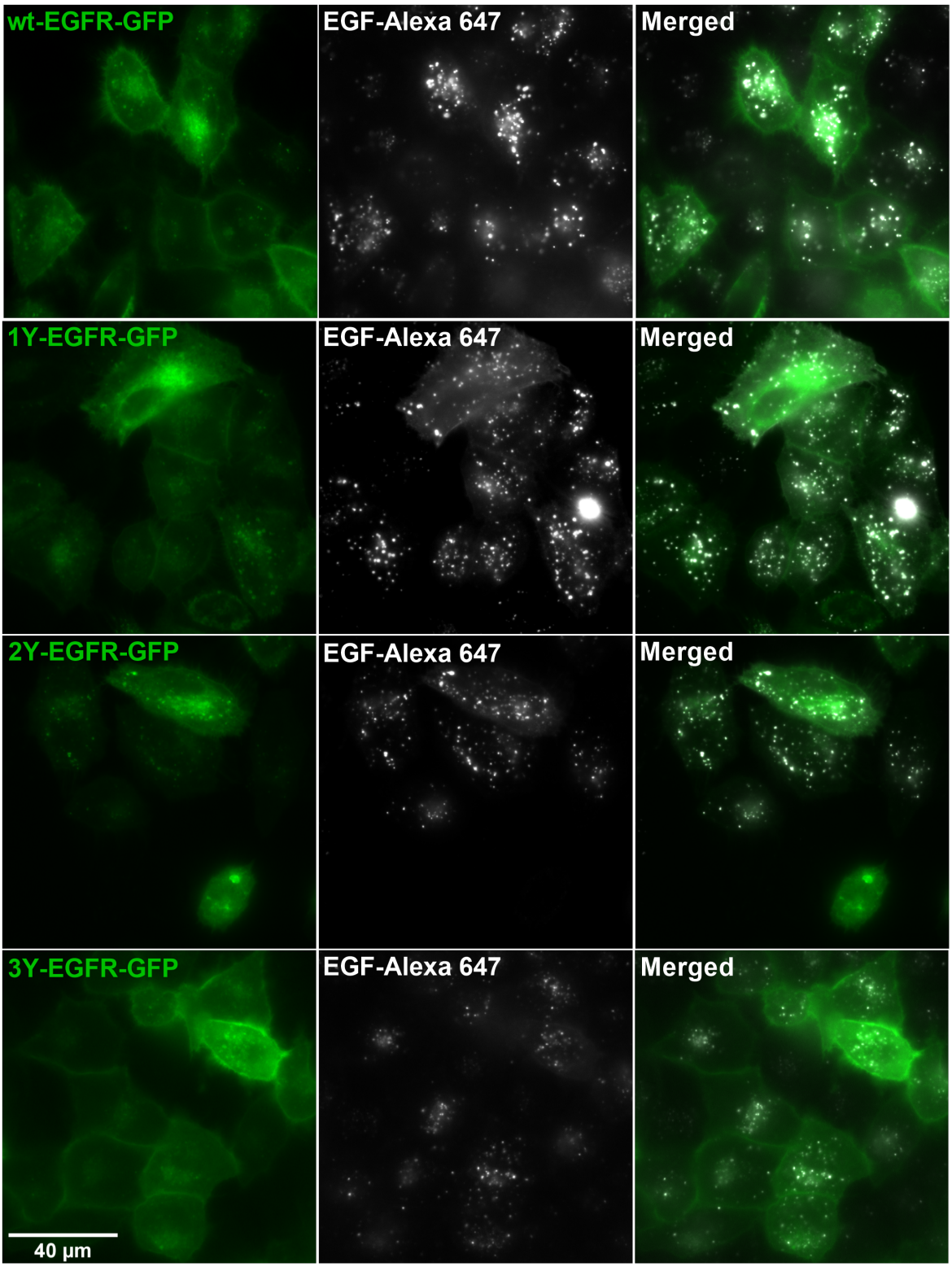

Figure 4.18: Montage of HeLa cells transfected with the various EGFRs 35 min after stimulation with EGF-Alexa 647 (50ng/ml). HeLa cells were transiently transfected with wt-, 1Y-, 2Y- or 3Y-EGFR-GFP. Cells were stimulated with EGF-Alexa 647 during imaging at ~20 seconds. Z-stack of five images was performed 35 min post EGF-Alexa 647 stimulation.

4.3 Trafficking and colocalization analysis: Knockdown of Rab22a

We have so far shown that mCh-Rab5 and Rab7a binding kinetics in HeLa cells (Figure 4.3, Figure 4.4), are altered in the presence of various EGFRs. In order to establish the role of phosphorylation and ubiquitination of the wt-EGFR-GFP and 3Y-EGFR-GFP we decided to knockdown Rab22a, which is important for the recruitment of Rabex-5. Rabex-5 have been shown to be recruited to the early endosome by ubiquitinated EGFR (Mattera, Bonifacino et al. 2006, Penengo, Mapelli et al. 2006, Zhang, Zhang et al. 2014). Rab22a is a GTPase located on early endosomes (Olkkonen, Dupree et al. 1993) and has also been shown to be important for endosomal trafficking and endosomal maturation in dendritic cells (Mesa, Salomón et al. 2001). Rab22a is part of the Rab22a-Rabex-5-Rab5 cascade which is important for EGFR trafficking and degradation (Zhu, Liang et al. 2009). Previous studies of HeLa cells with knockdown of Rab22a show a severe reduction in the Rab5 GEF Rabex-5 on early endosomes and reduced degradation of EGF (Zhu, Liang et al. 2009). Previous work from our lab (Anna Vik Rødseth, Master thesis 2021) have shown that knockdown of Rab22a in HeLa cells leads to a faster Rab5-Rab7a conversion on endosomes. For the knockdown experiments, we tested four different oligoes (Materials and methods, 3.2.4). Knockdown was successful using all four siRNA oligos (Figure 4.19). However, when imaging cells we observed a better cell survival and state when using siRNA#2. Therefore, this oligo was further used for transfection and imaging experiments.
Western blot analysis was performed to confirm Rab22a knockdown in HeLa cells (Figure 4.19).

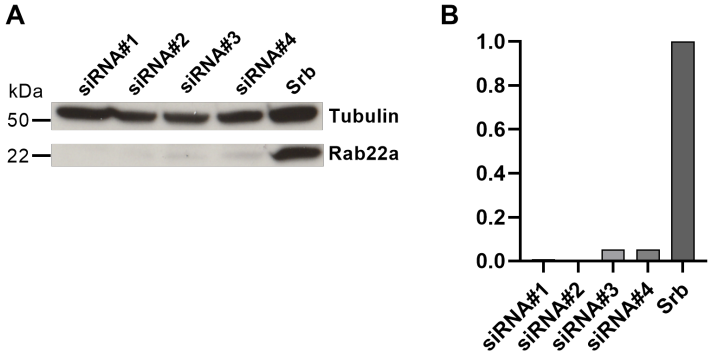

Figure 4.19: **Representative Western Blot with normalized quantification box plot. A)** Western Blot showing knockdown of Rab22a in HeLa cells (50ng) with the four different siRNA oligos, and Srb as the siRNA negative control. Tubulin was used as a loading control. **B)** Box plot of relative intensity of the siRNAs and scrambled (Srb) siRNA normalized by the tubulin values. The intensity of the bands was analyzed in ImageJ using the Gel analyzer plugin.

Western Blot analysis of the four siRNA oligos (4.19) showing the efficiency of the knockdown of Rab22a in HeLa cells. The same knockdown experiment had been performed several times in the Bakke lab showing the same knockdown efficiency (Anna Vik Rødseth, Master thesis 2021).

Further, we performed a colocalization analysis of mCh-Rab5 and EGF-Alexa 647 in cells co-transfected with wt- or 3Y-EGFR-GFP in knockdown Rab22a HeLa cells.

4.3.1 EGF-activated wt-EGFR-GFP/mCh-Rab5 trafficking in Knockdown Rab22a HeLa cells

We have here shown that phosphorylation deficient receptors change the binding dynamic of Rab5. Therefore, we wanted to investigate how the un-ubiquitinated 3Y-EGFR would be recruited to Rab5 positive endosomes in Rab22a known down cells. As our control experiment, we investigated the trafficking of EGF-activated wt-EGFR-GFP in Rab22a knockdown HeLa cells. Knockdown of Rab22a in HeLa cells was performed using siRNA#2 (Figure 4.19). Cells were transiently transfected with mCh-Rab5 and wt-EGFR-GFP and imaged every 10 seconds for 17 minutes. EGF-Alexa 647 (50ng/ml) stimulation was performed at ~20 seconds.

Before internalization of EGF-Alexa 647 we observed several endosomes positive for mCh-Rab5 and wt-EGFR-GFP (Figure 4.20). At 9 minutes EGF-Alexa 647 had been internalized and we observed major colocalization with endosomes positive for mCh-Rab5 and wt-EGFR-GFP. At 17 minutes mCh-Rab5/wt-EGFR-GFP-positive endosomes were still colocalized with EGF-Alexa 647.

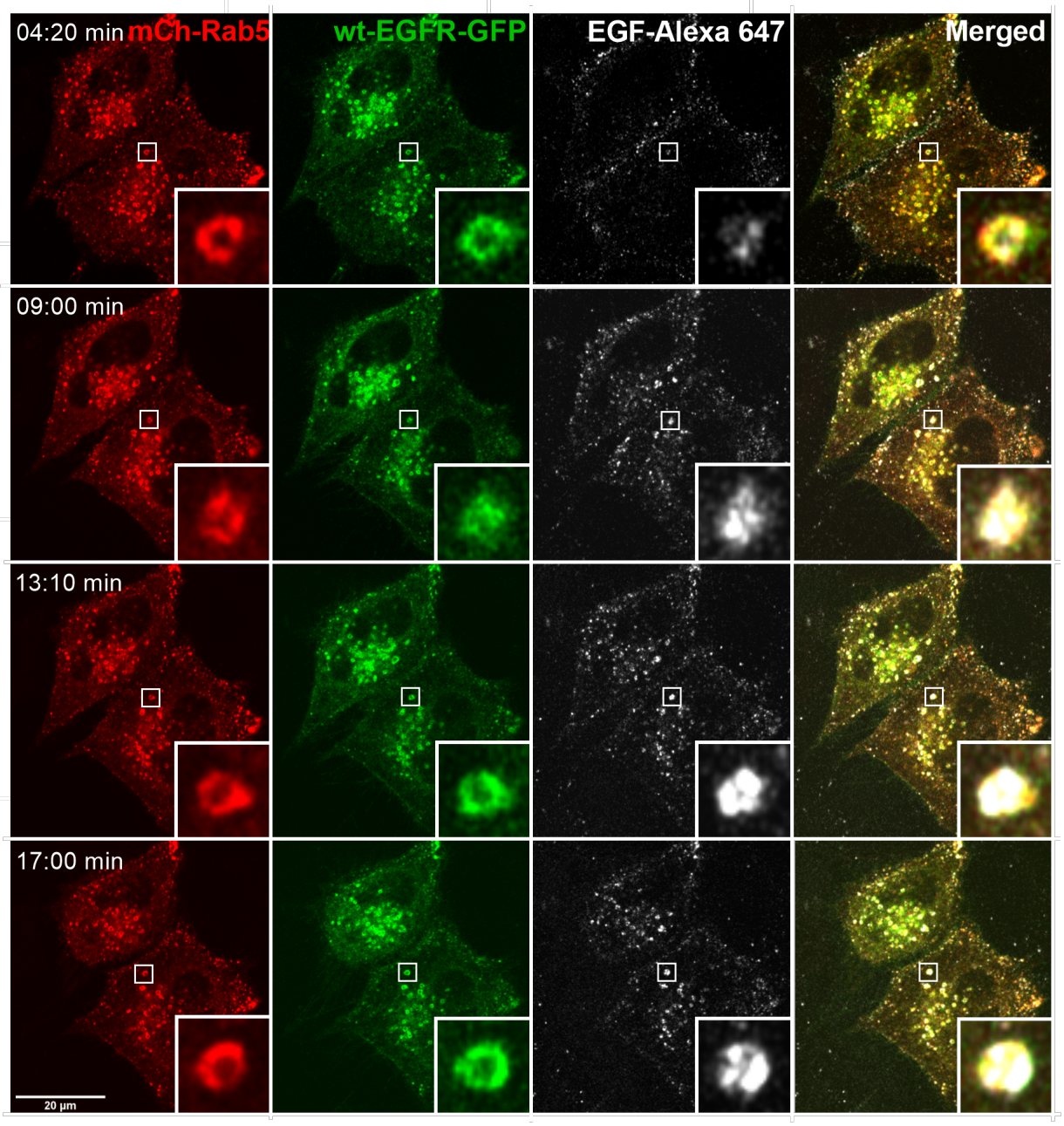

Figure 4.20: Montage of HeLa cells with knockdown of Rab22a using siRNA#2. Knockdown Rab22a HeLa cells were transiently transfected with wt-EGFR-GFP and mCh-Rab5. Stimulation with EGF-Alexa 647 (50ng/ml) was performed during imaging at 20 s.

We could here show that the wt-EGFR-GFP is rapidly internalized with EGF-Alexa 647 and colocalizes with mCh-Rab5 positive endosomes in HeLa cells with knockdown of Rab22a. Having established the wt-EGFR-GFP as a control we continued by investigating trafficking of EGF-activated 3Y-EGFR-GFP in knockdown Rab22a HeLa cells.

4.3.2 EGF-activated 3Y-EGFR-GFP/mCh-Rab5 trafficking in Knockdown Rab22a HeLa cells

As mentioned above our trafficking analysis of EGF-activated wt-EGFR-GFP was shown to be rapidly colocalized with mCh-Rab5 in Rab22a deficient HeLa cells (Figure 4.20). Our FRAP experiments showed an alteration in Rab5 $T_{1/2}$ when introducing the 3Y-EGFR-GFP and 3Y-EGFR in HeLa and PAE cells, respectively (Figure 4.3 B, Figure 4.5 B, Figure 4.6 B). Further we wanted to investigate the trafficking of EGF-activated 3Y-EGFR-GFP with mCh-Rab5 in HeLa cells where Rab22a was knocked down. Knockdown of Rab22a in HeLa cells was performed using siRNA#2 (Figure 4.19). Cells were transiently transfected with mCh-Rab5 and 3Y-EGFR-GFP and imaged every 10 seconds for 17 minutes. EGF-Alexa 647 stimulation (50ng/ml) was performed at ~20 seconds.

We could observe endosomes positive for mCh-Rab5 and 3Y-EGFR-GFP was mainly localized to the cytosol before stimulation with EGF-Alexa 647 (Figure 4.21). A weak EGF-Alexa 647 signal was detected at the plasma membrane at 4 minutes and 20 seconds. At 9 minutes we could observe some internalized of EGF-Alexa 647. We detected a slow, but constant increase in internalized EGF-Alexa 647 over time. However, only a few endosomes positive for mCh-Rab5 and 3Y-EGFR-GFP seemed to colocalize with EGF-Alexa 647. Throughout the movie we observed the major part of EGF-Alexa 647 to be located at the plasma membrane, indicating a low internalization rate in Rab22a knockdown HeLa cells co-transfected with 3Y-EGFR-GFP and mCh-Rab5.

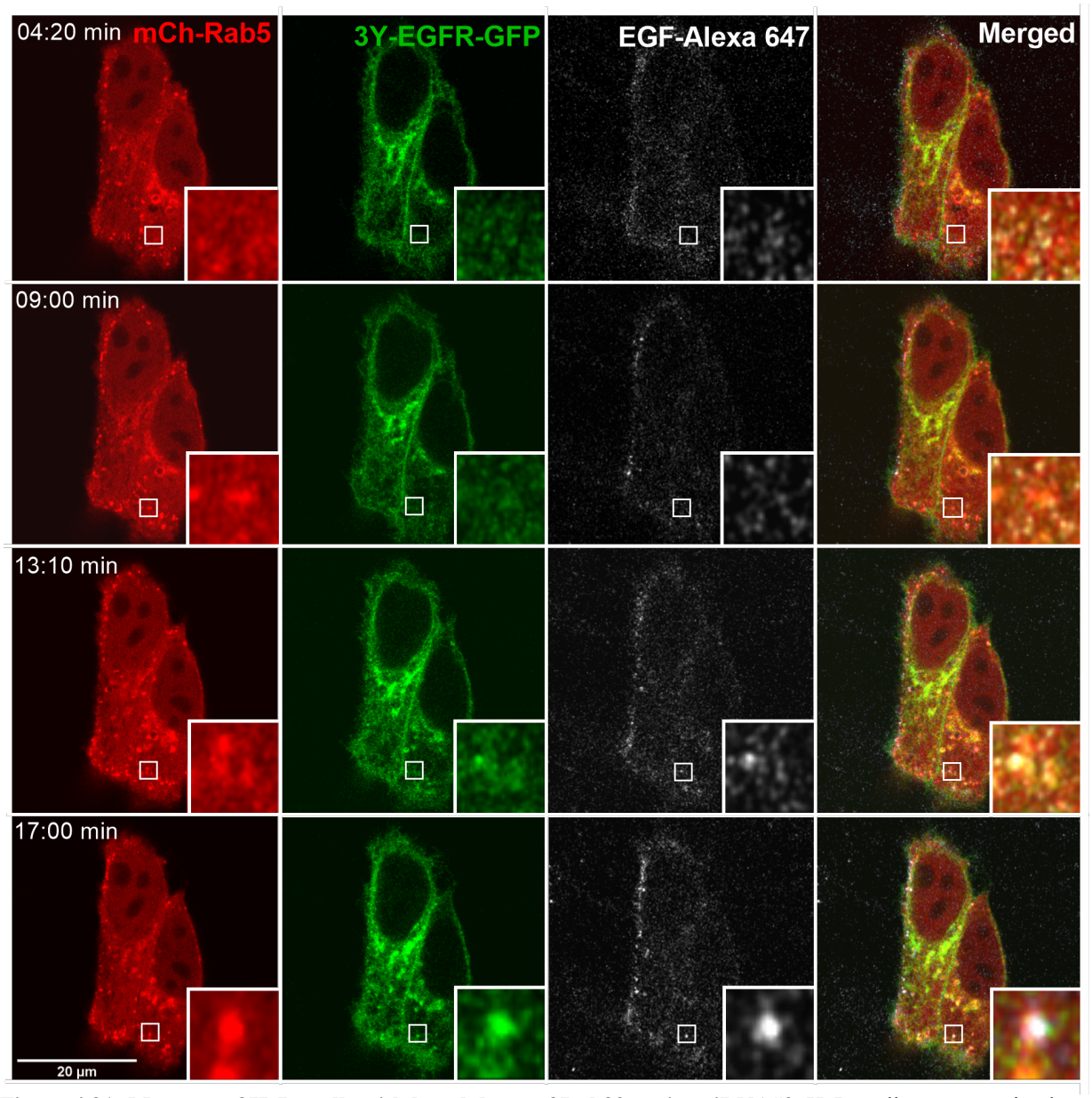

Figure 4.21: Montage of HeLa cells with knockdown of Rab22a using siRNA#2. HeLa cells were transiently transfected with 3Y-EGFR-GFP and mCh-Rab5. Stimulation with EGF-Alexa 647 (50ng/ml) was performed during imaging at 20 s.

The trafficking analysis could show a change in EGF-Alexa 647 internalization when comparing the wt- and 3Y-EGFR-GFP (Figure 4.20, Figure 4.21). Internalization of EGF-activated wt-EGFR-GFP was observed to be faster compared to the 3Y-EGFR-GFP. In addition, we observed an increase in the colocalization between mCh-Rab5/EGF-Alexa647 in cells transfected with the wt-EGFR-GFP.

4.3.3 Colocalization analysis of mCh-Rab5 and EGF-Alexa 647 in knockdown Rab22a HeLa cells with wt-/3Y-EGFR-GFP

We could show major differences in internalization and colocalization of EGF-Alexa 647 with mCh-Rab5 and wt-/3Y-EGFR-GFP in knockdown Rab22a HeLa cells (Figure 4.20, Figure 4.21). In cells transfected with wt-EGFR-GFP, EGF-Alexa 647 was rapidly internalized and colocalized with the receptor and mCh-Rab5. Cells transfected with 3Y-EGFR-GFP showed a delayed uptake of EGF-Alexa 647 and lower colocalization of EGF-Alexa 647 with mCh-Rab5 and 3Y-EGFR-GFP. We therefore wanted to analyze the percent colocalization of mCh-Rab5 and EGF-Alexa 647 over time. To investigate this, knockdown Rab22a HeLa cells were transfected with mCh-Rab5 and wt- or 3Y-EGFR-GFP and imaged every 10 seconds for 17 minutes. Cells were stimulated with EGF-Alexa 647 during imaging at ~20 seconds. We measured colocalization of mCh-Rab5 and EGF-Alexa 647 over time by percent pixel overlap in ImageJ. The colocalization analysis showed a major difference between cells transfected with wt- and 3Y-EGFR-GFP (Figure 4.22). We measured a ~70% higher colocalization of Rab5 and EGF-Alexa 647 in cells transfected with wt-EGFR-GFP compared to 3Y-EGFR-GFP at 17 minutes.

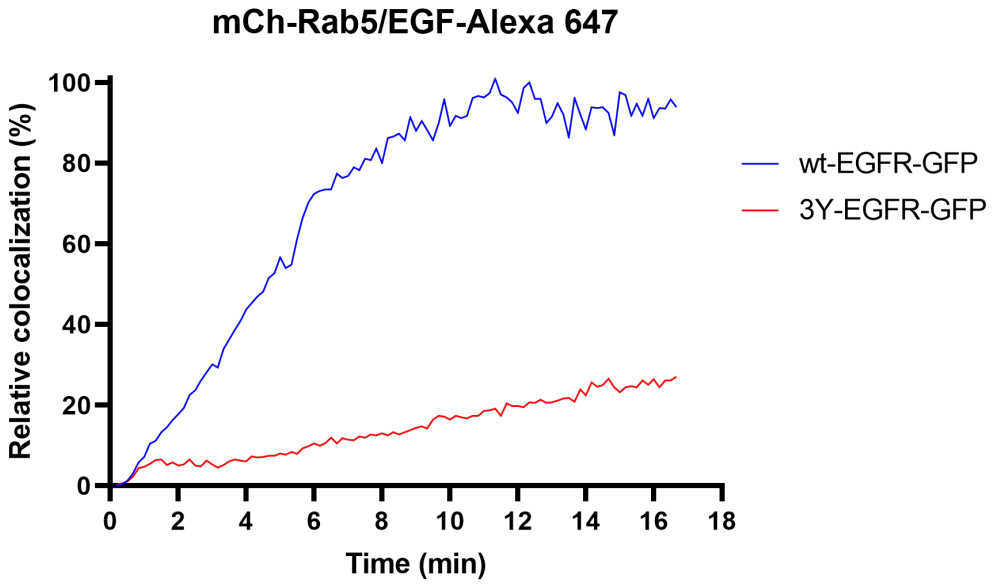

Figure 4.22: Relative percent colocalization of mCh-Rab5 and EGF-Alexa 647 in knockdown Rab22a HeLa cells transiently transfected with wt-/3Y-EGFR-GFP. EGF-Alexa 647 was added during imaging at 20 s. wt-EGFR-GFP n= 3, 3Y-EGFR-GFP n= 4.

Our data show a major decrease in colocalization of EGF-Alexa 647 and mCh-Rab5 in knockdown Rab22a HeLa cells in presence of 3Y-EGFR-GFP compared to wt-EGFR-GFP (Figure 4.22).

Overall, we show that the phosphorylation pattern of EGFR regulates the endosomal binding kinetics of Rab5 and Rab7a. An increasing number of deficient phosphorylation sites on the EGFR leads to a slower exchange of Rab5 and Rab7a on the early and late endosomes, respectively.

5. Discussion

The EGFR is a well-studied RTK and has been shown to be involved several cellular processes such as cell proliferation, migration, and tissue maintenance. EGFR is activated upon ligand binding leading to phosphorylation and internalization, and the receptor/ligand complex continues its signaling through the endosomal pathway (Wee and Wang 2017) (Conte and Sigismund 2016).

Unpublished work previously done in the Oddmund Bakke group as well as other published studies have shown that introducing mutations on the Cbl and/or Grb2 binding sites of the EGFR may affect the fate of the receptor upon internalization (Jiang, Huang et al. 2003). Degradation of EGFR was reduced upon inactivating the direct binding sites for Cbl and Grb2 (Merete Storflor, Master thesis 2015)(Fortian, Dionne et al. 2015).

Exchange of Rab5 to Rab7a is essential for endosomal maturation from early to late endosomes, respectively. Recent studies show that a redistribution in IF an MF of Rab5 is a mechanism to regulate the endosomal maturation of early endosomes (Skjeldal, Haugen et al. 2021). Since early endosomal maturation is crucial mechanism for receptor transport, we wanted to investigate whether the intrinsic phosphorylation properties of EGFR may regulate the binding kinetics of Rab5/Rab7a.

5.1 The endosomal binding kinetics of Rab5 are altered in presence of EGF-stimulated mutant EGFRs in HeLa and PAE cells

In this study we have utilized two different cellular systems, HeLa cells with endogenous EGFR and PAE cells lacking endogenous EGFR. HeLa cells have been transiently transfected with the various fluorescently tagged EGFRs and the PAE cells are stable cell-lines expressing different unlabeled EGFRs (wt-EGFR, 1Y-EGFR, 2Y-EGFR and 3Y-EGFR). Co-transfecting with mCh-/mAp-Rab5 or mAp-/EGFP-Rab7a we could follow EGF activated EGFRs until they colocalized with Rab5 or Rab7a positive endosomes. We measured their endosomal binding dynamics through FRAP experiments.

The binding dynamics of mCh-Rab5 on EGF-stimulated wt-EGFR positive endosomes in HeLa cells, was measured to $T_{1/2}$ of 27.43 ± 1.4 seconds (Figure 4.3 B, Table 4.1) which is similar to measured $T_{1/2}$ recovery for mCh-Rab5 in unstimulated cells (Anna Vik Rødseth, Master thesis 2021). This result indicates unaltered mCh-Rab5 binding dynamics on EGF-Alexa 647 and wt-EGFR-GFP positive endosomes. However, in EGF-Alexa 647 stimulated PAE cells the mAp-Rab5 binding dynamics seemed to be faster with a calculated $T_{1/2}$ recovery of 16.3 ± 2.7 seconds (Figure 4.6 B, Table 4.1). This difference may be caused by the combination of the transfected fluorescently labelled EGFR and the endogenous EGFR present in the HeLa cells. Hence, in the PAE system we can specifically study the activated stably transfected receptor without the interference of the endogenous receptor. Although the Rab5 $T_{1/2}$ in HeLa and PAE cells differed, we could calculate a similar IF and MF of Rab5 in the two cellular systems showing an IF of 16% and MF of 86% in HeLa cells (Figure 4.3 C, Table 4.1) and IF of 20% and MF of 80% in PAE cells (Figure 4.6 C, Table 4.1). The measured difference in Rab5 $T_{1/2}$ between the two cellular systems might be due to the expression of endogenous receptor in the HeLa cells. As we stimulate the HeLa cells with EGF we will activate the endogenous receptor as well as the transfected. Hence, the concentration of the receptor on Rab5 positive endosomes might differ in HeLa and PAE and the concentration of the phosphorylated endosomal receptor might change the Rab5 $T_{1/2}$ between the two cell-lines.

Interestingly, when introducing mutant EGFRs stimulated with EGF in HeLa cells we could measure a cumulative increase in mCh-Rab5 $T_{1/2}$ throughout the mutants, showing an increase of mCh-Rab5 $T_{1/2}$ from 30.50 ± 1.5 seconds with 1Y-EGFR-GFP to 39.20 ± 1.8 seconds with 3Y-EGFR-GFP (Figure 4.3 B, Table 4.1). A similar cumulative pattern of mAp-Rab5 $T_{1/2}$ was measured throughout the EGF-stimulated mutants in PAE cells, showing an increase from 21.6 ± 0.9 seconds with 1Y-EGFR to 31.9 ± 2.7 seconds with 3Y-EGFR (Figure 4.6 B, Table 4.1). Results combined from HeLa and PAE cells on Rab5 binding dynamics suggest a phosphorylation dependent gradient changing the binding dynamics of endosomal Rab5.

Further analysis of mAp-Rab5 binding dynamics with EGF-stimulated mutant EGFRs in PAE cells we could not detect any specific change in the IF and MF (Figure 4.6 C, Table 4.1). However, we could measure a major change in the fractions for mCh-Rab5 in EGF-stimulated HeLa cells. On mCh-Rab5 positive endosomes we could measure a 50% reduction in IF of Rab5 from wt- to 1Y-EGFR-GFP and a complete loss of the IF of Rab5 with 2Y- and 3Y-

EGFR-GFP (Figure 4.3 C, Table 4.1). These results further validates that the degree of EGFR phosphorylation induces different binding kinetics of Rab5.

5.2 EGFR mutations affects the endosomal binding kinetics of Rab7a in PAE and HeLa cells

A pivotal moment in the trafficking of EGFR is the endosomal maturation regulated by the conversion from a Rab5 positive endosome to a Rab7a (Rink, Ghigo et al. 2005, Skjeldal, Haugen et al. 2021). For the internalized receptor this crucial step is important to maintain the progression to lysosomal degradation (Ceresa and Bahr 2006). Each individual receptor presented in this work internalized and could reach the Rab7a positive endosomes. As the binding dynamics of Rab5 was found to be altered according to the unique phosphorylation of the mutated receptors, we also wanted to understand if the later Rab GTPase, Rab7a, could also be affected by the degree of phosphorylation. Analyzing the $T_{1/2}$ of mAp-Rab7a positive endosomes in EGF-stimulated HeLa cells transfected with wt-EGFR-GFP we could measure a mAp-Rab7a $T_{1/2}$ to be 22.6 ± 2.5 seconds (Figure 4.4 B, Table 4.1), similar to previous published data (Distefano, Haugen et al. 2018). However, in EGF-stimulated wt-EGFR PAE cells we could measure an altered EGFP-Rab7a binding kinetics showing a faster EGFP-Rab7a $T_{1/2}$ of 15.6 ± 4.1 seconds (Figure 4.8 B, Table 4.1). This difference in Rab7a $T_{1/2}$ between the two cellular systems may be due to the presence of endogenous EGFR in HeLa cells that may reduce the exchange rate of Rab7a on the EGFR positive endosomes.

We could further measure a different fraction distribution of mAp-Rab7a/EGFP-Rab7a, when expressing the wt-receptor, calculating an IF and MF of mAp-Rab7a in stimulated HeLa cells to 59% and 41% (Figure 4.4 C, Table 4.1) vs. 7% and 93% for EGFP-Rab7a in stimulated PAE cells (Figure 4.8 C, Table 4.1). This shows that the typical fraction distribution of Rab7a in the two cellular systems are completely different and we might expect variances in the binding dynamics of Rab7a introducing the diverse mutants. Analysis of the mAp-Rab7 IF and MF in EGF stimulated HeLa cells transfected with the various EGFR mutants could show a complete rearrangement of the fractions. Not only the binding dynamics with an increased $T_{1/2}$ but also a complete rearrangement of the fractions was induced by various mutated receptors. This indicates that the phosphorylation state of transfected EGFRs in HeLa cells inherently changes the binding dynamics of mAp-Rab7a.

Subsequent analysis of the EGFP-Rab7a endosomal binding dynamics in the 1Y-, and 2Y-EGFR PAE cell-lines revealed a slight increase in $T_{1/2}$ of EGFP-Rab7a when stimulated with EGF-Alexa 647 (Figure 4.8 B, Table 4.1). However, when analyzing the binding dynamics of EGFP-Rab7a in stimulated 3Y-EGFR PAE cells we could measure a significant and strong increase in $T_{1/2}$ of mAp-Rab7a compared to the wt-, 1Y-, and 2Y-EGFR. From the EGFP-Rab7a $T_{1/2}$ in the 1Y- and 2Y-EGFR we could measure a ~30-fold increase of EGFP-Rab7a $T_{1/2}$ in 3Y-EGFR PAE cells, $T_{1/2} = 543.6 \pm 186.6$ seconds. This major change in EGFP-Rab7a $T_{1/2}$ in the EGF stimulated cells shows how important the phosphorylation of the EGFR present on the endosome is to specifically regulate the binding dynamics of EGFP-Rab7a. This also indicates the differences within the systems where PAE cells express a human EGFR, either wild-type or mutant and have no background/endogenous to assist the system when a phosphorylation deficient EGFR is transported through the endocytic pathway.

Compared to mAp-Rab7a in EGF-stimulated HeLa cells (Figure 4.4 C, Table 4.1), we did not detect a specific change in EGFP-Rab7a fractions in EGF-stimulated PAE cells (Figure 4.8 C). The fractions of EGFP-Rab7a in PAE cells did not change throughout the various EGFRs whereas in HeLa cells we could measure a total redistribution of the fractions of mAp-Rab7a. These differences may be due to the two different cellular systems in which the PAE system lack endogenous EGFR.

EGF stimulation of the various receptors induced an overall change in binding dynamics of Rab5 and Rab7a. Similar experiments with unstimulated PAE (wt-, 1Y-, 2Y-, 3Y-EGFR) could show a concomitant result with a cumulative increase in $T_{1/2}$ and a stable distribution of the endosomal MF and IF fractions (Figure 4.5, Figure 4.6). These results indicate that there is some kind of receptor activation before EGF stimulation, which might be due to the FBS (which contain receptor ligands), that was added to the imaging medium (Yan, Hui et al. 2007). However, the various receptors in the PAE cells are very sensitive to ligand stimuli and induce the same changes in the binding dynamics of mAp-Rab5 and EGFP-Rab7a, except from the changes induced by the 3Y-EGFR mutant. $T_{1/2}$ of EGFP-Rab7a in unstimulated 3Y-EGFR PAE was reduced by ~50% due to less receptor activation, indicating that a stronger endosomal signal from the 3Y-EGFR receptor enhances the alteration of the EGFP-Rab7a binding dynamics.

In HeLa cells with endogenous EGFR and in PAE cells lacking endogenous EGFR we found a cumulating increase in Rab7a $T_{1/2}$ in both EGF-stimulated and unstimulated cells. However, in PAE cells we could measure a significant and strong increase in Rab7a $T_{1/2}$ when colocalized with the 3Y-EGFR mutant. In contrast to in HeLa cells which express endogenous EGFR, 3Y-EGFR in the PAE cell system may only dimerize with a receptor containing the same mutations on all three phosphorylation sites. This indicates that without direct binding sites for Cbl and Grb2 on the EGFR, the exchange of Rab7a on the late endosomal membrane is strongly abrogated, restricting the further trafficking to lysosomes for degradation. This result is in agreement with earlier studies indicating that the packaging of phosphorylated EGFRs in endosome is a mechanism to specify signaling response and cell-fate (Ceresa and Bahr 2006, Villasenor, Nonaka et al. 2015). The IF and MF of EGFP-Rab7a did not change throughout the various receptors in PAE cells. However, we could measure a total redistribution of the IF and MF of mAp-Rab7a in EGF-stimulated HeLa cells. This might be due to the HeLa cells expressing endogenous EGFR.

5.3 EGFR mutants show different recruitment and internalization characteristics on the plasma membrane

We have shown that the EGFR phosphorylation characteristics alters the binding dynamics of Rab5 and Rab7a. Previous studies have shown alterations in the internalization, trafficking and the degradation of the EGFR mutants (Merete Storflor, Master thesis 2015)(Jiang, Huang et al. 2003, Fortian, Dionne et al. 2015). We wanted to study the effects of these specific EGFR mutations on the activation, uptake and recycling of the receptor. HeLa cells were transiently transfected with the various fluorescently tagged EGFRs and imaged by TIRF microscopy. Similar to previous experiments the HeLa cells were EGF-stimulated and we could temporarily follow the activation, internalization and recycling.

All the four different EGFRs were activated by EGF stimulation and appeared as receptor clusters on the plasma membrane. wt-EGFR-GFP seemed to be recruited faster than the 1Y-, 2Y- and 3Y-EGFR-GFP. The wt-EGFR-GFP had a maximum activation after ~3 minutes (Figure 4.9). 1Y-EGFR-GFP showed a delay in the recruitment to the plasma membrane compared to wt-EGFR-GFP and had a maximum activation after ~8 minutes (Figure 4.11). Both the wt-EGFR and 1Y-EGFR-GFP were internalized as we detected a decrease in the signal overtime. 1Y-EGFR-GFP lack the direct binding site for Cbl which is important for the

ubiquitination of the receptor. Earlier studies have shown that some of the endocytosed receptors escapes the Cbl-meditated ubiquitination. Some receptors can also become dephosphorylated before recycling (Levkowitz, Waterman et al. 1998, Bao, Alroy et al. 2000). Our results support that there is some recycling both for the wt- and 1Y-EGFR-GFP. However, for the 2Y-EGFR-GFP we could measure a delay in the recruitment to the membrane, with a maximum at 8 minutes (Figure 4.13). We detected a very low signal ~20 minutes after EGF-Alexa 647 stimulation. This mutant lacks the two direct binding sites for Grb2. For the 3Y-EGFR-GFP we observed a slow recruitment to the plasma membrane with a maximum after ~6 minutes and we could also detect a high EGF-Alexa647 signal after ~22 minutes (Figure 4.15).

We measured 70% of 3Y-EGFR-GFP clusters present on the plasma membrane at the end of the experiment, in addition to strong signals of EGF-Alexa 647 (Figure 4.16, Figure 4.17). This may indicate EGF-bound 3Y-EGFR-GFP on the plasma membrane with impaired internalization due to loss of binding sites Y1045/1068/1086 for Grb2, which has been shown to be important for receptor internalization (Jiang, Huang et al. 2003). Further, the presence of EGF-/3Y-EGFR-GFP complex on the plasma membrane towards the end of the experiment may in addition be due to enhanced recycling of internalized receptor/ligand complex. This is supported by earlier studies which has shown that ubiquitination-deficient EGFRs is overwhelmingly trafficked through the recycling route, evading degradation (Sigismund, Woelk et al. 2005).

5.4 Knockdown of Rab22a alters trafficking of wt- and 3Y-EGFR-GFP

Ubiquitinated EGFR recruits Rabex-5 which in turn will recruit Rab5 to the early endosomal membrane (Mattera, Tsai et al. 2006). Rab22a is a known effector of Rabex-5 and is part of the Rab22a-Rabex-5-Rab5 cascade important for EGFR degradation. Studies have shown that the degradation of EGFR in Rabex-5-deficient NF73 cells is strongly decelerated, and Rabex-5 is poorly recruited to the early endosome upon Rab22a knockdown (Zhu, Liang et al. 2009). Having shown altered binding kinetics of Rab5 when colocalized with wt- and 3Y-EGFR we further investigated the trafficking of the two receptors in knockdown Rab22a HeLa cells. These cells were also co-transfected with Rab5 and stimulated with EGF-Alexa 647.

HeLa cells co-transfected with wt-EGFR-GFP and mCh-Rab5, after knockdown of Rab22a, were stimulated with EGF-Alexa647 which was rapidly internalized. After internalization we could observe colocalization between EGF-Alexa647 and mCh-Rab5 after one minute (Figure 4.20). Following the trafficking of EGF-Alexa 647 as a function of mCh-Rab5 colocalization we could measure a steady increase until 10 minutes (Figure 4.22). However, after 10 minutes the EGF-Alexa647 colocalization with mCh-Rab5 came to a steady state which continued until 17 minutes. Under normal conditions, without Rab22a knockdown, we would expect to see a decrease of EGF-Alexa647/mCh-Rab5 colocalization after 10 minutes as the mCh-Rab5 would begin to detach from the EGF-Alexa647 positive endosomes. This standard endosomal maturation pattern has previously been shown in the preceding work of this thesis (Merete Storflor, Master thesis 2015). By knocking down Rab22a we confer the previous findings that Rab22a is important for EGFR trafficking due to the abrogation of the important Rab22a-Rabex-5-Rab5 (Zhu, Liang et al. 2009).

Interestingly, in HeLa cells with a Rab22a knockdown and co-transfected with 3Y-EGFR-GFP and mCh-Rab5, we could observe very few mCh-Rab5 positive endosomes prior to EGF-Alexa 647 activation (Figure 4.21). After activation we could observe 3Y-EGFR-GFP and EGF-Alexa647 remaining on the PM for a longer time period than in the wt-EGFR-GFP condition. This indicates an inhibited internalization of the 3Y-EGFR-GFP as previously shown (Merete Storflor, Master thesis 2015)(Fortian, Dionne et al. 2015). However, tracking similar colocalization as described above we could measure colocalization after one minute, but on very few mCh-Rab5 positive vesicles. Subsequently following the colocalization we could measure a very slow increase in colocalization and after 17 minutes we could detect 70% less colocalization of EGF-Alexa647/mCh-Rab5 in cells with 3Y-EGFR-GFP compared to cells with EGF-647Alexa/mCh-Rab5 in cells with wt-EGFR-GFP (Figure 4.22).

Combined, this may indicate that the Rab5 GEF Rabex-5 can bind ubiquitinated wt-EGFR which allows for activation and further recruitment of Rab5 to early endosomes. 3Y-EGFR has been shown to be un-ubiquitinated (Merete Storflor, Master thesis 2015) and as previously published ubiquitinated EGFR recruits Rabex-5 through the Ub-binding site (Mattera, Tsai et al. 2006). Abrogated Ub-binding site for Rabex-5 evidently inhibits the recruitment of Rab5 to the receptor positive endosome and the trafficking is inhibited through an altered maturation pattern.

The finding in this work is highly relevant in the process of understanding the trafficking of receptors in the endocytic pathway and to understand how the pivotal endosomal maturation can be regulated. The fact that a mutated receptor can rearrange the binding dynamics locally on the early and late endosome is a novel finding and may help us understanding the molecular mechanisms of endosomal maturation.

In conclusion, here we show that the EGFR regulates its progression through the endosomal pathway by controlling the endosomal maturation, or more specifically by regulating the endosomal binding kinetics of Rab5 and Rab7a.

6. Future perspectives

Our studies show that the EGFR regulates its progression through the endosomal pathway by regulating endosomal binding kinetics of the GTPases Rab5 and Rab7a in a phosphorylation-dependent manner. We have found that the $T_{1/2}$ increases and the IF and MF is reorganized, specifically the results from the HeLa studies. Previous work in the lab have shown that the IF and MF of Hepatocyte growth factor regulated tyrosine kinase substrate (Hrs) and epidermal growth factor receptor pathway substrate 15 (Eps15) can be reorganized due to a change in phosphorylation (Haugen, Skjeldal et al. 2017). It would be interesting to study if this receptor phosphorylation induced reorganization of the endosomal binding fractions applies to other membrane associated proteins such as, Hrs, Eps15, Rab4 and Rab22a, and would be altered similarly as shown in this study. It seems like the changes in the binding dynamics, activated by a phosphorylation impaired receptor, might be a generic mechanism to regulate its progression and degradation.

When the mutated receptor reached the late endosomal compartment, we could show a gradual change in binding dynamic of Rab7a based on the inherent phosphorylation deficiency. This apparently hindered the internalization and progression of the late endosome by slowing down the binding dynamics of Rab7a. Searching for the molecular mechanism in which the impaired receptors may alter the Rab7a binding dynamics on the late endosome by inhibition of specific interaction with phosphatase and tensin homologue deleted on chromosome 10 (PTEN). A previous study could show a critical role for PTEN in EGFR signal termination (Vivanco, Rohle et al. 2010) and suggests that PTEN could be an interesting candidate to understand more about the receptor induced binding dynamics of Rab7a.

Further quantitative colocalization analysis with photoactivation of the various mutant receptors in combinations with each other. Previous unpublished work in the Bakke lab could show that the wt-EGFR and the 3Y-EGFR was internalized together and were transported to the late endocytic compartment. At this compartment the wt-receptor was sorted intraluminal, and the 3Y-EGFR remained on the late endosomal membrane. It would be very interesting to figure out if the 3Y-EGFR on the late endosomal membrane was recycled back to the PM by

photoactivating the fluorophore to specifically follow the activated late endosomal 3Y-EGFR by TIRF imaging.

In HeLa cells with knockdown of Rab22a we found that the entire trafficking of EGF through Rab5 positive endosomes was specifically slower. The same kind of experiment should be carried out with the other two mutants, 1Y- and 2Y-EGFR, to understand how the phosphorylation impaired receptor would recruit a change in the Rab5 detachment pattern and study the transition to Rab7a. We should also perform FRAP experiments to understand more of the binding dynamics in the absence of Rab22a. This experiment should also be performed with the Rab5 effector protein EEA1.

7. References

1. Antonin, W., C. Holroyd, D. Fasshauer, S. Pabst, G. F. von Mollard and R. Jahn (2000). "A SNARE complex mediating fusion of late endosomes defines conserved properties of SNARE structure and function." EMBO J **19**(23): 6453-6464.
2. Ballabio, A. and J. S. Bonifacino (2020). "Lysosomes as dynamic regulators of cell and organismal homeostasis." Nat Rev Mol Cell Biol **21**(2): 101-118.
3. Barbieri, M. A., S. Hoffenberg, R. Roberts, A. Mukhopadhyay, A. Pomrehn, B. F. Dickey and P. D. Stahl (1998). "Evidence for a Symmetrical Requirement for Rab5-GTP in in Vitro Endosome-Endosome Fusion." J Biol Chem **273**(40): 25850-25855.
4. Batzer, A. G., D. Rotin, J. M. Urena, E. Y. Skolnik and J. Schlessinger (1994). "Hierarchy of binding sites for Grb2 and Shc on the epidermal growth factor receptor." Mol Cell Biol **14**(8): 5192-5201.
5. Bitsikas, V., I. R. Corrêa and B. J. Nichols (2014). "Clathrin-independent pathways do not contribute significantly to endocytic flux." Elife **2014,3**(3): 1,e03970-03926.
6. Bonifacino, J. S. and B. S. Glick (2004). "The Mechanisms of Vesicle Budding and Fusion." Cell **116**(2): 153-166.
7. Bucci, C., P. Thomsen, P. Nicoziani, J. McCarthy and B. Van Deurs (2000). "Rab7: A key to lysosome biogenesis." Mol Biol Cell **11**(2): 467-480.
8. Carpenter, G., L. King and S. Cohen (1978). "Epidermal growth factor stimulates phosphorylation in membrane preparations in vitro." Nature **276**(5686): 409-410.
9. Ceresa, B. P. and S. J. Bahr (2006). "rab7 Activity Affects Epidermal Growth Factor:Epidermal Growth Factor Receptor Degradation by Regulating Endocytic Trafficking from the Late Endosome." J Biol Chem **281**(2): 1099-1106.
10. Conte, A. and S. Sigismund (2016). "Chapter Six - The Ubiquitin Network in the Control of EGFR Endocytosis and Signaling." Prog Mol Biol Transl Sci **141**: 225-276.
11. Cooper, G. M. (2000). The cell : a molecular approach. cell. Washington, D.C. :,Sunderland, Mass., ASM Press ; Sinauer Associates.
12. De Duve, C. and R. Wattiaux (1966). "Functions of lysosomes." Annu Rev Physiol **28**(1): 435-492.

13. Decker, S. J. (1990). "Epidermal growth factor and transforming growth factor- alpha induce differential processing of the epidermal growth factor receptor." Biochem Biophys Res Commun **166**(2): 615-621.
14. Desjardins, M., L. A. Huber, R. G. Parton and G. Griffiths (1994). "Biogenesis of Phagolysosomes Proceeds through a Sequential Series of Interactions with the Endocytic Apparatus." J Cell Biol **124**(5): 677-688.
15. Distefano, M. B., L. H. Haugen, Y. Wang, H. Perdreau-Dahl, I. Kjos, D. Jia, J. P. Morth, J. Neefjes, O. Bakke and C. Progida (2018). "TBC1D5 controls the GTPase cycle of Rab7b." J Cell Sci **131**(17).
16. Dunn, K. W., T. E. McGraw and F. R. Maxfield (1989). "Iterative Fractionation of Recycling Receptors from Lysosomally Destined Ligands in an Early Sorting Endosome." J Cell Biol **109**(6): 3303-3314.
17. Eathiraj, S., X. Pan, D. G. Lambright and C. Ritacco (2005). "Structural basis of family-wide Rab GTPase recognition by rabenosyn-5." Nature **436**(7049): 415-419.
18. Ebner, R. and R. Derynck (1991). "Epidermal growth factor and transforming growth factor-α: Differential intracellular routing and processing of ligand-receptor complexes." Cell Regul **2**(8): 599-612.
19. EMBL, E. (2004). "Determination of the halftime of the recovery (thalf)."
20. Ferguson, K. M. (2008). "Structure-based view of epidermal growth factor receptor regulation." Annu Rev Biophys **37**(1): 353-373.
21. Ferguson, K. M., M. B. Berger, J. M. Mendrola, H.-S. Cho, D. J. Leahy and M. A. Lemmon (2003). "EGF Activates Its Receptor by Removing Interactions that Autoinhibit Ectodomain Dimerization." Mol Cell **11**(2): 507-517.
22. Fish, K. N. (2009). "Total Internal Reflection Fluorescence (TIRF) Microscopy." Current Protocols in Cytometry **50**(1): 12.18.11-12.18.13.
23. Fortian, A., L. K. Dionne, S. H. Hong, W. Kim, S. P. Gygi, S. C. Watkins and A. Sorkin (2015). "Endocytosis of Ubiquitylation-Deficient EGFR Mutants via Clathrin-Coated Pits is Mediated by Ubiquitylation." Traffic **16**(11): 1137-1154.
24. Gabe Lee, M. T., A. Mishra and D. G. Lambright (2009). "Structural Mechanisms for Regulation of Membrane Traffic by Rab GTPases." Traffic **10**(10): 1377-1389.
25. Garrett, T. P. J., N. M. McKern, M. Lou, T. C. Elleman, T. E. Adams, G. O. Lovrecz, H.-J. Zhu, F. Walker, M. J. Frenkel, P. A. Hoyne, R. N. Jorissen, E. C. Nice, A. W. Burgess and

C. W. Ward (2002). "Crystal Structure of a Truncated Epidermal Growth Factor Receptor Extracellular Domain Bound to Transforming Growth Factor α." Cell **110**(6): 763-773.

26. Gillingham, Alison K., R. Sinka, Isabel L. Torres, Kathryn S. Lilley and S. Munro (2014). "Toward a Comprehensive Map of the Effectors of Rab GTPases." Dev Cell **31**(3): 358-373.
27. Goh, L. K., F. Huang, W. Kim, S. Gygi and A. Sorkin (2010). "Multiple mechanisms collectively regulate clathrin-mediated endocytosis of the epidermal growth factor receptor." J Cell Biol **189**(5): 871-883.
28. Gorvel, J.-P., P. Chavrier, M. Zerial and J. Gruenberg (1991). "rab5 controls early endosome fusion in vitro." Cell **64**(5): 915-925.
29. Grandal, M. V. and I. H. Madshus (2008). "Epidermal growth factor receptor and cancer: control of oncogenic signalling by endocytosis." J Cell Mol Med **12**(5a): 1527-1534.
30. Grant, B. D. and J. G. Donaldson (2009). "Pathways and mechanisms of endocytic recycling." Nat Rev Mol Cell Biol **10**(9): 597-608.
31. Griffiths, G. (1989). "The structure and function of a mannose 6-phosphate receptor-enriched, pre-lysosomal compartment in animal cells." Journal of cell science. Supplement **11,93**(11): 139-147.
32. Griscelli, C. and M. Prunieras (1978). "PIGMENT DILUTION AND IMMUNODEFICIENCY: A NEW SYNDROME." Int J Dermatol **17**(10): 788-791.
33. Grovdal, L. M., E. Stang, A. Sorkin and I. H. Madshus (2004). "Direct interaction of Cbl with pTyr 1045 of the EGF receptor (EGFR) is required to sort the EGFR to lysosomes for degradation." Exp Cell Res **300**(2): 388-395.
34. Grøvdal, L. M., E. Stang, A. Sorkin and I. H. Madshus (2004). "Direct interaction of Cbl with pTyr 1045 of the EGF receptor (EGFR) is required to sort the EGFR to lysosomes for degradation." Exp Cell Res **300**(2): 388-395.
35. Guy, P. M., J. V. Platko, L. C. Cantley, R. A. Cerione and K L Carraway, 3rd (1994). "Insect cell-expressed p180erbB3 possesses an impaired tyrosine kinase activity." Proc Natl Acad Sci U S A **91**(17): 8132-8136.

36. Haugen, L. H., F. M. Skjeldal, T. Bergeland and O. Bakke (2017). "Endosomal binding kinetics of Eps15 and Hrs specifically regulate the degradation of RTKs." Sci Rep **7**(1): 17962-17962.
37. Hehnly, H. and S. Doxsey (2014). "Rab11 Endosomes Contribute to Mitotic Spindle Organization and Orientation." Dev Cell **28**(5): 497-507.
38. Helenius, A., J. Kartenbeck and L. Pelkmans (2001). "Caveolar endocytosis of simian virus 40 reveals a new two-step vesicular-transport pathway to the ER." Nat Cell Biol **3**(5): 473-483.
39. Helenius, A., I. Mellman, D. Wall and A. Hubbard (1983). "Endosomes." Trends in Biochemical Sciences **8**(7): 245-250.
40. Hopkins, C. R. (1983). "Intracellular routing of transferrin and transferrin receptors in epidermoid carcinoma A431 cells." Cell **35**(1): 321-330.
41. Horiuchi, H., R. Lippé, H. M. McBride, M. Rubino, P. Woodman, H. Stenmark, V. Rybin, M. Wilm, K. Ashman, M. Mann and M. Zerial (1997). "A Novel Rab5 GDP/GTP Exchange Factor Complexed to Rabaptin-5 Links Nucleotide Exchange to Effector Recruitment and Function." Cell **90**(6): 1149-1159.
42. Hu, Y.-B., E. B. Dammer, R.-J. Ren and G. Wang (2015). "The endosomal-lysosomal system: From acidification and cargo sorting to neurodegeneration." Transl Neurodegener **4**(1): 18-18.
43. Huang, F., D. Kirkpatrick, X. Jiang, S. Gygi and A. Sorkin (2006). "Differential regulation of EGF receptor internalization and degradation by multiubiquitination within the kinase domain." Mol Cell **21**(6): 737-748.
44. Jiang, X., F. Huang, A. Marusyk and A. Sorkin (2003). "Grb2 regulates internalization of EGF receptors through clathrin-coated pits." Mol Biol Cell **14**(3): 858-870.
45. Kaksonen, M. and A. Roux (2018). "Mechanisms of clathrin-mediated endocytosis." Nat Rev Mol Cell Biol **19**(5): 313-326.
46. Khan, I. and P. S. Steeg (2021). "Endocytosis: a pivotal pathway for regulating metastasis." Br J Cancer **124**(1): 66-75.
47. Kim, S., Y. Sato, P. S. Mohan, C. Peterhoff, A. Pensalfini, A. Rigoglioso, Y. Jiang and R. A. Nixon (2016). "Evidence that the rab5 effector APPL1 mediates APP-βCTF-induced dysfunction of endosomes in Down syndrome and Alzheimer's disease." Mol Psychiatry **21**(5): 707-716.

48. King, J. S. and R. R. Kay (2019). "The origins and evolution of macropinocytosis." Philos Trans R Soc Lond B Biol Sci **374**(1765): 20180158-20180158.
49. Kiss, A. L. and E. Botos (2009). "Endocytosis via caveolae: alternative pathway with distinct cellular compartments to avoid lysosomal degradation?" J Cell Mol Med **13**(7): 1228-1237.
50. Klinkert, K., M. Rocancourt, A. Houdusse and A. Echard (2016). "Rab35 GTPase couples cell division with initiation of epithelial apico-basal polarity and lumen opening." Nat Commun **7**(1): 11166-11166.
51. Klumperman, J. and G. Raposo (2014). "The complex ultrastructure of the endolysosomal system." Cold Spring Harb Perspect Biol **6**(10): a016857-a016857.
52. Langemeyer, L., A.-C. Borchers, E. Herrmann, N. Füllbrunn, Y. Han, A. Perz, K. Auffarth, D. Kümmel and C. Ungermann (2020). "A conserved and regulated mechanism drives endosomal rab transition." Elife **9**.
53. Lewis, W. H. (1937). "Pinocytosis by malignant cells." American Journal of Cancer **29**(4): 666-679.
54. Lippé, R., M. Miaczynska, V. Rybin, A. Runge and M. Zerial (2001). "Functional synergy between Rab5 effector Rabaptin-5 and exchange factor Rabex-5 when physically associated in a complex." Mol Biol Cell **12**(7): 2219-2228.
55. Lippincott-Schwartz, J., E. Snapp and A. Kenworthy (2001). "Studying protein dynamics in living cells." Nat Rev Mol Cell Biol **2**(6): 444-456.
56. Lock, J. G. and J. L. Stow (2005). "Rab11 in recycling endosomes regulates the sorting and basolateral transport of E-cadherin." Mol Biol Cell **16**(4): 1744-1755.
57. Lowenstein, E. J., R. J. Daly, A. G. Batzer, W. Li, B. Margolis, R. Lammers, A. Ullrich, E. Y. Skolnik, D. Bar-Sagi and J. Schlessinger (1992). "The SH2 and SH3 domain-containing protein GRB2 links receptor tyrosine kinases to ras signaling." Cell **70**(3): 431-442.
58. Massol, R. H., W. Boll, A. M. Griffin and T. Kirchhausen (2006). "A Burst of Auxilin Recruitment Determines the Onset of Clathrin-Coated Vesicle Uncoating." Proc Natl Acad Sci U S A **103**(27): 10265-10270.
59. Mattera, R., J. S. Bonifacino, S. Lee, W. J. Smith, J. H. Hurley, M. S. Kostelansky, Y. C. Tsai and A. M. Weissman (2006). "Structural basis for ubiquitin recognition and autoubiquitination by Rabex-5." Nat Struct Mol Biol **13**(3): 264-271.

60. Mattera, R., Y. C. Tsai, A. M. Weissman and J. S. Bonifacino (2006). "The Rab5 Guanine Nucleotide Exchange Factor Rabex-5 Binds Ubiquitin (Ub) and Functions as a Ub Ligase through an Atypical Ub-interacting Motif and a Zinc Finger Domain." J Biol Chem **281**(10): 6874-6883.
61. Maxfield, F. R. and T. E. McGraw (2004). "Endocytic recycling." Nat Rev Mol Cell Biol **5**(2): 121-132.
62. Mayor, S. and R. E. Pagano (2007). "Pathways of clathrin-independent endocytosis." Nat Rev Mol Cell Biol **8**(8): 603-612.
63. McBride, H. and M. Zerial (2001). "Rab proteins as membrane organizers." Nat Rev Mol Cell Biol **2**(2): 107-117.
64. Mesa, R., C. Salomón, M. Roggero, P. D. Stahl and L. S. Mayorga (2001). "Rab22a affects the morphology and function of the endocytic pathway." J Cell Sci **114**(22): 4041-4049.
65. Miaczynska, M., S. Christoforidis, A. Giner, A. Shevchenko, S. Uttenweiler-Joseph, B. Habermann, M. Wilm, R. G. Parton and M. Zerial (2004). "APPL Proteins Link Rab5 to Nuclear Signal Transduction via an Endosomal Compartment." Cell **116**(3): 445-456.
66. Mills, G. B., Y. Mosesson and Y. Yarden (2008). "Derailed endocytosis: an emerging feature of cancer." Nat Rev Cancer **8**(11): 835-850.
67. Minsky, M. (1961). "Steps toward Artificial Intelligence." Proceedings of the IRE **49**(1): 8-30.
68. Naslavsky, N., J. Rahajeng, M. Sharma, M. Jović and S. Caplan (2006). "Interactions between EHD proteins and Rab11-FIP2: A role for EHD3 in early endosomal transport." Mol Biol Cell **17**(1): 163-177.
69. Nevo, J. (2021). "Novel Players in the Integrin Signaling Orchestra: TCPTP and MDGI."
70. Nishikimi, A., S. Ishihara, M. Ozawa, K. Etoh, M. Fukuda, T. Kinashi and K. Katagiri (2014). "Rab13 acts downstream of the kinase Mst1 to deliver the integrin LFA-1 to the cell surface for lymphocyte trafficking." Sci Signal **7**(336): ra72-ra72.
71. Ogiso, H., R. Ishitani, O. Nureki, S. Fukai, M. Yamanaka, J.-H. Kim, K. Saito, A. Sakamoto, M. Inoue, M. Shirouzu and S. Yokoyama (2002). "Crystal Structure of the Complex of Human Epidermal Growth Factor and Receptor Extracellular Domains." Cell **110**(6): 775-787.

72. Okutani, T., Y. Okabayashi, Y. Kido, Y. Sugimoto, K. Sakaguchi, K. Matuoka, T. Takenawa and M. Kasuga (1994). "Grb2/Ash binds directly to tyrosines 1068 and 1086 and indirectly to tyrosine 1148 of activated human epidermal growth factor receptors in intact cells." J Biol Chem **269**(49): 31310-31314.
73. Olkkonen, V. M., P. Dupree, I. Killisch, A. Lutcke, M. Zerial and K. Simons (1993). "Molecular cloning and subcellular localization of three GTP-binding proteins of the rab subfamily." J Cell Sci **106**(4): 1249-1261.
74. Palade, G. (1975). "Intracellular Aspects of the Process of Protein Synthesis." Science **189**(4200): 347-358.
75. Pawson, T. and J. Schlessingert (1993). "SH2 and SH3 domains." Curr Biol **3**(7): 434-442.
76. Penengo, L., M. Mapelli, A. G. Murachelli, S. Confalonieri, L. Magri, A. Musacchio, P. P. Di Fiore, S. Polo and T. R. Schneider (2006). "Crystal Structure of the Ubiquitin Binding Domains of Rabex-5 Reveals Two Modes of Interaction with Ubiquitin." Cell **124**(6): 1183-1195.
77. Pfeffer, S. R. (2013). "Rab GTPase regulation of membrane identity." Curr Opin Cell Biol **25**(4): 414-419.
78. Pfeffer, S. R., D. Aivazian and U. Sivars (2003). "Yip3 catalyses the dissociation of endosomal Rab-GDI complexes." Nature **425**(6960): 856-859.
79. Pincet, F., V. Adrien, R. Yang, J. Delacotte, J. E. Rothman, W. Urbach and D. Tareste (2016). "FRAP to characterize molecular diffusion and interaction in various membrane environments." PLoS One **11**(7): e0158457-e0158457.
80. Pinilla-Macua, I., A. Grassart, U. Duvvuri, S. C. Watkins and A. Sorkin (2017). "EGF receptor signaling, phosphorylation, ubiquitylation and endocytosis in tumors in vivo." Elife **6**.
81. Poteryaev, D., S. Datta, K. Ackema, M. Zerial and A. Spang (2010). "Identification of the Switch in Early-to-Late Endosome Transition." Cell **141**(3): 497-508.
82. Progida, C., L. Cogli, F. Piro, A. De Luca, O. Bakke and C. Bucci (2010). "Rab7b controls trafficking from endosomes to the TGN." J Cell Sci **123**(9): 1480-1491.
83. Progida, C., M. S. Nielsen, G. Koster, C. Bucci and O. Bakke (2012). "Dynamics of Rab7b-Dependent Transport of Sorting Receptors." Traffic **13**(9): 1273-1285.

84. Pylypenko, O., H. Hammich, I. M. Yu and A. Houdusse (2018). "Rab GTPases and their interacting protein partners: Structural insights into Rab functional diversity." Small GTPases **9**(1-2): 22-48.

85. Rink, J., E. Ghigo, Y. Kalaidzidis and M. Zerial (2005). "Rab Conversion as a Mechanism of Progression from Early to Late Endosomes." Cell **122**(5): 735-749.

86. Rozakis-Adcock, M., A. Batzer, P. G. Pelicci, W. Li, J. Schlessinger, G. Pelicci, J. McGlade, G. Mbamalu, R. Daly, J. Brugge, S. Thomas and T. Pawson (1992). "Association of the Shc and Grb2/Sem5 SH2-containing proteins is implicated in activation of the Ras pathway by tyrosine kinases." Nature **360**(6405): 689-692.

87. Rubino, M., M. Miaczynska, R. Lippé and M. Zerial (2000). "Selective Membrane Recruitment of EEA1 Suggests a Role in Directional Transport of Clathrin-coated Vesicles to Early Endosomes." J Biol Chem **275**(6): 3745-3748.

88. Satori, C. P., M. M. Henderson, E. A. Krautkramer, V. Kostal, M. M. Distefano and E. A. Arriaga (2013). "Bioanalysis of Eukaryotic Organelles." Chem. Rev **113**(4): 2733-2811.

89. Schmidt, O. and D. Teis (2012). "The ESCRT machinery." Curr Biol **22**(4): R116-R120.

90. Schneider, M. R. and E. Wolf (2009). "The epidermal growth factor receptor ligands at a glance." J. Cell. Physiol **218**(3): 460-466.

91. Schnettger, L., A. Rodgers, U. Repnik, R. P. Lai, G. Pei, M. Verdoes, R. J. Wilkinson, D. B. Young and M. G. Gutierrez (2017). "A Rab20-Dependent Membrane Trafficking Pathway Controls M. tuberculosis Replication by Regulating Phagosome Spaciousness and Integrity." Cell Host Microbe **21**(5): 619-628.e615.

92. Schonteich, E., G. M. Wilson, J. Burden, C. R. Hopkins, K. Anderson, J. R. Goldenring and R. Prekeris (2008). "The Rip11/Rab11-FIP5 and kinesin II complex regulates endocytic protein recycling." J Cell Sci **121**(22): 3824-3833.

93. Scott, C. C., F. Vacca and J. Gruenberg (2014). "Endosome maturation, transport and functions." Semin Cell Dev Biol **31**: 2-10.

94. Sharma, M., N. Naslavsky and S. Caplan (2008). "A Role for EHD4 in the Regulation of Early Endosomal Transport." Traffic **9**(6): 995-1018.

95. Sigismund, S., V. Algisi, G. Nappo, A. Conte, R. Pascolutti, A. Cuomo, T. Bonaldi, E. Argenzio, L. G. Verhoef, E. Maspero, F. Bianchi, F. Capuani, A. Ciliberto, S. Polo and P. P. Di Fiore (2013). "Threshold-controlled ubiquitination of the EGFR directs receptor fate." EMBO J **32**(15): 2140-2157.

96. Sigismund, S., T. Woelk, C. Puri, E. Maspero, C. Tacchetti, P. Transidico, P. P. Di Fiore and S. Polo (2005). "Clathrin-Independent Endocytosis of Ubiquitinated Cargos." Proc Natl Acad Sci U S A **102**(8): 2760-2765.

97. Singh, B., G. Carpenter and R. J. Coffey (2016). "EGF receptor ligands: recent advances [version 1; peer review: 3 approved]." F1000Res **5**: 2270.

98. Sipe, D. M. and R. F. Murphy (1987). "High-Resolution Kinetics of Transferrin Acidification in BALB/c 3T3 Cells: Exposure to pH 6 Followed by Temperature-Sensitive Alkalinization during Recycling." Proc Natl Acad Sci U S A **84**(20): 7119-7123.

99. Skjeldal, F. M., L. H. Haugen, D. Mateus, D. M. Frei, A. V. Rødseth, X. Hu and O. Bakke (2021). "De novo formation of early endosomes during Rab5 to Rab7 transition." Journal of cell science: jcs.254185.

100. Skjeldal, F. M., L. H. Haugen, D. Mateus, D. M. Frei, A. V. Rødseth, X. Hu and O. Bakke (2021). "De novo formation of early endosomes during Rab5-to-Rab7a transition." J Cell Sci **134**(8).

101. Sorkin, A. and L. K. Goh (2009). "Endocytosis and intracellular trafficking of ErbBs." Experimental cell research **315**(4): 683-696.

102. Sprague, B. L. and J. G. McNally (2005). "FRAP analysis of binding: proper and fitting." Trends Cell Biol **15**(2): 84-91.

103. Stenmark, H. (2009). "Rab GTPases as coordinators of vesicle traffic." Nat Rev Mol Cell Biol **10**(8): 513-525.

104. Swanson, J. A. (2008). "Shaping cups into phagosomes and macropinosomes." Nat Rev Mol Cell Biol **9**(8): 639-649.

105. Takahashi, S., K. Kubo, S. Waguri, A. Yabashi, H.-W. Shin, Y. Katoh and K. Nakayama (2012). "Rab11 regulates exocytosis of recycling vesicles at the plasma membrane." J Cell Sci **125**(17): 4049-4057.

106. Taylor, M. J., D. Perrais and C. J. Merrifield (2011). "A high precision survey of the molecular dynamics of mammalian clathrin-mediated endocytosis." PLoS Biol **9**(3): e1000604-e1000604.

107. Tokarev, A. A., A. Alfonso and N. Segev Overview of Intracellular Compartments and Trafficking Pathways. New York, NY, New York, NY: Springer New York**:** 3-14.

108. Tomas, A., C. E. Futter and E. R. Eden (2013). "EGF receptor trafficking: consequences for signaling and cancer." Trends Cell Biol **24**(1): 26-34.

109. Tzahar, E., H. Waterman, X. Chen, G. Levkowitz, D. Karunagaran, S. Lavi, B. J. Ratzkin and Y. Yarden (1996). "A hierarchical network of interreceptor interactions determines signal transduction by Neu differentiation factor/neuregulin and epidermal growth factor." Mol Cell Biol **16**(10): 5276-5287.

110. van der Sluijs, P., M. Hull, P. Webster, P. Mâle, B. Goud and I. Mellman (1992). "The small GTP-binding protein rab4 controls an early sorting event on the endocytic pathway." Cell **70**(5): 729-740.

111. Van Gele, M., P. Dynoodt and J. Lambert (2009). "Griscelli syndrome: a model system to study vesicular trafficking." Pigment Cell Melanoma Res **22**(3): 268-282.

112. Vanlandingham, P. A. and B. P. Ceresa (2009). "Rab7 Regulates Late Endocytic Trafficking Downstream of Multivesicular Body Biogenesis and Cargo Sequestration." J Biol Chem **284**(18): 12110-12124.

113. Villasenor, R., H. Nonaka, P. D. Conte-Zerial, Y. Kalaidzidis and M. Zerial (2015). "Regulation of EGFR signal transduction by analogue-to-digital conversion in Endosomes." Elife **4**(4): 1-74.

114. Vivanco, I., D. Rohle, M. Versele, A. Iwanami, D. Kuga, B. Oldrini, K. Tanaka, J. Dang, S. Kubek, N. Palaskas, T. Hsueh, M. Evans, D. Mulholland, D. Wolle, S. Rajasekaran, A. Rajasekaran, L. M. Liau, T. F. Cloughesy, I. Dikic, C. Brennan, H. Wu, P. S. Mischel, T. Perera and I. K. Mellinghoff (2010). "The phosphatase and tensin homolog regulates epidermal growth factor receptor (EGFR) inhibitor response by targeting EGFR for degradation." Proc Natl Acad Sci U S A **107**(14): 6459-6464.

115. Wandinger-Ness, A. and M. Zerial (2014). "Rab proteins and the compartmentalization of the endosomal system." Cold Spring Harb Perspect Biol **6**(11): a022616-a022616.

116. Wee, P. and Z. Wang (2017). "Epidermal growth factor receptor cell proliferation signaling pathways." Cancers (Basel) **9**(5): 52.

117. Weigert, R., A. C. Yeung, J. Li and J. G. Donaldson (2004). "Rab22a regulates the recycling of membrane proteins internalized independently of clathrin." Mol Biol Cell **15**(8): 3758-3770.

118. Wieduwilt, M. J. and M. M. Moasser (2008). "The epidermal growth factor receptor family: Biology driving targeted therapeutics." Cell Mol Life Sci **65**(10): 1566-1584.

119. Yamashiro, D. J., B. Tycko, S. R. Fluss and F. R. Maxfield (1984). "Segregation of transferrin to a mildly acidic (pH 6.5) para-golgi compartment in the recycling pathway." Cell **37**(3): 789-800.

120. Yan, F., Y.-n. Hui, Y.-j. Li, C.-m. Guo and H. Meng (2007). "Epidermal Growth Factor Receptor in Cultured Human Retinal Pigment Epithelial Cells." Ophthalmologica **221**(4): 244-250.

121. Zerial, M., H. M. McBride, S. Christoforidis and R. D. Burgoyne (1999). "The Rab5 effector EEA1 is a core component of endosome docking." Nature **397**(6720): 621-625.

122. Zerial, M., F. Severin, E. Nielsen, A. A. Hyman and J. M. Backer (1999). "Rab5 regulates motility of early endosomes on microtubules." Nat Cell Biol **1**(6): 376-382.

123. Zhang, Z., T. Zhang, F. Yu, J. Chen and J. Ding (2014). "Molecular basis of the activation of the Rabex-5 GEF activity by Rabaptin-5 in endocytosis (802.27)." The FASEB journal **28**(S1).

124. Zhen, Y. and H. Stenmark (2015). "Cellular functions of Rab GTPases at a glance." J Cell Sci **128**(17): 3171-3176.

125. Zhou, Y., N. Ariotti, J. Rae, H. Liang, V. Tillu, S. Tee, M. Bastiani, A. T. Bademosi, B. M. Collins, F. A. Meunier, J. F. Hancock and R. G. Parton (2021). "Caveolin-1 and cavin1 act synergistically to generate a unique lipid environment in caveolae." J Cell Biol **220**(3).

126. Zhu, H., Z. Liang and G. Li (2009). "Rabex-5 is a rab22 effector and mediates a rab22-rab5 signaling cascade in endocytosis." Mol Biol Cell **20**(22): 4720-4729.

127. Distefano, M. B., L. H. Haugen, Y. Wang, H. Perdreau-Dahl, I. Kjos, D. Jia, J. P. Morth, J. Neefjes, O. Bakke and C. Progida (2018). "TBC1D5 controls the GTPase cycle of Rab7b." J Cell Sci **131**(17).

128. Goh, L. K., F. Huang, W. Kim, S. Gygi and A. Sorkin (2010). "Multiple mechanisms collectively regulate clathrin-mediated endocytosis of the epidermal growth factor receptor." J Cell Biol **189**(5): 871-883.

129. Grovdal, L. M., E. Stang, A. Sorkin and I. H. Madshus (2004). "Direct interaction of Cbl with pTyr 1045 of the EGF receptor (EGFR) is required to sort the EGFR to lysosomes for degradation." Exp Cell Res **300**(2): 388-395.

130. Grøvdal, L. M., E. Stang, A. Sorkin and I. H. Madshus (2004). "Direct interaction of Cbl with pTyr 1045 of the EGF receptor (EGFR) is required to sort the EGFR to lysosomes for degradation." Exp Cell Res **300**(2): 388-395.

131. Huang, F., D. Kirkpatrick, X. Jiang, S. Gygi and A. Sorkin (2006). "Differential regulation of EGF receptor internalization and degradation by multiubiquitination within the kinase domain." Mol Cell **21**(6): 737-748.

132. Mattera, R., J. S. Bonifacino, S. Lee, W. J. Smith, J. H. Hurley, M. S. Kostelansky, Y. C. Tsai and A. M. Weissman (2006). "Structural basis for ubiquitin recognition and autoubiquitination by Rabex-5." Nat Struct Mol Biol **13**(3): 264-271.

133. Mesa, R., C. Salomón, M. Roggero, P. D. Stahl and L. S. Mayorga (2001). "Rab22a affects the morphology and function of the endocytic pathway." J Cell Sci **114**(22): 4041-4049.

134. Olkkonen, V. M., P. Dupree, I. Killisch, A. Lutcke, M. Zerial and K. Simons (1993). "Molecular cloning and subcellular localization of three GTP-binding proteins of the rab subfamily." J Cell Sci **106**(4): 1249-1261.

135. Penengo, L., M. Mapelli, A. G. Murachelli, S. Confalonieri, L. Magri, A. Musacchio, P. P. Di Fiore, S. Polo and T. R. Schneider (2006). "Crystal Structure of the Ubiquitin Binding Domains of Rabex-5 Reveals Two Modes of Interaction with Ubiquitin." Cell **124**(6): 1183-1195.

136. Rink, J., E. Ghigo, Y. Kalaidzidis and M. Zerial (2005). "Rab Conversion as a Mechanism of Progression from Early to Late Endosomes." Cell **122**(5): 735-749.

137. Sigismund, S., V. Algisi, G. Nappo, A. Conte, R. Pascolutti, A. Cuomo, T. Bonaldi, E. Argenzio, L. G. Verhoef, E. Maspero, F. Bianchi, F. Capuani, A. Ciliberto, S. Polo and P. P. Di Fiore (2013). "Threshold-controlled ubiquitination of the EGFR directs receptor fate." EMBO J **32**(15): 2140-2157.

138. Skjeldal, F. M., L. H. Haugen, D. Mateus, D. M. Frei, A. V. Rødseth, X. Hu and O. Bakke (2021). "De novo formation of early endosomes during Rab5-to-Rab7a transition." J Cell Sci **134**(8).

139. Zhang, Z., T. Zhang, F. Yu, J. Chen and J. Ding (2014). "Molecular basis of the activation of the Rabex-5 GEF activity by Rabaptin-5 in endocytosis (802.27)." The FASEB journal **28**(S1).

140. Zhu, H., Z. Liang and G. Li (2009). "Rabex-5 is a rab22 effector and mediates a rab22-rab5 signaling cascade in endocytosis." Mol Biol Cell **20**(22): 4720-4729.

Supplementary

Table S1: Lysogeny broth (LB) medium

Bacto-tryptone	10 g/L
Bacto yeast extract	5 g/L
NaCl	10 g/L
NaOH	1 mM

Adjusted with dH_2O to desired volume

Table S2: Wizard™ Plus Midiprep kit protocol (Promega)

Wizard™ Plus Midiprep kit protocol
1. Pellet 100 ml of cells by centrifugation at 4000 rpm for 10-20 minutes at 4°C. Pour off the supernatant and blot the tube upside down on a paper towel to remove excess liquid.
2. Completely resuspend the cell pellet in 3ml of Cell Resuspension Solution. (Complete resuspension is critical for optimal yields.)
3. Add 3ml of Cell Lysis Solution and mix by inverting the tube four times. Do not vortex. The cell suspension should clear immediately.
4. Add 3ml of Neutralization Solution and mix by inverting the tube 4 times.
5. Centrifuge at 4000 rpm for 10 minutes at 4°C. If a tight pellet has not formed by the end of the centrifugation, centrifuge for another 15 minutes.
6. Carefully decant the supernatant to a new centrifuge tube, avoiding the white precipitate.
7. Add 10ml of resuspended Wizard® Midipreps DNA Purification Resin (preheated 37°C) to the DNA solutions. Swirl to mix.
8. For each Midiprep, use one Midicolumn. Insert the Midicolumn tip into the vacuum manifold port.
9. Transfer the resin/DNA mixture into the Midicolumn. Apply a vacuum of at least 15 inches of Hg to pull the resin/DNA mix into the Midicolumn. When the entire sample has passed through the column, break the vacuum at the source.
10. Add 15ml of Column Wash Solution to the Midicolumn and apply a vacuum to draw the solution through the Midicolumn.
Break the vacuum at the source and add another 15ml of Column Wash Solution to the Midicolumn. Reapply a vacuum to draw the solution through the Midicolumn.
11. Dry the resin by continuing to draw a vacuum for 30 seconds after the solution has been pulled through the column. Remove the 12. Midicolumn from the vacuum source.
13. Separate the Reservoir from the Midicolumn by breaking or cutting with sharp scissors.
14. Transfer the Midicolumn to a 1.5ml microcentrifuge tube.
15. Centrifuge the Midicolumn at 10,000 × *g* in a microcentrifuge for 2 minutes to remove any residual Column Wash Solution.
16. Transfer the Midicolumn to a new microcentrifuge tube.
17. Add 300µl of preheated (65-70°C) Nuclease-Free Water to the Midicolumn and wait 1 minute.
18. Elute the DNA by centrifuging the Midicolumn at 10,000 × *g* for 20 seconds in a microcentrifuge. Remove and discard the Midicolumn.

19. A white pellet of resin fines may be present in the final eluate. Whether visible or not, it is important to separate the fines from the DNA.
20. Centrifuge the sample at 10,000 × *g* in a microcentrifuge for 5 minutes to pellet the fines. Carefully transfer the DNA-containing supernatant to a clean microcentrifuge tube.
21. Store the eluted DNA at -20°C

Table S3: RIPA buffer (Lysis buffer)

NaCl	150 mM
Tris-HCl (pH 7.8)	50 mM
Sodium Deoxycholate	1 %
SDS	0.1 %
Triton X-100	1.5 %

Adjusted with dH_2O to desired volume
25xPhosphate inhibitor added prior to use

Tabell S4: Laemmli sampling buffer 2x

1M Tris-HCl (pH 6.8)	100 mM
Glycerol	20 %
SDS	4%
Bromophenol Blue	0.2 %

Adjusted with dH_2O to desired volume
200 mM DTT was added prior to use

Table S5: Tris/Glycine/SDS Running buffer 10x

Tris Base	29 g/L
Glycine	144 g/L
SDS	10 g/L
dH_2O	1L

Mixed in 1L dH_2O
Diluted 1:10 with dH_2O prior to use.

Table S6: Transfer buffer 1x

Tris	6.06 g/L
Glycin	28.8 g/L
Methanol	200 ml
dH_2O	1L

Table S7: Antibodies used for Western blotting

	Antibody	**Concentration**	**Class**	**Acquired from**
pAb	Anti-Rab 22a	1:200	Rabbit IgG	Proteintech
sAb	ECL™ Anti-Rabbit IgG, Horseradish Peroxidase linked whole antibody	1:10 000	Donkey	GE Healthcare
pAb	Anti-Tubulin	1:120 000	Mouse IgG	Sigma-Aldrich
sAb	ECL™ Anti-mouse IgG, Horseradish Peroxidase linked whole antibody (from sheep)	1:10 000	Sheep	GE Healthcare